Sediment Provenance using Detrital-Zircons, Nd-Sr Isotopes, and Bulk Rock Geochemistry: Implications for Sediment Routing in the Neoproterozoic Windermere Supergroup, southern Canadian Cordillera

Alexandra Pipe

A thesis submitted in partial fulfillment of the requirements for the M.Sc. degree in Earth Sciences

Department of Earth and Environmental Sciences
Faculty of Science
University of Ottawa

Abstract

High-resolution sampling of Neoproterozoic basin-floor to slope deposits in the Windermere Supergroup, east-central British Columbia indicates three distinct stratigraphically ascending clusters suggesting temporal changes in sediment provenance. Assemblage 1 has a characteristic northwestern Laurentia bimodal detrital zircon distribution with low ε_{Nd} values, and intermediate to mafic igneous provenance as indicated by discriminant function analysis of major elements, low Th/Sc and Zr/Sc, high Co/Th, and high Cr abundance. This suggests derivation from western Laurentia basement rocks and Archean mafic and ultramafic suites from the Central Hearne province supracrustal belt. Assemblage 2, although compositionally similar, has an additional 655 Ma detrital zircon age population, higher ε_{Nd} values, and felsic igneous to recycled provenance, suggesting a significant Neoproterozoic igneous rift-related source. Assemblage 3 marks the end of input from the juvenile ca. 655 Ma source and felsic igneous to recycled provenance, suggesting a return to western Laurentian cratonic sources.

Résumé

L'échantillonnage à haute résolution de dépôts néoprotérozoïques du bassin, du plancher et de la pente dans le supergroupe de Windermere, dans le centre-est de la Colombie-Britannique, indique trois assemblages avec des ascendents stratigraphiques distincts, suggérant des changements temporels dans la provenance des sédiments. L'assemblage 1 a une distribution bimodale caractéristique du nord-ouest de la Laurentie avec de faibles valeurs de εNd, et une provenance ignée intermédiaire à mafique comme l'indique l'analyse de la fonction discriminante, un faible Th/Sc et Zr/Sc, un Co/Th élevé, une forte abondance de Cr. Ceci suggère une provenance des roches du socle de la Laurentie occidentale et des suites mafiques et ultramafiques archéennes de la ceinture supracrustale de la province de Central Hearne. L'assemblage 2, bien que de composition similaire, présente une population supplémentaire avec des âges de zircons détritiques de 655 Ma, des valeurs εNd plus élevées et une provenance d'igné felsique recyclé, ce qui suggère une source importante liée à un rift igné néoprotérozoïque situé à proximité ou au sud. L'assemblage 3 marque la fin de l'apport de la source juvénile d'env. 655 Ma et de la provenance ignée felsique à recyclée, ce qui suggère un retour aux sources cratoniques du Laurentien occidental.

Extended Abstract

Resolving events associated with the origin of the passive margin forming the western edge of Laurentia (ancestral North America) are an important constraint on the breakup of the Rodinia supercontinent and set the stage for the Phanerozoic evolution of western Laurentia. One of the prime areas to study this history is the 7–9 km-thick Neoproterozoic Windermere Supergroup (WSG) in the southern Canadian Cordillera. At the Castle Creek study area (CC) in east-central British Columbia a continuous succession of sheetlike, sandstone-rich basin-floor (upper Kaza Group (UKG)) conformably overlain by continental slope deposits (Isaac Formation) comprising 7 informal channel complexes (ICC0-ICC6) were sampled ~ 10 m stratigraphically upward over the 2000 m-thick section. Geochemical data derived from these mudrock samples were combined with detrital zircon data from sandstones to provide a highly resolved understanding of temporal changes in sediment provenance and sediment supply during development of the continent-margin Neoproterozoic Windermere turbidite system in the southern Canadian Cordillera. Based on their geochemical characteristics strata in the study are subdivided into four compositionally unique groups: Assemblage 1, comprising UKG up to ICC1, Assemblage 2, comprising ICC3, ICC4 and ICC5, and Assemblage 3, comprising ICC6 and all strata above to the base of the Cunningham Formation.

Detrital zircon ages in Assemblage 1 have a characteristic northwestern Laurentia bimodal distribution with major populations between 3.0 to 2.5 Ga and 1.9-1.75 Ga, and an absence of grains between 2.5 and 2.0 Ga. This zircon age distribution, in addition to εNd(*600 Ma*) values that range from -19.1 to -17.6, are consistent with derivation from nearby Precambrian basement domains in the subsurface of western Canada, specifically the Rimbey domain and adjacent domains in the southern Hearne province. Geochemical data from

Assemblage 1 suggest a mafic component in some of the strata, specifically: a flatter REE pattern (La/Yb_N = 25.3), a low Zr/Sc ratio, and smaller negative Eu anomaly that is higher than in standard UCC (Eu/Eu* = 0.7 versus 0.64 – the latter being the UCC). Additionally, Assemblage 1 has a higher Cr/Th ratio (Cr/Th = 7.5) and lower $^{87}Sr/^{86}Sr(0)$ values (0.7320 to 0.7582) compared to other assemblages. Two potential sources for the additional intermediate-mafic source include the Wopmay Orogen, specifically the Fort Simpson, Hottah, Great Bear terranes and Archean mafic and ultramafic suites in the central Hearne province supracrustal belt of northern Saskatchewan, Manitoba and Nunavut. Problematic with Scenario A is the absence of 2.4-2.0 Ga detrital zircons from the area between the CC study area and the Wopmay Orogen magmatic belts (i.e. Kiskatinaw, Ksituan, Chinchaga, and Buffalo Head terranes), whereas Scenario B is more consistent with the general east-to-west sediment dispersal pattern during the Neoproterozoic.

Detrial zircon ages in Assemblage 2 are consistent with a northwestern Laurentia provenance, but rather than being bimodal are trimodal. This includes major populations between 3.0 to 2.5 Ga, 1.9-1.8 Ga, and a third at 655 Ma. The resulting detrital signature reflects mixing of two distinct sources. Like Assemblage 1, the Mesoproterozoic and Archean detrital zircon signatures are attributed to the southern Hearne and associated Rimbey domain. The source of the ca. 655 Ma age peak, however, is more uncertain. Assemblage 2 exhibits a range of $\varepsilon Nd(600\ Ma)$ values from -16.5 to -9.9, which is broader than in Assemblage 1 and significantly lower than lithostratigraphically similar strata in the Horsethief Creek and Miette groups (-22.0 to -20.3). This would suggest input from a more juvenile source, which is consistent with the prominent 655 Ma detrital zircon age population. On the provenance discrimination diagram, most of these samples plot in fields for felsic igneous and quartzose sedimentary provenance

based on their relatively low MgO, Fe_2O_3 and TiO_2 content. Furthermore, trace element ratios, such as high Th/Sc (0.68-1.85) and Zr/Sc (7.4-24), and low concentrations of Cr and Ni, suggest a mostly continental source. REE patterns are similar to PAAS with LREE enrichment and negative Eu anomalies ranging from 0.57 to 0.74 (average = 0.68). These geochemical data, in addition to the 655 Ma detrital zircon age population and the more positive Nd isotopic ratios, are suggestive of a highly recycled continental source, but with a significant Neoproterozoic igneous rift-related source for Assemblage 2. Currently the only known occurrence of igneous rocks crystallized between ~ 660-640 Ma are a suite of 665-651 Ma alkalic felsic plutons in central Idaho and the 650-640 Ma Pool Creek syenite in the Yukon Territory. If detrital zircons were sourced from the Pool Creek syenite to the north, the absence of 2.4-2.0 Ga zircons and lack of north to south paleocurrent indicators is problematic. More likely the 655 Ma age population was sourced from the south-east, for example from the alkalic plutonic suites in central Idaho, although the possibility of isolated intrusive units related to late-stage rifting in the SCC or even more local anorogenic magmatism cannot be ruled out.

Like Assemblage 1, detrital zircons in Assemblage 3 exhibit the characteristic bimodal age distribution, namely 3.0 to 2.5 Ga and 1.9-1.8 Ga, suggesting derivation from adjacent Precambrian basement domains in the subsurface of western Canada. In the provenance discrimination diagram, samples from Assemblage 3 plot mostly in the felsic igneous provenance field, but stratigraphically upward trend towards a more intermediate/mafic igneous composition reflecting the upward increase in MgO, Fe_2O_3 and TiO_2. Assemblage 3 is interpreted to mark the end of the input of juvenile ca. 655 Ma sources, and a return to the characteristic bimodal detrital zircon Laurentian signature.

Acknowledgements

This thesis would not have been possible without the help of many individuals along the way, to whom I am grateful. First and foremost, I would like to thank my supervisor, Dr. Bill Arnott. Thank you for providing me with the opportunity to work on this unique project. Although this project started out with one specific goal, it ended up unexpectedly going in a completely different direction. Thank you for allowing me the independence to explore new ideas, while always providing meaningful guidance and support, and pushing me to ensure no stone was left unturned.

I would like to thank Dr. Clement Bataille and Dr. Lyle Nelson for serving on my defense committee. Your insight and feedback on this thesis were invaluable, and greatly improved the final work.

Thank you to the lab members who were involved in the geochemistry analyses used in this thesis. Thank you to Smita Mohanty and Nimal De Silva of the Geochemistry Lab for teaching me how to perform sample digestions, for your meticulous work with the ICP-MS to ensure all measurements were precise, and for your insight regarding data interpretation. Thank you to Shuangquan Zhang at the Carleton University Isotope Geochemistry and Geochronology Research Centre for allowing me to use the lab space, and for your assistance in measuring Sr and Nd isotopes. Additionally, thank you to Martina Boddy for helping to prepare my samples for isotopic analysis. Thank you to Lilianne Dagenais and Jeffrey Ovens for your work in the X-Ray Core Facility completing XRF analyses for our many mudrock samples. Thank you to Will Matthews at the University of Calgary for your effort measuring and analysing U-Pb geochronology data for our samples, and for your helpful feedback.

Thank you to Celeste Cunningham for helping me in my first field season at Castle Creek, and for your continued support throughout my time at uOttawa. Your incredible knowledge and experience in sedimentology helped me to learn quickly in the field and beyond! Additionally, thank you to all other past and present Windy members: Jag, Omar, Simona, Rae, Patty and Mike. Your feedback during weekly meetings was invaluable, and I always came out of them with something new in hand. I also thank my fellow graduate students at uOttawa, family and friends for your continued support.

Finally, I would like to thank the Windermere Consortium partners OXY Petroleum, Husky Energy, Cenovus Energy, and the NSERC Discovery Grant, for continued and generous financial support. Thank you to the University of Ottawa, as well as the Husky Energy Graduate Scholarship, and the NSERC Graduate Scholarship, for providing scholarships and funding that supported the completion of this project.

Table of Contents

Abstract ii

Résumé iii

Extended Abstract iv

Acknowledgements vii

List of Figures xi

List of Tables xv

List of Abbreviations xvi

Chapter 1: Introduction 1

1.1 Thesis Rationale 1

1.2 Regional Geology of the Windermere Supergroup 3

1.2.1 Windermere Supergroup Location and Overview 3

1.2.2 Tectonic History 5

1.2.3 Regional Stratigraphy 9

1.2.4 Castle Creek Study Area 14

1.3 Sedimentary Rock Geochemistry 17

1.3.1 The geochemical evolution of the continental crust 17

1.3.3 Application of Isotope Systematics to Provenance Studies 28

1.4 Tectonic subdivisions of western Laurentia 35

1.5 Previous Geochemical Work in Proterozoic Passive Margin Western Laurentia Sediments 43

Chapter 2: Methodology 45

2.1 Detrital Zircon Geochronology 45

2.2 Sample Collection and Preparation 45

2.3 Whole Rock Geochemistry 46

2.4 Trace Element Geochemistry 46

2.5 Isotopic Analysis 47

Chapter 3: Results 50

3.1 Detrital-Zircon U-Pb Type Populations 50

3.1.1 Type 1 Detrital Zircon Signature 51

3.1.2 Type 2 Detrital Zircon Signature 51

3.1.3 Anomalous detrital zircon populations in ICC4B 54

3.2 Major Element Geochemistry 56

3.3 Trace Element Geochemistry 60

3.3.1 Large-ion lithophile elements (LILE, Rb, Cs, Ba, Sr), Th and U 61

3.3.2 High field strength elements (HFSE, Zr, Hf, Y, Nb and Ta) 62

3.3.3 Transition trace elements (TTE, Cr, V, Co, Ni and Sc) 63

3.3.4 Rare earth elements (REE) 64

3.4 Isotope Geochemistry 69

Chapter 4: Discussion 77

4.1 Source rock composition 77

4.1.1 Weathering 77
4.1.2 Major Element Discriminant Function 81
4.1.3 Tectonic Setting Discrimination 84
4.1.4 Th/Sc, Th/U, and Zr/Sc Ratios (Sediment Sorting and Recycling) 86
4.1.5 Transition Metals (Derivation from Ultramafic/Mafic Sources) 87
4.1.6 Rare Earth Elements 89

4.2 Comparison to Isotope Data 91

4.3 Provenance and tectonic setting discriminations 95

4.3.1 Assemblage 1: UKG, LIF, ICC1 96
4.3.2 Assemblage 2 (ICC3, ICC4, ICC5) 102
4.3.3 Assemblage 3 (ICC6 to base of Cunningham) 107
4.3.4 Anomalous Signatures within Assemblage 2 109

4.4 Sediment routing patterns in the Neoproterozoic Windermere Supergroup, southern Canadian Cordillera 113

Chapter 5: Summary and Future Work 120

5.1 Contributions 120

5.2 Future Work 125

References 127

List of Figures

Figure 1.1. A) Distribution of the Windermere Supergroup and correlative units exposed in western North America. Black rectangle indicates the southern Canadian Cordillera where deep-marine strata of the Windermere turbidite system crop out. B) Simplified geological map of Mesoproterozoic-Early Paleozoic rocks in the Cariboo Mountains of the southern Canadian Cordillera. Neoproterozoic-Paleozoic rocks discussed in the thesis are located in the Foreland Fold and Thrust and Omineca tectonic belts. Geological dataset obtained from Canada Open Government portal and BC Geological Survey Digital Geology. 4
Figure 1.2. Distribution of Precambrian tectonic elements within the North American craton (modified from Box et al., 2020). BH, Buffalo Head; CB, Cumberland batholith; FS, Fort Simpson magmatic arc; GB, Great Bear magmatic arc; GF, Great Fall tectonic zone; H, Hottah terrane; STZ, Snowbird tectonic zone; W, Wopmay orogen....6
Figure 1.3. Global paleogeographic reconstruction by Li et al. (2013) showing a model for the pattern of continent dispersal at three periods during the Neoproterozoic. 8
Figure 1.4. Regional stratigraphy of the Windermere Supergroup in the Southern Canadian Cordillera (modified from Ross & Arnott, 2007). Geochronological dates from Ross et al. (1995), Lund et al. (2003), Kendall et al. (2004) and Colpron et al. (2002). 10
Figure 1.5. Stratigraphic nomenclature of Neoproterozoic strata in the Rocky and Cariboo mountains (from McMechan et al., 2015). 12
Figure 1.6. Schematic cross-section of western North America ca. ~ 600 Ma. In the western United States strata of the WSG consist of shelf deposits, shelf-edge and upper slope facies in Mackenzie Mountains, and deep-marine base-of-slope and basin floor deposits in the southern Canadian Cordillera. 14
Figure 1.7. Composite stratigraphic column for the Castle Creek study area, showing the general stratigraphic levels (from Ross and Arnott, 2007) 15
Figure 1.8. Plot of ionic radius versus ionic charge for incompatible trace elements of geological interest. Major elements (in red) indicate where trace element ionic substitutions will most readily occur. An ionic potential (charge to size ratio) of 0.02 subdivides the incompatible elements into low field strength (LFS) elements (also known as large ion lithophile elements, LILE) and high field strength elements (HFSE) (Rollinson and Pease, 2021, from Shannon, 1976) 18
Figure 1.9. Values of the K_2O/Al_2O_3 ratio for K-feldspars and clay minerals. Crosses represent values for the specific minerals indicated (from Cox et al., 1995, after Deer et al., 1966) 22
Figure 1.10. Goldschmidt's classification of the elements (from White, 2013). 25
Figure 1.11. Plots of REE concentration. (a) REE concentrations in ppm for selected CI chondrites plotted against atomic number. REE with even atomic numbers have higher concentrations than those with odd atomic numbers. These values are used to normalise rock REE concentrations. (b) an example of a chondrite normalised plot showing the REE plotted by atomic number of the x-axis and CI chondrite normalised concentrations plotted on a log scale y-axis (from Rollinson and Pease, 2021). 27
Figure 1.12. Schematic map of the Cordilleran miogeocline, showing basement domains of the western Canadian Shield, modified from Gehrels and Ross (1998). Ages are based on U-

Pb dates. Except for limited regions in the Great Bear, Trans-Hudson, and Rimbey domains, all basement of western Canada has Archean Nd signature. 35
Figure 3.1. Example of cathodoluminescence (CL) images of zircons. The solid circles represent U-Pb analysis pits. U-Pb spot ages given here and elsewhere are $^{206}Pb/^{238}U$ ages for zircon components younger than 1.0 Ga and $^{207}Pb/^{206}Pb$ ages for those older than 1.0 Ga. 50
Figure 3.2. Tera-Wasserburg diagrams (left side) show U-Pb data for the middle Kaza Group, upper Kaza Group, and ICC1 (Type 1 signature). Each ellipse represents a single spot analysis and its 2σ standard error. Kernel density estimation (KDE) diagrams (right side) show distribution of ages. 52
Figure 3.3. Tera-Wasserburg diagrams (left side) show U-Pb data for ICC3, ICC4, and ICC5 (Type 2 signature). Each ellipse represents a single spot analysis and its 2σ standard error. Kernel density estimation (KDE) diagrams (right side) show distribution of ages. 54
Figure 3.4. Tera-Wasserburg diagrams (left side) show U-Pb data for anomalous signatures in strata of ICC4B. Each ellipse represents a single spot analysis and its 2σ standard error. Kernel density estimation (KDE) diagrams (right side) show distribution of ages. 55
Figure 3.5. Major elemental oxides normalized to PAAS values for average shale, for: a) UKG to ICC1; b) ICC2; c) ICC3 to ICC5; d) ICC6 and above. 56
Figure 3.6. Distribution of samples for Al_2O_3 vs. other major oxides: a) K_2O, b) TiO2, c) MgO. Left side of page displays data by individual units; right side of page displays data as units categorized by similar characteristics into four separate groups. 58
Figure 3.7. Distribution of samples for sum of major oxides Fe_2O_3 + MgO vs. ratios of other major oxies: a) Al_2O_3/SiO_2; B) K_2O/Na_2O. Left side of page displays data by individual units; right side of page displays data as units categorized by similar characteristics into four separate groups. 59
Figure 3.8. Distribution patterns of selected trace elements normalized by Post-Archean Average Shale (PAAS), for: a) UKG to ICC1; b) ICC2; c) ICC3 to ICC5. 60
Figure 3.9. Stratigraphic trends for LILE, from UKG to ICC6. 62
Figure 3.10. Stratigraphic trends for HFSE, from UKG to ICC6. 63
Figure 3.11. Stratigraphic trends for transition trace elements, from UKG to ICC6. 64
Figure 3.12. Chondrite-normalized REEs patterns for mudstone samples. The chondrite values are from (Boynton, 1984). 65
Figure 3.13. Stratigraphic trends for various ratios of REEs, from UKG to ICC6. 67
Figure 3.14. Provenance ages against stratigraphic position of Windermere Supergroup strata at Castle Creek. 71
Figure 3.15. $^{147}Sm/^{144}Nd$ vs. εNd (0) plot for the Castle Creek samples 75
Figure 3.16. Plots of $^{87}Sr/^{86}Sr$ (0) and εNd (0) versus (a) SiO_2, (b) K_2O, (c) Fe_2O_3 + MgO for samples from the UKG and IF. 76
Figure 4.1. Major element ternary diagrams showing the weathering control on the composition of the Windermere supergroup siliciclastic samples. Various unweathered igneous rocks are represented by hollow squares, and unweathered rock-forming minerals are represented by black circles. Reference values of source rocks from McLennan et al., (1993) after Nesbitt and Young (1984, 1989). Arrows indicate weathering trends for different source rocks. The solid line separates the non-weathered and the weathered fields. a) Al_2O_3–$CaO+Na_2O$–K_2O (A-CN-K) diagram; also a measure of CIA. (1) represents the weathering trend of UCC; (2) represents effects of K metasomatism. B)

Al_2O_3+K_2O–CaO–Na_2O (A-C-N) diagram; also a measure of PIA. c) Al_2O_3 – Fe_2O_3+MgO–CaO+Na_2O+K_2O diagram. The samples indicate a trend that is interpreted as a variation of the composition of the source rocks. 78
Figure 4.2. Two indicators of weathering, Chemical Index of Alteration (CIA) and Index of Chemical Variation (ICV) in samples from Castle Creek (reference data from Lee 2002). The grey area represents the range of CIA values of Neoproterozoic shale. 81
Figure 4.3. Two discriminant function diagrams for the provenance signatures of Castle Creek samples using major elements (after Roser and Korsch, 1988), using: a) oxide/Al_2O_3 ratios. Discriminant Function 3 = (30.638 TiO_2/Al_2O_3) + (-12.541 Fe_2O_3/Al_2O_3) + (7.329 MgO/Al_2O_3) + (12.031 Na_2O/Al_2O_3) + (35.402 K_2O/Al_2O_3) – 6.382. Discriminant Function 4 = (56.500 TiO_2/Al_2O_3) + (-10.879 Fe_2O_3/Al_2O_3) + (30.875 MgO/Al_2O_3) + (-5.404 Na_2O/Al_2O_3) + (11.112 K_2O/Al_2O_3) – 3.890. b) oxide abundances. Discriminant Function 1 = (-1.773TiO_2) + (0.607Al_2O_3) + (0.760Fe_2O_3) + (-1.500MgO) + (0.616CaO) + (0.509Na_2O) + (-1.224K_2O) + (-9.090); Discriminant Function 2 = (0.445TiO_2) + (0.070Al_2O_3) + (-0.250Fe_2O_3) + (-1.142MgO) + (0.438CaO) + (1.475Na_2O) + (-1.426K_2O) + (-6.861). 83
Figure 4.4. A) La/Th vs. Hf diagram (after Floyd and Leveridge, 1987). B) La-Th-Sc discrimination diagram differentiating ocean island arc (OIA), continental island arc (CIA), passive margin (PM), and active continental margin (ACM) (after Bhatia and Crook, 1986), d) Th/Sc discrimination diagram illustrating acidic to intermediate compositions for the studied samples. D) Discrimination diagram illustrating continental sedimentary provenance of the studied samples. E) Co/Th vs. La/Sc diagram (after McLennan et al., 1995).....85
Figure 4.5. a) Th/Sc vs. Zr/Sc discrimination diagram (after McLennan et al., 1993) illustrating compositional variations and sediment recycling of sediments in the shales and sandstones. B) Th vs. Th/U discrimination diagram illustrating moderate weathering and sediment recycling (after McLennan et al., 1993).....87
Figure 4.6. Cross-plot of: a) Y/Ni vs Cr/V; b) Cr/Th vs Th/Sc.....88
Figure 4.7. Cross-plot of $^{87}Sr/^{86}Sr$ vs. eNd(0), showing distribution of samples in Assemblage 1 and Assemblage 2.....91
Figure 4.8. ε_{Nd} vs $^{147}Sm/^{144}Nd$ diagram. Also shown are western Laurentia basement source terranes. Red circles indicate Assemblage 1 samples; green circles indicate Assemblage 2 samples. Black diamonds represent literature values for correlative units from the Horsethief Creek Formation (Boghossian et al., 1996). Isotopic data for Laurentian basement rocks taken from Canadian Geochronology Knowledgebase (https://atlas.gc.ca/geochron/en/). Also shown are potential felsic and mafic igneous sources approximated from similar igneous sources with crystallization ages ca. 700-650 Ma.....92
Figure 4.9. Composite kernel density estimation for all U-Pb zircon data for Assemblage 1 UKG, LIF, ICC1. Dates are $^{206}Pb/^{238}U$ for dates <1500 Ma, and $^{207}Pb/^{206}Pb$ for dates >1500 Ma. Samples with <1% probability of concordance were filtered from the data set. N is the number of samples; n is the number of measurements. Coloured regions correspond to major crystalline provenances of the Laurentian craton. Significant proximal sources are noted on the diagram with age ranges. 97

Figure 4.10. Bivariate plots for the interval between the UKG and ICC1 (Assemblage 1): a) Discriminant function diagram based on normalized major element oxides b) Bivariate Th versus Sc diagram. 98
Figure 4.11. Composite kernel density estimation for all U-Pb zircon data for Assemblage 2 ICC3 to ICC5. Dates are $^{206}Pb/^{238}U$ for dates <1500 Ma, and $^{207}Pb/^{206}Pb$ for dates >1500 Ma. Samples with <1% probability of concordance were filtered from the data set. N is the number of samples; n is the number of measurements. Coloured regions correspond to major crystalline provenances of the Laurentian craton. Significant proximal sources are noted on the diagram with age ranges. 103
Figure 4.12. Bivariate plots for Assemblage 2 (ICC3, ICC4, ICC5): a) discriminant function diagram; b) Th/Sc diagram. 105
Figure 4.13. Composite kernel density estimation for all U-Pb zircon data for Assemblage 3 ICC6 to the base of the Cunningham Fm. Dates are $^{206}Pb/^{238}U$ for dates <1500 Ma, and $^{207}Pb/^{206}Pb$ for dates >1500 Ma. Samples with <1% probability of concordance were filtered from the data set. N is the number of samples; n is the number of measurements. Coloured regions correspond to major crystalline provenances of the Laurentian craton. Significant proximal sources are noted on the diagram with age ranges. 107
Figure 4.14. Bivariate plots for Assemblage 3 (ICC6 and above) showing discriminant functions. 108
Figure 4.15. Location of ICC4B within the Isaac Formation at the Castle Creek study area. Yellow star marks the stratigraphic location of the anomalous samples....110
Figure 4.16. Composite kernel density estimation for all U-Pb zircon data for the anomalous samples of ICC4B, with <1% probability of concordance were filtered from the data set. N is the number of samples; n is the number of measurements. Coloured regions correspond to major crystalline provenances of the Laurentian craton. Significant proximal sources are noted on the diagram with age ranges. 111
Figure 4.17. Summary of provenance proxies for assemblages 1, 2 and 3, showing major and trace element ratios: a) discriminant function; b) Cr/Nb, c) Zr/Sc, d) Eu/Eu*. Also shown are compiled detrital zircon U-Pb data for each assemblage, showing most common age populations. 113
Figure 4.18. Map of basement terranes (exposed and subsurface) in western Laurentia. Black shaded area represents Windermere Supergroup deposits; red star is the location of the Castle Creek study area. Geological data from Open Government Canada, BC Geological Survey Digital Geology, Government of Alberta Open Data, USGS Open Data Bedrock Geology maps. 114
Figure 4.19. Hypothetical sediment catchment and drainage pathways based on detrital zircon signatures superimposed on sub-Paleozoic subcrop map. Darker tinted areas represent non-sourced areas; lighter areas represent the potential regional drainage basin. Black solid and dotted arrows represent most likely and less likely sediment source pathways, respectively. 115
Figure 4.20. Hypothetical sediment catchment and drainage pathways for anomalous ICC4B sample based on detrital zircon signatures superimposed on sub-Paleozoic subcrop map. Highlighted area indicates the probable sediment catchment and the solid black arrow the most likely drainage pathway. 118

List of Tables

Table 3.1. Nd isotopic data of sedimentary rocks from the Neoproterozoic Windermere Supergroup. 70
Table 3.2. Sr isotopic data from Windermere mudrocks at the Castle Creek study area. 73
Table 4.1. Turbidite provenance associations showing averages for selected geochemical proxies 99

List of Abbreviations

Abbreviation	Definition
2σ	Two standard deviations of the mean
B.C.	British Columbia
CC	Castle Creek Study Area
CHUR	Chondritic uniform reservoir
CIA	Chemical index of alteration
FIC	First Isaac Carbonate
HFSE	High field strength element
ICC	Isaac Channel Complex
ICC0	Isaac Channel Complex 0
ICC1	Isaac Channel Complex 1
ICC2	Isaac Channel Complex 2
ICC3	Isaac Channel Complex 3
ICC4	Isaac Channel Complex 4
ICC4B	Isaac Channel Complex 4B
ICC5	Isaac Channel Complex 5
ICC6	Isaac Channel Complex 6
ICV	Index of compositional variation
LA-ICP-MS	Laser ablation inductively coupled plasma mass spectrometry
LILE	Large ion lithophile elements
Ma	Mega annum (million years ago)
MC-ICP-MS	Multi collector inductively coupled plasma mass spectrometry
Moho	Mohorovičić discontinuity
OFP	Old Fort Point
PAAS	Post-Archean average shale
REE	Rare earth elements
T_{DM}	Depleted mantle crustal residence age
UCC	Upper continental crust
UKG	Upper Kaza Group
WSG	Windermere Supergroup

Chapter 1: Introduction

1.1 Thesis Rationale

Events surrounding the origin of the passive margin forming the western edge of Laurentia (ancestral North America) are an important constraint on the breakup of the Rodinia supercontinent and set the stage for the Phanerozoic tectonic evolution of western Laurentia. One of the prime areas to study this history is the Neoproterozoic Windermere Supergroup (WSG) in the southern Canadian Cordillera. The WSG is a 7–9 km-thick continental rift-to-drift succession of mostly siliciclastic deep-marine strata associated with the breakup of Rodinia and later development of a passive continental margin and deposition. This study presents a variety of geochemical datasets from a 2.5 km-thick succession of basin-floor to base-of-slope deposits exposed in the Castle Creek study area in east-central British Columbia in order to understand changes in provenance within these strata and better constrain the regional tectonic history.

Recent detrital zircon geochronology of deep-water WSG strata across the southern Canadian Cordillera showed a consistent bimodal distribution of Paleoproterozoic (~1.8 Ga) and Archean (> 2.5 Ga) U-Pb dates, suggesting a long-standing and stable continental drainage system with an eastward-lying cratonic sediment source (Hadlari et al., 2021). However, one sample from continental slope channel deposits at the Castle Creek study area (termed ICC4B) displayed anomalous age probabilities between 2.4-2.0 Ga, suggesting a major but only temporary change in sediment provenance. However, no associated changes in sedimentological or stratigraphic details were noted. To investigate this marked change in provenance, strontium (Sr) and neodymium (Nd) isotope values, in association with elemental compositions (i.e. REE, Zr, Sc) were measured. Since sandstones provide limited information on provenance beyond the dating

of detrital zircons, we chose to investigate this change in mudstones of fine-grained levees that bound channel ICC4B. Mudstones are useful for studying sediment provenance due to their impermeable nature and consequent retention of most the mineral constituents inherited from the sediment source rock.

The principal objective of this thesis is to document the geochemical changes in proximity to ICC4B and therein elucidate changes on the pattern of regional sediment supply. However, early in the project it became clear that the unusual nature of the ICC4B sample was isolated to a single observation, which then led to a secondary objective to study the broad-scale provenance trends through the entire transect of basin floor to continental slope strata exposed at Castle Creek. Samples were collected with ~ 10 m vertical sample spacing over a 2000 m-thick stratigraphic succession. This novel dataset was then combined with compiled detrital zircon data to provide a highly resolved understanding of temporal changes in sediment provenance and sediment supply during deposition of the Neoproterozoic Windermere turbidite system and development of the northwestern Laurentian continent margin in the southern Canadian Cordillera.

1.2 Regional Geology of the Windermere Supergroup

1.2.1 Windermere Supergroup Location and Overview

The Windermere Supergroup (WSG), along with the unconformably underlying Belt-Purcell Supergroup, is the most extensively exposed late Proterozoic sedimentary sequence in the Canadian Cordillera (Young et al., 1973). First termed the "Windermere System" by Walker (1926) to classify poorly sorted pebble conglomerate, feldspathic grit and phyllite of the Toby Conglomerate and Horsethief Creek Formation in the Windermere valley of southeastern British Columbia (B.C.), it now encompasses a succession of Neoproterozoic rocks exposed locally across the western North American Cordillera, stretching from northern Mexico northward to the Yukon-Alaska border (Figure 1.1.A) (Ross and Arnott, 2007; Walker, 1926; Young et al., 1973). In the southern Canadian Cordillera, the WSG, therefore, encompasses all rocks that occur between the Mesoproterozoic Purcell Supergroup, and the early Cambrian Gog and Hamill groups, or other age-correlative units (Young et al., 1973).

Neoproterozoic-strata of the WSG record the rift and subsequent drift of the supercontinent Rodinia during the Cryogenian, which led to the formation of the western Laurentian passive margin and opening of the proto-Pacific passive margin (Link, 1993; Ross, 1991; Young et al., 1973; Young, 1984). The sedimentological characteristics of the WSG vary dramatically at the regional scale, reflecting the temporal and spatial changes in depositional facies along the incipient western margin of Laurentia. In northern Mexico and the western United States, the WSG comprises siliciclastic continental and shallow marine strata (Link, 1993; Stewart, 2005; Stewart et al., 1999). In the southern Canadian Cordillera, particularly in the Cariboo Mountains, rocks of the WSG are well exposed, with outcrops principally in the Foreland Fold and Thrust and Omineca belts (Figure 1.1.B) (Murphy, 1987; Price, 1981). Here,

the WSG is dominated by deep-marine, turbiditic clastic rocks but also includes shallow-water carbonate, local diamictites, and rare volcanic rocks (McMechan, 2015; Ross and Arnott, 2007). In the northern Canadian Cordillera, specifically the Mackenzie Mountains, the WSG is 5 – 7 km thick and comprises carbonate-rich shallow-marine and upper continental slope strata (Jefferson and Parrish, 1988; Narbonne and Aitken, 1995).

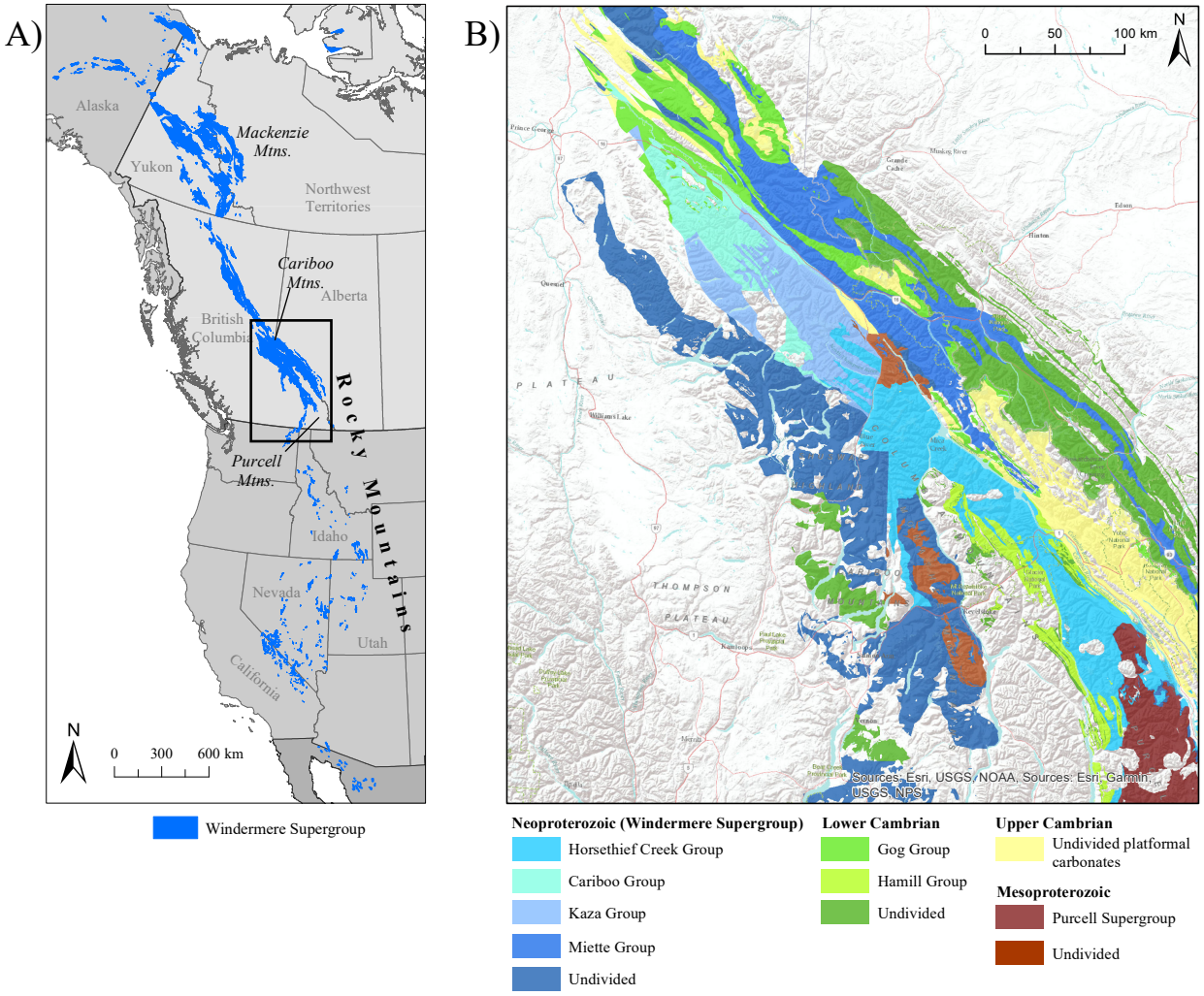

Figure 1.1. A) Distribution of the Windermere Supergroup and correlative units exposed in western North America. Black rectangle indicates the southern Canadian Cordillera where deep-marine strata of the Windermere turbidite system crop out. B) Simplified geological map of Mesoproterozoic-Early Paleozoic rocks in the Cariboo Mountains of the southern Canadian Cordillera. Neoproterozoic-Paleozoic rocks discussed in the thesis crop out in the Foreland Fold and Thrust and Omineca tectonic belts. Geological dataset obtained from Canada Open Government portal and BC Geological Survey Digital Geology.

1.2.2 Tectonic History

The setting of the Windermere Supergroup (WSG) in the context of Neoproterozoic Laurentia necessitates an understanding of long-term behaviour of continental crust and mantle formation and modification. The North American craton, named Laurentia, consists of the Precambrian basement terranes of Canada which extend to Greenland and the United States, interior platform and basin sedimentary rocks, and the reactivated Cordilleran foreland basin of western North America (Hoffman, 1988). The North American craton was formed in the Paleoproterozoic (2.0-1.8 Ga) by a series of plate collisions between large Archean provinces (i.e. Slave, Rae-Hearne, Superior) and smaller continental fragments (i.e. Wyoming, Medicine Hat, Sask, Marshfield, Nain), resulting in closure of expansive oceans (Hoffman, 1988; Whitmeyer and Karlstrom, 2007). The Precambrian evolution of the northern North American continent comprises six main events: 1) assembly of Archean provinces 2.4-2.0 Ga; 2) Thelon Orogen 2.02-1.91 Ga; 3) Wopmay Orogen 1.95-1.84 Ga; 4) Hearne/Rae collision 1.85-1.75 Ga; 5) Wyoming/Hearne collision ~1.9 Ga; 6) Trans-Hudson Orogen: Hearne-Wyoming/Superior collision 1.9-1.8 Ga. The southern part of the North American continent, which includes much of the continental United States, was assembled later, between 1.8-1.0 Ga, by accretion of a series of juvenile volcanic arcs and ocean terranes to the southern margin of Laurentia (Whitmeyer and Karlstrom, 2007). Accretionary provinces include the Yavapai province (1.80-1.70 Ga), the Mazatzal province (1.70-1.65 Ga), the Granite-Rhyolite province (1.50-1.30 Ga), and the Llano-Grenville province (1.30-1.00 Ga) (Whitmeyer and Karlstrom, 2007). The main tectonic elements of Laurentia are broadly subdivided into Archean and Proterozoic provinces (Figure 1.2.). The Archean provinces consist of the Slave, Rae, Hearne, Wyoming, Superior, and Nain, and most of the Canadian Shield. Each of these provinces consists of a granite-greenstone

Archean basement complex overlain by recycled products of Early Proterozoic platformal sedimentary rocks (Hoffman, 1988). Early Proterozoic reactivation of orogenic belts resulted in varying levels of deformation and metamorphism in the provinces (Hoffman, 1988). During the Neoproterozoic (1000 – 544 Ma), Laurentia, as well as most of the other continental landmasses,

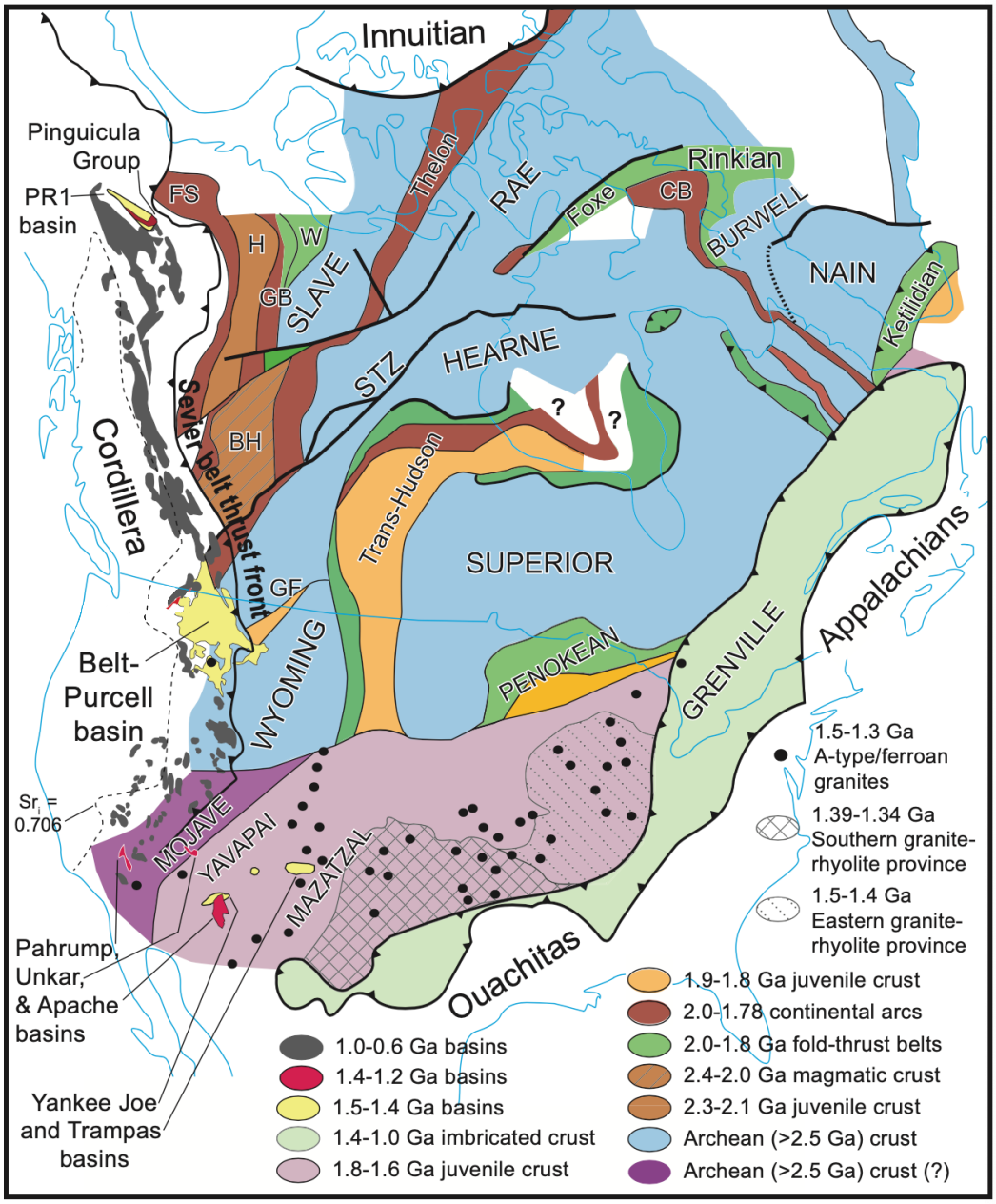

Figure 1.2. Distribution of Precambrian tectonic elements within the North American craton (modified from Box et al., 2020). BH, Buffalo Head; CB, Cumberland batholith; FS, Fort Simpson magmatic arc; GB, Great Bear magmatic arc; GF, Great Fall tectonic zone; H, Hottah terrane; STZ, Snowbird tectonic zone; W, Wopmay orogen.

were part of the supercontinent Rodinia, which was centered at equatorial latitudes for most of its history, but may have temporarily extended to polar regions (Hoffman, 1988; Li et al., 2013). In addition to major tectonic change and continent rearrangement, the Neoproterozoic saw major global climatic changes, including global-scale glaciations, and changes in marine chemistry and biology that eventually culminated in the appearance of the first evidence of complex life on Earth during the Ediacaran (635-541 Ma). Between 780 and 680 Ma, rifting began along the western margin of Laurentia, followed by the main pulse of rifting along the western margin of Laurentia between 680 and 580 Ma (Figure 1.3) (Li et al., 2013; Whitmeyer and Karlstrom, 2007; Young, 1984). This resulted in formation of an extensive passive continental margin marking the expansion of the paleo-Pacific Ocean (Panthalassa) (Devlin and Bond, 1988; Devlin et al., 1985). The Windermere Supergroup records the syn-rift to passive margin sequences associated with the breakup of Rodinia, including the progradation of the passive margin of Laurentia into the proto-Pacific ocean basin (Bond and Kominz, 1984; Ross et al., 1995; Stewart, 1972)

Later, a second rift beginning at ~550 Ma and associated subsidence occurred followed by mostly shallow-marine carbonate sedimentation (Bond and Kominz, 1984; Ross, 1991; Ross et al., 1995). In the late Paleozoic, the western passive margin of Laurentia became a tectonically-active continental arc system, where accretion of allochthonous terranes formed the North American Cordillera (Price, 1981). The Canadian Cordillera is subdivided into five morphogeological belts: the Insular Belt; Coast Belt; Intermontane Belt, Omineca Belt; and Foreland Fold and Thrust Belt. Each of these belts are distinguished by unique deformational styles and metamorphic grades. As a result of deformation associated with the Mesozoic Cordilleran Orogeny, rocks of the WSG have experienced varying grades of metamorphism,

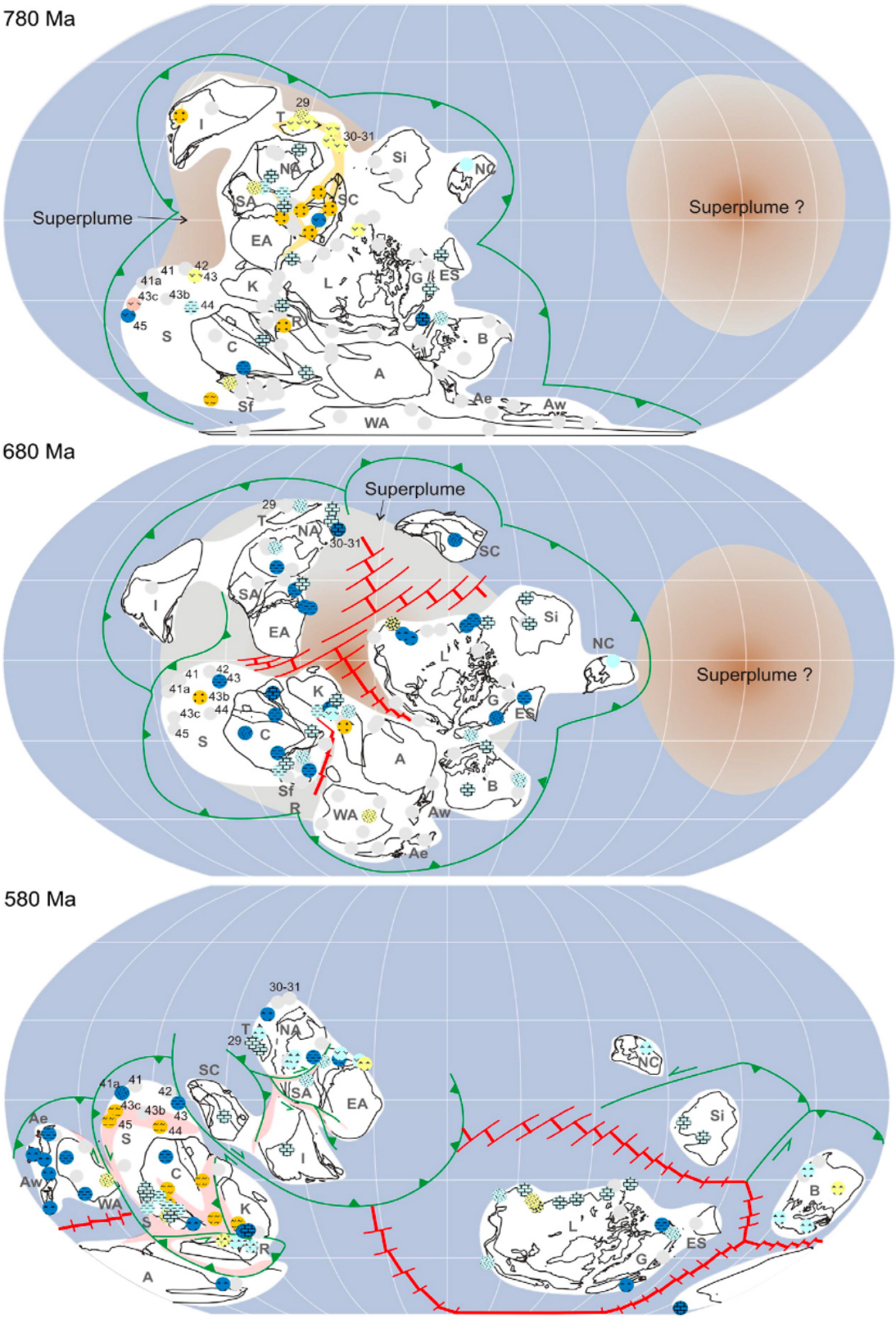

Figure 1.3. Global paleogeographic reconstruction by Li et al. (2013) showing a model for the pattern of continent dispersal at three periods during the Neoproterozoic.

which has also changed its overall thickness (Murphy, 1987). For example, in the southern Canadian Cordillera, metamorphic grade ranges from sub-greenschist in the northern Cariboo Mountains to upper amphibolite in the southern Cariboo and western Purcell Mountains (Crowley, 1999; Murphy, 1987).

1.2.3 Regional Stratigraphy

Preceding the Windermere Supergroup, the Mesoproterozoic rock record of western North America consists primarily of metamorphic rocks formed during the creation of the supercontinent Columbia (1.7-1.3 Ma) and Rodinia (1.1-0.75 Ma) (Box et al., 2020). In the southern Canadian Cordillera, exposures of Precambrian crystalline basement rock are restricted to the Omineca Belt where these sequences make up the basement of Laurentia and record collisional tectonics (McDonough and Parrish, 1991). In the southern Canadian Cordillera, the WSG lies unconformably above Mesoproterozoic strata of the Belt-Purcell Supergroup (1.5-1.4 Ga), or Archean to Paleoproterozoic, highly metamorphosed crystalline basement that ranges in age from 2.2-1.7 Ga (Crowley, 1999; Ross and Arnott, 2007). Crystalline basement that underlies the WSG is exposed in two main regions and comprises the Malton and Monashee complexes, interpreted to have crystallized between 2.1-1.9 (Crowley, 1999; Murphy et al., 1991; Ross and Bowring, 1990). The WSG consists of two distinct tectonostratigraphic sequences: a syn-rift, and a post-rift sequence (Figure 1.4.). At the base of the WSG, the Toby and Irene formations are an up to 2.5 km-thick succession of intercalated conglomerate, glaciogenic diamictite and local mafic volcanic rocks (Aalto, 1971). The Toby Formation is thought to be a glaciomarine in nature, based on observations of striated clasts and dropstones, representing resedimented glacial deposits associated with the Sturtian glaciation (~720 – 660 Ma) (Aalto, 1971; Rooney et al., 2014). In the southern Canadian Cordillera, the Toby Formation

is conformably overlain by volcanic rocks of the Irene Formation, consisting of andesitic greenstone, tuff, breccia and volcanic conglomerate (Aalto, 1971). Correlative metavolcanic rocks in northeastern Washington (Huckleberry Formation), central Idaho (Gospel Peaks sequence) and northern British Columbia have been dated between 735-696 Ma, suggesting regional-scale glaciomarine deposition and volcanic activity associated with the breakup of Rodinia (Devlin et al., 1985; Devlin et al., 1988; Eyster et al., 2018; Fanning and Link, 2004; Lund et al., 2003). The tops of these lower rift assemblages are marked by siltstone or limestone

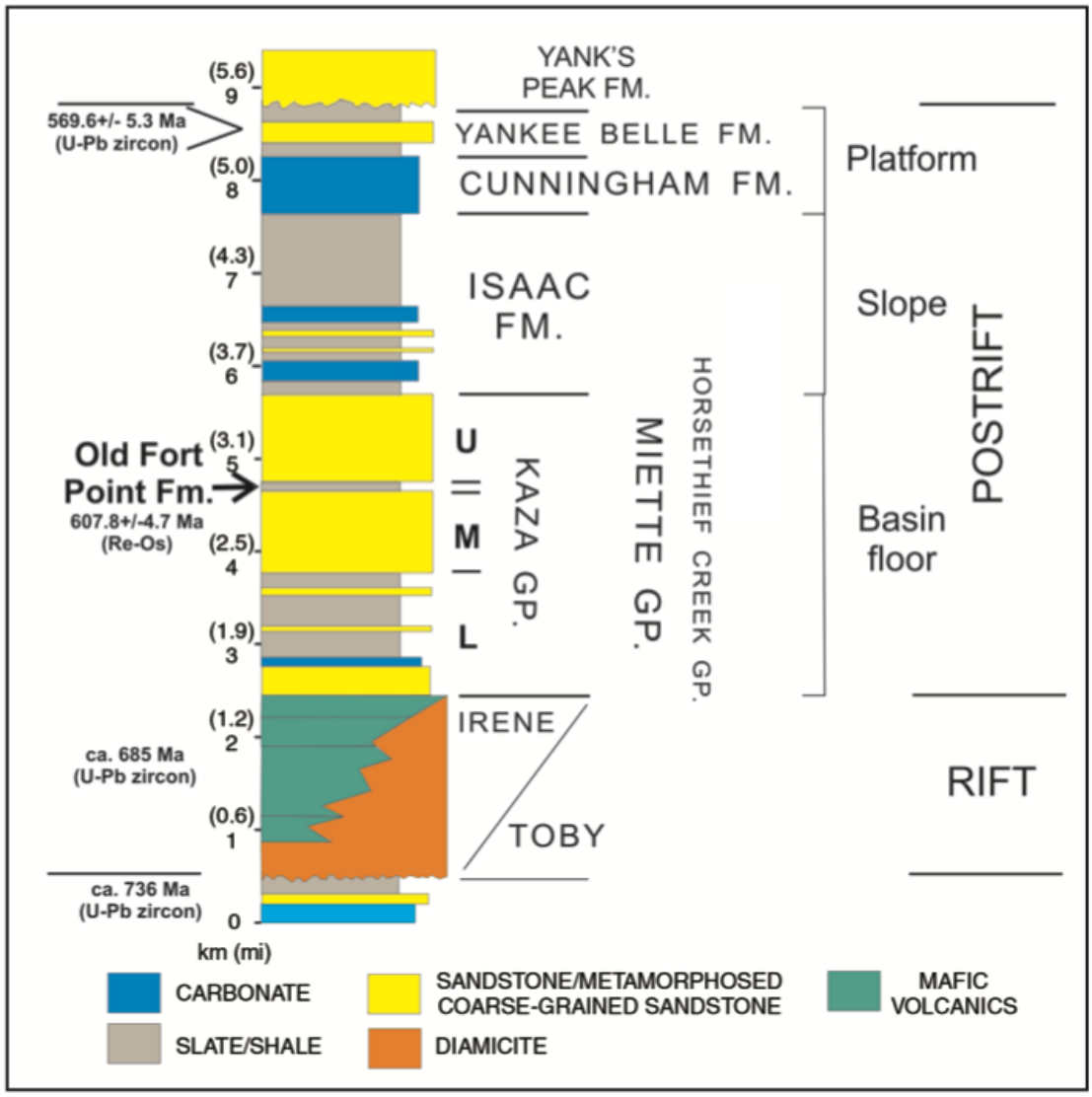

Figure 1.4. Regional stratigraphy of the Windermere Supergroup in the Southern Canadian Cordillera (modified from Ross & Arnott, 2007). Geochronological dates from Ross et al. (1995), Lund et al. (2003), Kendall et al. (2004) and Colpron et al. (2002).

laminites, passing upward into thick turbiditic successions, signifying deposition in a continental slope environment, and thus transformation to a post-rift to passive-margin succession (Eisbacher, 1985).

Rift-phase strata of the Toby and Irene formations are overlain by a 5 – 7 km-thick succession of basin floor to shelf strata, marking the initiation of post-rift deposition along the passive continental margin of Laurentia developed as a result of thermally-driven subsidence (Bond and Kominz, 1984). However, revisions to the geological timescale may suggest that subsidence took place in the mid-Cambrian, around 540 Ma, possibly conflicting with the subsidence-driven model (Dickinson, 2004; Dillard et al., 2007; Post and Long, 2008). Strata are dominated by coarse-grained sandstone turbidites intercalated with mudstone, minor carbonate and one diamictite (Vreeland Formation) (Ross and Arnott, 2007). In the Cariboo Mountains, these strata comprise the Kaza and Cariboo groups, and correlate with the Miette Group in the southern Rocky Mountains, the Misinchinka Group in the central to northern Rocky Mountains, and the Horsethief Creek Group in the Purcell Mountains (Figure 1.5.) (Smith et al., 2014).

Strata in the basal 2 – 4 km of the post-rift succession make up the Kaza Group in the east-central Cariboo Mountains, which consists of a lower part dominated by mudstone, and middle and upper parts dominated by sandstone (Murphy, 1987; Ross and Arnott, 2007). The lower Kaza Group consists of calc-schist, marble and meta-sandstone. Strata in the middle Kaza consist of metamorphosed sub-feldspathic sandstone interstratified with graphitic and non-graphitic phyllite (metamorphosed mudstone), and rare thin marble beds. The upper Kaza is marked by a notable increase in the sandstone to mudstone ratio (75:25) (Arnott, 2007; Murphy, 1987) and development of sheet-like stratal geometries interpreted to represent stacked depositional lobes formed in a weakly channelized environment on the basin floor (Terlaky et al.,

2014; Terlaky et al., 2015). Separating the middle and upper Kaza groups is the Old Fort Point Formation (OFP), a lithologically and geochemically distinct unit composed of thin-bedded siliciclastic and carbonate turbidites, local purple and green slates, and an up to 100 – 150 m-thick black shale unit (Ross and Murphy, 1988; Smith et al., 2014). The fine-grained nature of the OFP represents a significant local rise in sea-level that significantly reduced siliciclastic input to the system, resulting in development of anoxic conditions and primarily chemogenic sedimentation represented by limestone turbidites and organic-rich black shale (Ross and Murphy, 1988). The depositional age of the OFP is constrained by a precise Re-Os isochron age of 607.8 ± 4.7 Ma, providing a maximum depositional age for the overlying WSG (Kendall et al., 2004). In the central and northern Canadian Cordillera, diamictites of the Vreeland Formation underlie the OFP, but are absent in the southern Canadian Cordillera, changing facies laterally to deep-marine turbidites of the Kaza Group (Figure 1.5.) (McMechan, 2000;

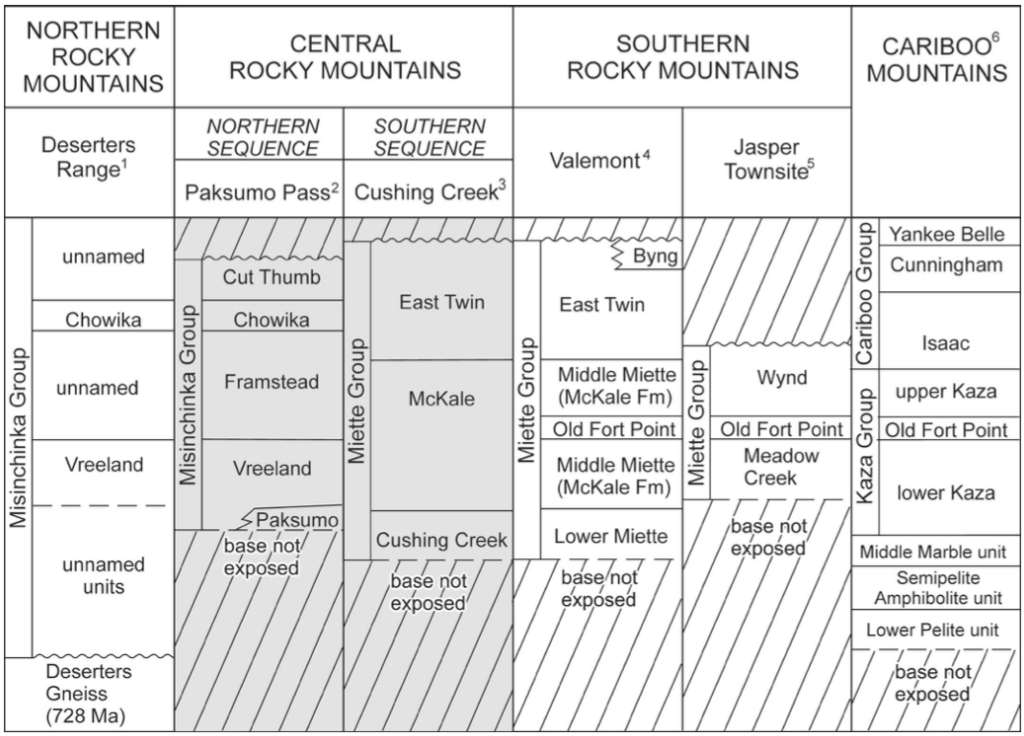

Figure 1.5. Stratigraphic nomenclature of Neoproterozoic strata in the Rocky and Cariboo mountains (from McMechan et al., 2015).

McMechan, 2015; Ross et al., 1995). The Vreeland Formation diamictites record high volumes of glaciogenic sediment transport from the shelf to the slope by unconfined debris flows, associated with the Marinoan glaciation (650-635 Ma) (Hoffman et al., 2017; Kendall et al., 2004; McMechan, 2000)

The upper Kaza Group is then overlain by the Cariboo Group, an up to 5 km-thick succession that is subdivided into the Isaac, Cunningham and Yankee Belle formations. The Isaac Formation consists primarily of fine-grained mudstones (sandstone:mudstone ratio of 25:75), interbedded with 20 – 200 m-thick, laterally discontinuous sandstone, and less common conglomerate units (Arnott, 2007). These units represent stacked leveed-channel complexes and complex sets formed in a slope to base-of-slope setting (Fraino et al., 2022). The presence of mass movement deposits, including slump, slide, and debrites, suggest greater gravitational instability compared to the underlying Kaza Group (Arnott, 2007; Ross et al., 1995).

The Cunningham and Yankee Belle formations conformably overlie the Isaac Formation, and represent upper continental slope and high-energy continental shelf deposits, respectively (Ross et al., 1995). The Cunningham Formation is dominated by limestone and dolostone with minor mudstone, siltstone and shale. Carbonates are bedded or massive, and consist of recrystallized micrite and non-skeletal arenite, including pisolites, oolites, pellets and intraclasts, whereas dolostone units are commonly sandy or silty (Campbell et al., 1973). The Yankee Belle Formation conformably overlies the Cunningham and is composed of three main facies. The basal unit consists of a coarse-grained sandstone (Zig-Zag Member), overlain by interbedded limestone, siltstone and shale, with an upper unit consisting mostly of shale and sandstone (Campbell et al., 1973). Above the Yankee Belle Formation is a regional unconformity that separates the WSG from Lower Cambrian Yank’s Peak Formation or its correlatives (lower Gog

Group of northern Rocky Mountains, Hamill Group in the Purcell Mountains) (Aitken, 1969). The unconformity is thought to be related to a second, younger rift event that preceded Cambro-Ordovician passive margin formation, and resulted in substantial uplift and erosional removal of coeval shallow-water facies in the eastern part of the basin (Ross et al., 1995).

Collectively, the Kaza and Cariboo groups form a several-km-thick, upward-shallowing succession of basin floor to continental shelf deposits (Figure 1.6.). These are interpreted to represent the westward progradation of the passive continental margin of Laurentia into the developing proto-Pacific ocean (Ross and Arnott, 2007; Ross et al., 1995).

1.2.4 Castle Creek Study Area

Strata of the upper Kaza and Isaac Formation are well exposed at the Castle Creek study area (CC) located in the northern Cariboo Mountains of east-central British Columbia. Here,

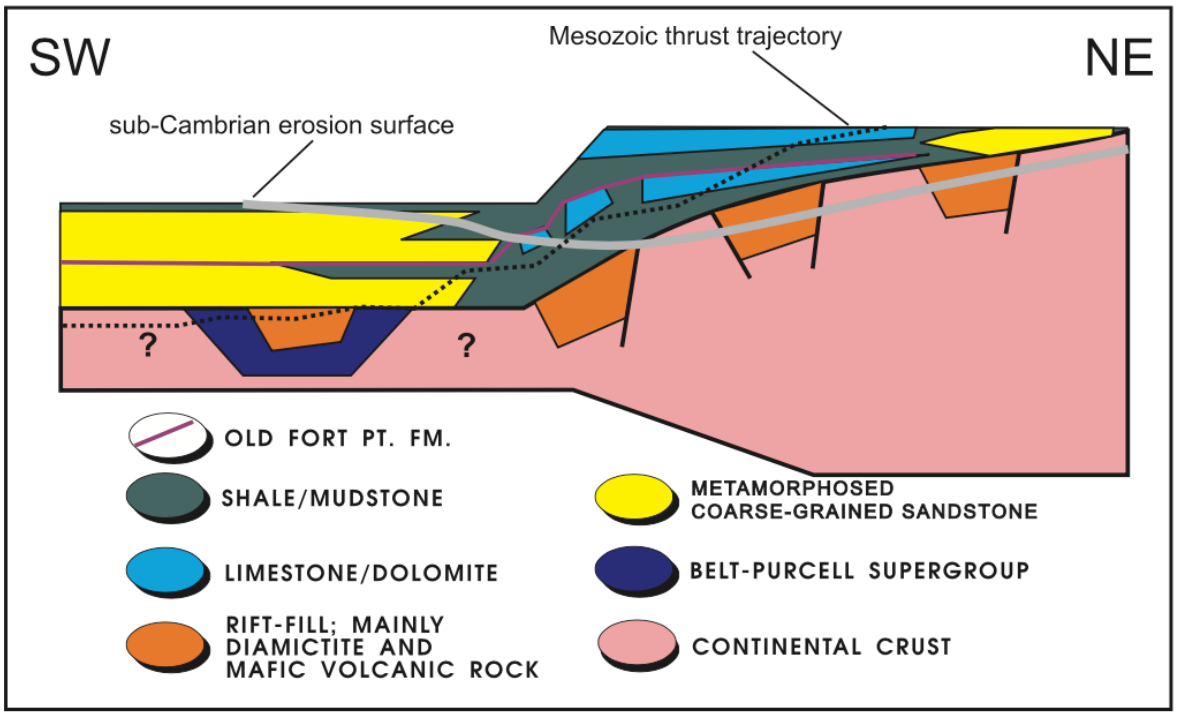

Figure 1.6. Schematic cross-section of western North America ca. ~ 600 Ma. In the western United States strata of the WSG consist of shelf deposits, shelf-edge and upper slope facies in Mackenzie Mountains, and deep-marine base-of-slope and basin floor deposits in the southern Canadian Cordillera.

strata are vertically-dipping and form an extensive exposure ~ 2.5 km-thick (perpendicular to bedding) and 7 km-wide (parallel to bedding) (Arnott, 2007). Recent deglaciation has removed surface vegetation and polished the rock surface, allowing for detailed sedimentological investigation of exposed strata.

Strata of the upper Kaza Group comprise the lower 800 m of outcrop at CC, and consist of decametre-thick, laterally continuous units of sheetlike to lobate coarse-grained sandstone to pebble conglomerate units interbedded with mud-rich, thin-bedded turbidites (Figure 1.7.)

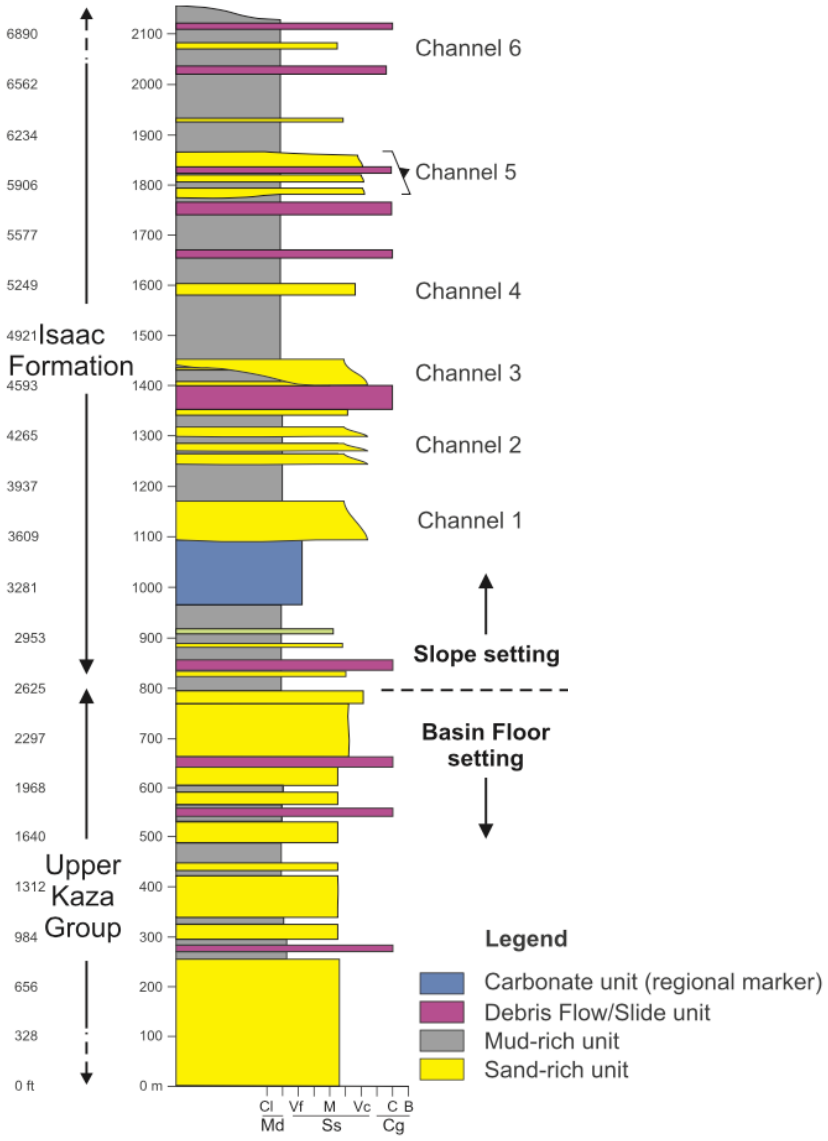

Figure 1.7. Composite stratigraphic column for the Castle Creek study area, showing the general stratigraphic levels (from Ross and Arnott, 2007)

(Arnott, 2007). These strata represent depositional lobes deposited by poorly confined flows on the basin floor. The Isaac Formation, making up the upper 1600 m of exposed stratigraphy at CC. conformably overlies the upper Kaza Group and consists of coarse-grained sandstone and conglomerate that form laterally discontinuous 10-200 m-thick stratal units, bounded on all sides by thin-bedded turbidites. These deposits represent continental slope channel fills bound by genetically related fine-grained levees (Bergen et al., 2022; Gammon et al., 2007; Ross and Arnott, 2007). There are seven channel-levee complexes present in the Isaac Formation at CC. Together, strata exposed at CC represent a several-kilometers-thick, upward-shallowing succession from proximal basin floor deposits of the upper Kaza Group to slope deposits of the Isaac Formation (Arnott, 2007; Ross and Arnott, 2007; Ross and Parrish, 1991).

The southern Canadian Cordillera been affected by four phases of deformation and two phases of low-grade metamorphism, associated with mid-Jurassic to Eocene accretion of exotic terranes onto the western margin of Canada (Reid et al., 2002). Strata at CC are exposed within the Isaac Lake Synclinorium, a structural depression formed by pre- to mid-Jurassic southwest-verging overturned folds and associated bounding dextral strike-slip faults (Reid et al., 2002). Quartz grains in sandstones exhibit lobate grain boundaries due to grain boundary bulging recrystallization, and all original clay minerals have been recrystallized to muscovite and chlorite. Based on this, Lee (2016) determined deformational temperature in the southern Cariboo Mountains to range from 280-400 °C, which is consistent with lower greenschist facies mineral assemblages. This is slightly lower than the 350-450 °C regional temperature corresponding to an upper amphibolite metamorphic grade in the northern Cariboo Mountains (Murphy, 1987).

1.3 Sedimentary Rock Geochemistry

1.3.1 The geochemical evolution of the continental crust

The silicic continental crust found on Earth is unique among the terrestrial planets in our solar system, which tend to be dominated by basalts (Taylor and McLennan, 1985). The existence of this continental crust reflects differentiation associated with plate tectonics on Earth. The continental crust is vertically stratified based on its composition, defined seismically as the upper-, middle-, and lower crustal layers, and extends from the Earth's surface to the Mohorovicic discontinuity (Moho), marking the crust-mantle boundary (Rudnick, 1995). The layers of the continental crust display gradational variations in bulk composition. The upper crust is most accessible to direct observation and sampling, and is largely granodioritic in composition, constrained by analysis of igneous exposures, as well as terrigenous clastic sedimentary rocks, which provide an average sample of the exposed crust from which they were derived (Taylor and McLennan, 1985). The lower continental crust is less accessible for study at the surface, hence its composition is largely estimated by indirect means such as seismic studies (Rudnick and Gao, 2014). Nonetheless, it has been observed that on average, the lower continental crust is similar in composition to unmodified basalts (Hawkesworth and Kemp, 2006). This suggests that the average lower continental crust may be a good approximation of the basaltic protolith to the continental crust. It is generally accepted that the continental crust undergoes differentiation by intracrustal melting, with most models involving at least two stages of differentiation (Hawkesworth and Kemp, 2006; Taylor and McLennan, 1995). This involves the extraction of basaltic magma from the mantle, followed by remelting or fractional crystallization of the basalt (Hawkesworth and Kemp, 2006). The composition of the upper and

lower continental crust is therefore an important constraint on all geochemical models of bulk Earth composition and evolution since it is not easily recycled back into the mantle.

Despite comprising only 0.6% of the mass of the silicate Earth, the continental crust, especially the upper crust, is a major geochemical reservoir, and contains a large proportion of incompatible elements — as much as a thousand-fold relative to the mantle (Rudnick and Gao, 2014; Taylor and McLennan, 1995). Incompatible elements are those that preferentially occur in the liquid rather than solid phase of a melt due to unsuitable size and/or charge relative to the cation sites in the minerals crystallizing from the melt. In basaltic and ultramafic rocks, the major minerals have two common kinds of cationic lattice sites: a smaller tetrahedral site occupied by Si and Al (minor Fe, Ti), and a larger octahedral site occupied by Ca, Mg, Fe and Na (White,

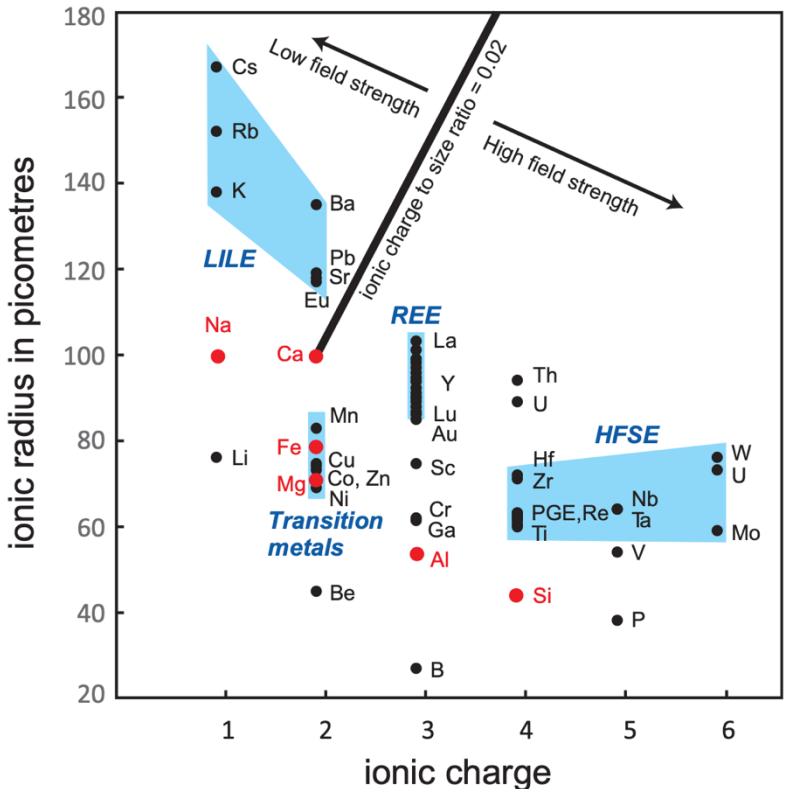

Figure 1.8. Plot of ionic radius versus ionic charge for incompatible trace elements of geological interest. Major elements (in red) indicate where trace element ionic substitutions will most readily occur. An ionic potential (charge to size ratio) of 0.02 subdivides the incompatible elements into low field strength (LFS) elements (also known as large ion lithophile elements, LILE) and high field strength elements (HFSE) (Rollinson and Pease, 2021, from Shannon, 1976)

2013). Incompatible elements with difficulty entering the solid phase are primarily classified into two groups (Figure 1.8.). One group includes those with large ionic radius (large-ion lithophile elements; LILE), namely K, Rb, Cs, Sr and Br. The other group includes those with high ionic charge (high-field-strength elements; HFSE), such as Zr, Nb, Hf, rare-earth elements (REE), Th, U and Ta. Partial melting of the mantle results in enrichment of incompatible elements in continental crusts relative to the residuum in the mantle melt. Of note, these incompatible elements include the radiogenic heat producing elements (K, Th, and U) that partially fuel mantle convection driving plate tectonics, and members of a number of radiogenic-isotope systems (i.e. Rb-Sr, U-Pb, Sm-Nd, Lu-Hf) (Rudnick and Gao, 2014; Taylor and McLennan, 1995). As a result, the residual mantle reservoir, formed following extraction of continental crust formation, is very different from the average continental crust by being strongly depleted in incompatible element abundance.

1.3.2 Application of rock geochemistry in sediment provenance studies

Many recent studies have used elemental composition of sedimentary rocks to determine provenance (Armstrong-Altrin et al., 2015; Armstrong-Altrin et al., 2018; Chaudhuri et al., 2020; Chen et al., 2019; Kuiper et al., 2014; Phan et al., 2018). These analyses are based on the observation that some elements, for example rare earth elements, or REEs, occur in extremely low concentrations in river water and seawater (Taylor and McLennan, 1995) and that these concentrations show little change from source rock to depositional sink.

Of particular interest in provenance studies is the continental margin, where significant growth and differentiation of continental crust occurs. Basin clastic sedimentary rocks, including turbidites, are an important component of the sediment that accumulates along the edges of continents and are common in the geological record, making them important sources of

information (McLennan et al., 1990). The composition of these deposits is controlled primarily by tectonic setting and source rock composition, although weathering, transport, sedimentary processes and diagenesis may also be factors (Cox et al., 1995). While various types of lithologies may be studied, fine-grained sedimentary rocks, such as mudstones and shales, are the most suitable rock type to study provenance due to their impermeable nature, and therefore retention of most mineral constituents inherited from the source rock. Furthermore, fine-grained rocks are more effective at averaging sources than coarse-grained counterparts due to suspension transport and deposition and are less affected by grain-size effects. Therefore, the composition of mudstones reflects best the composition of their source rocks, and on a global scale, the average continental crust (Cox et al., 1995).

Clay minerals, which are the principal constituent in mudstones, are labile and prone to recrystallization and mineralogical change during diagenesis and low-grade metamorphism (Cox et al., 1995). However, since these processes are largely isochemical, bulk composition changes little. Therefore, chemistry is the best index of compositional difference between mudrocks of different age, provenance and diagenetic history. Researchers have established a variety of valuable geochemical discriminants, based primarily on the relative mobility of elements, to study clastic rock provenance and tectonic setting. The immobile major and trace elements (e.g., Al_2O_3, Fe_2O_3, TiO_2, Th, Sc, Co, Zr, REEs) are carried in the suspended load, and accordingly are especially useful provenance indicators. Since these elements are relatively insoluble in aqueous systems, these elements are relatively undisturbed by sedimentary processes and retain the original source concentration. An effective technique that has been widely used to quantify provenance is the application of trace element ratios. For instance, La and Th are more abundant in silicic igneous rocks, whereas Co, Sc, and Cr are more abundant in basic igneous rocks. Also,

silicic igneous rocks have a negative Eu anomaly, defined as depletion of Eu relative to other REE, whereas basic igneous rocks contain little to no Eu anomaly. These same trends within fine-grained sediments reflect their sources, suggesting that trace element and REE ratios may be used as indicators of provenance (Cullers, 1988; Cullers, 2002).

1.3.2.1 Major element geochemistry

Relative proportions of different minerals in clastic grains reflect the composition in the source terrane. In terms of major elements, clay minerals and nonclay silicate minerals have different proportions of aluminum oxide, thus chemical composition and oxide ratios are useful indicators of compositional changes in detrital mineralogy. The Index of Compositional Variability (ICV), proposed by Cox et al. (1995) is one such ratio, defined as:

(1) $ICV = (Fe_2O_3 + K_2O + Na_2O + CaO + MgO + TiO_2) / Al_2O_3$

measures the abundance of alumina relative to other major cations, while excluding silica to eliminate problems of quartz dilution, such that alumina-poor nonclay silicates have a higher ICV relative to clay minerals. Furthermore, there is a compositional gradient — ICV tends to be highest in minerals with higher susceptibility to weathering, such as pyroxene and amphibole, decreasing in more stable minerals such as alkali feldspar, followed by the montmorillonite group of clay minerals, and is lowest in the kaolinite group (Cox et al., 1995). Another index of mudrock composition is the ratio K_2O/Al_2O_3, which can be used as an indicator of compositional variation due to the differing values for this ratio in clay minerals and feldspars (Figure 1.9.).

ICV is also sensitive to the intensity of chemical weathering and may also be used as a measure of compositional maturity of mudrocks (Cox et al., 1995). The upper crust consists of approximately 21% by volume quartz, 41% plagioclase, and 21% potassium feldspar (Nesbitt and Young, 1982). Chemical weathering during erosion and transport causes rapid degradation of labile minerals such as feldspars, micas and apatites (Middelburg et al., 1988). Feldspars are the most abundant of the labile minerals, and therefore dominate chemical weathering of the upper crust. Mixed-layer clays (i.e. smectites, chlorites), which contain Ca, Na, K, Fe, and Mn, undergo alteration into compositionally simpler cation-poor clays such as the kandites (Middelburg et al., 1988). Elements released during this process are removed in solution, which

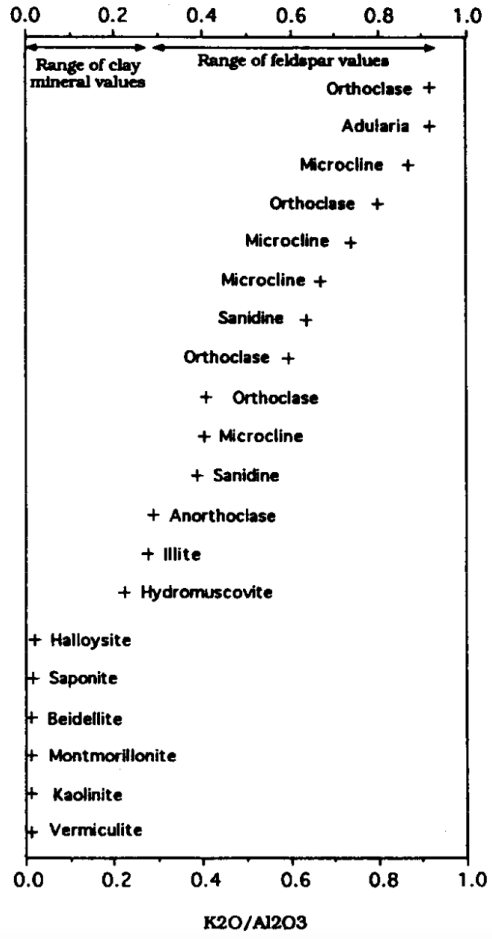

Figure 1.9. Values of the K_2O/Al_2O_3 ratio for K-feldspars and clay minerals. Crosses represent values for the specific minerals indicated (from Cox et al., 1995, after Deer et al., 1966)

then leads to their depletion but concomitant enrichment in less soluble elements like Al and Fe. Although K has a high aqueous solubility, it tends to be conserved in mudrocks because of the chemical stability of illite. Therefore detrital mud recycled from older mudrocks generally contain abundant illite, and as a consequence are rich in potassium (Potter et al., 1980).

Calcium, Na, and K are removed from feldspars by chemical weathering resulting in an increase in the proportion of aluminum oxide to alkalis in the weathered residue (Nesbitt and Young, 1982). A good measure of the degree of weathering can be obtained by calculation of the chemical index of alteration (CIA) using molecular proportions:

(2) $CIA = [Al_2O_3 / (Al_2O_3 + CaO^* + Na_2O + K_2O] \times 100$

where CaO^* is the amount of CaO incorporated in the silicate fraction of the rock, and carbonate and apatite content are corrected for. The resultant value measures the proportion of Al_2O_3 versus the labile oxides in the mudrock. Values of the index range between 30 and 45 for fresh basalt with abundant albite, anorthite, potassic feldspars and diopside, and 45 to 55 for granite and granodiorite. The average mudstone ranges from 70 to 75, reflecting the abundance of clay minerals. Mudstones containing more intensely altered materials will have correspondingly high CIA values due to the abundance of aluminum-rich kaolinites and beidellites (Nesbitt and Young, 1982).

1.3.2.2 Trace element geochemistry

Trace element chemistry of mudrocks has been used in numerous studies to compare mudrocks of different ages or provenance, or to establish the relative contribution of fractionated igneous material to the sedimentary system (Armstrong-Altrin et al., 2015; Cox et al., 1995). Trace elements constitute only a small elemental fraction in the upper continental crust yet provide important geochemical and geological information. These elements have a wide range of

chemical properties and behaviours, allowing for their sensitivity to processes to which major elements are insensitive (Rollinson and Pease, 2021; White, 2013). Since many trace elements have very low solubility in aqueous systems, they are transferred from source rock to sediment without significant fractionation (Nesbitt, 1979). Rather than forming mineral frameworks, they generally occur in association with clay minerals as sorbed particles on surfaces or incorporated into interlayer cation sites, and hence their occurrence is not strongly related to mineralogy or bulk composition (Cox et al., 1995; Taylor and McLennan, 1985). Additionally, most hydrothermal fluids have low concentrations of insoluble trace elements, so alteration of whole-rock trace element patterns during hydrothermal alteration and metamorphism has little effect (Taylor and McLennan, 1995). Therefore, ratios of low-solubility trace elements in mudrocks generally reflect those of the source rocks, making such elements a valuable tool for provenance analysis.

The behaviour of elements can be divided into four categories: atmophile, lithophile, chalcophile, and siderophile. Atmophile elements (e.g. H, C, N, He) are generally volatile and concentrated in the atmosphere and hydrosphere, whereas lithophile (e.g. Al, Ti, Ba, Na), siderophile (e.g. Co, As, Sb, Re) and chalcophile (e.g. Cu, Ni, Pb, In) elements tend to partition into a silicate, metal, or sulfide liquid respectively. The distribution of the electropositive elements in these phases is controlled by the free energies of formation of the corresponding sulfides and silicates (White, 2013). Lithophile elements have either very low or very high electronegativities, and tend to form ionic bonds, whereas siderophile and chalcophile elements have intermediate electronegativities and tend to form covalent or metallic bonds (White, 2013). Overabundance of oxygen in the outer part of the Earth means that metallic liquids do not occur naturally, and only trace sulfide liquids form. As a result, siderophile and chalcophile elements

occur mainly in silicate phases in the continental crust and mantle (White, 2013). Elements can also be grouped based on their behaviour in the silicate portion of the Earth: volatiles, semi-volatiles, major elements, first series transition metals, high field strength elements, noble metals, alkali/alkaline earth trace elements, rare earths and related elements, and U/Th decay series elements (Figure 1.10).

Many elements in the periodic table, including the alkali and alkaline earth metals (K, Na, Ca, Sr), and U, are fractionated to varying degrees during secondary processes. The trace elements that are of greatest interest in provenance studies are those that are the least mobile under the expected range of geological conditions (Rollinson and Pease, 2021). These include certain first series transition metals (Sc), HFSE (Zr, Nb, Hf, Ta), REE, and Th (White, 2013). Insensitive to weathering, alteration, metamorphism, and diagenesis, these elements should be

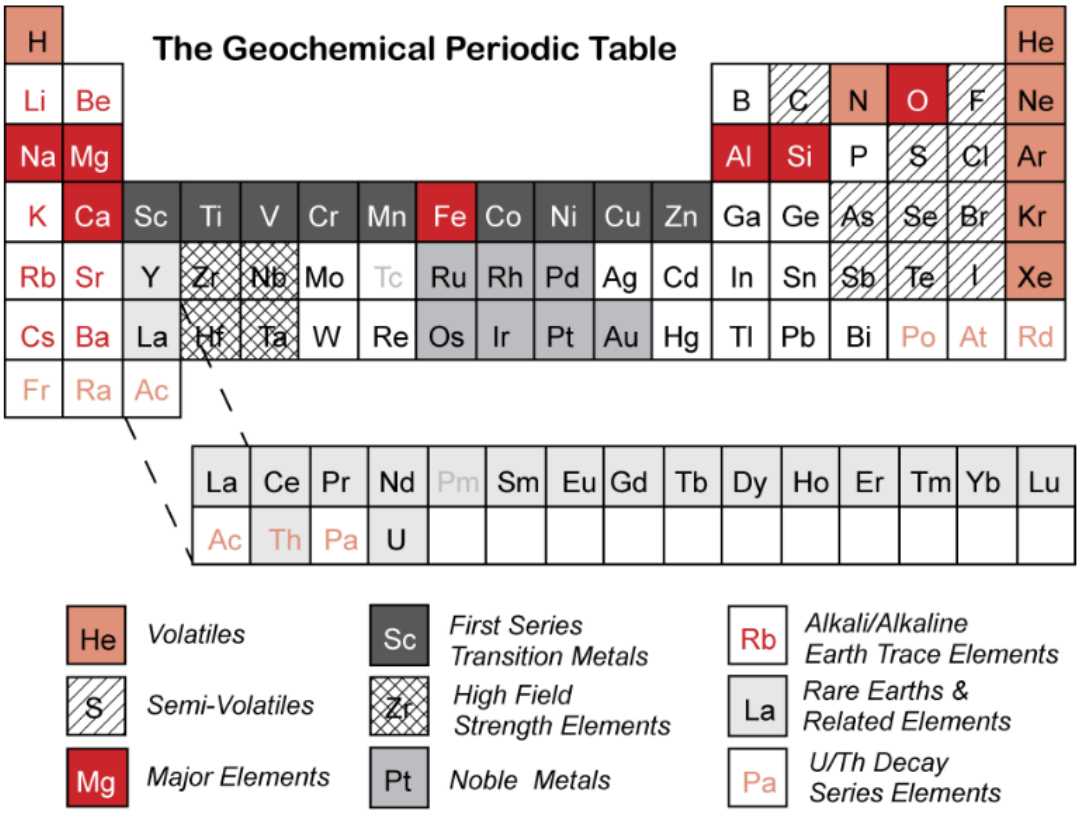

Figure 1.10. Goldschmidt's classification of the elements (from White, 2013).

transferred with little change in abundance from source to sink, and be representative of the average composition of the source rock (Rollinson and Pease, 2021; White, 2013).

The alkali and alkaline earth elements have electronegativities less than 1.5, a single valence state (+1 for alkali and +2 for alkaline earth elements) that tends to form ionic bonds, and include the LILE (White, 2013). Due to their large ionic radii, these elements tend to be concentrated in the melt phase during crystallization or melting and are termed incompatible elements. Their low ionic potential makes these elements relatively soluble in aqueous solutions, and thus mobile during weathering and diagenesis (Figure 1.8.) (Rollinson and Pease, 2021).

Rare earth elements are subdivided into the lanthanide and actinide rare earths, although the term is usually applied only to the lanthanide rare earths, as only two of the actinides, U and Th, have nuclei sufficiently stable to survive over geological time (Rollinson and Pease, 2021). Y has similar chemical properties, including charge and ionic radius, to the heavy rare earth elements (HREE), and thus behaves similarly (White, 2013). The lanthanide rare earths generally have a +3 valence state over a wide range of redox states, although two of the REE display unique properties: Ce can be oxidized to the +4 oxidation state, and Eu can be reduced to the +2 oxidation state at low oxygen fugacities in the Earth's interior. Th is always in +4 state, whereas U can be +4 or +6 depending on oxygen fugacity. Similar to the alkalis and alkaline earths, REE+Y are strongly electropositive, with electronegativities of 1.2 or less, so form mostly ionic bonds (White, 2013). However, they are relatively insoluble in aqueous solutions due to their high charge and ionic potential (except U, which forms a soluble oxyanion complex). The REE are typically incompatible, although the level of incompatibility varies as a result of the progressive decrease in ionic radius from La (115 pm) to Lu (93 pm) (White, 2013). As a result, the lightest rare earths (LREE; La-Gd), in addition to highly charged U and Th, are highly

incompatible. The heavy rare earths (HREE; Tb-Lu) and Y have sufficiently small radii that they can be accommodated in certain minerals (White, 2013). Europium in its +2 state substitutes for Ca in plagioclase feldspar at a higher rate than other REE and so phases in equilibrium with plagioclase are depleted in Eu. Systemic variation in REE behaviour may be illustrated by plotting the log of the relative abundances against atomic number (Figure 1.11.). Even numbered elements in the solar system have greater abundances than odd-numbered elements, producing a saw tooth pattern of decreasing abundances in CI chondrites (a class of meteorites representing average concentrations of non-volatiles in the solar system) (White, 2013).

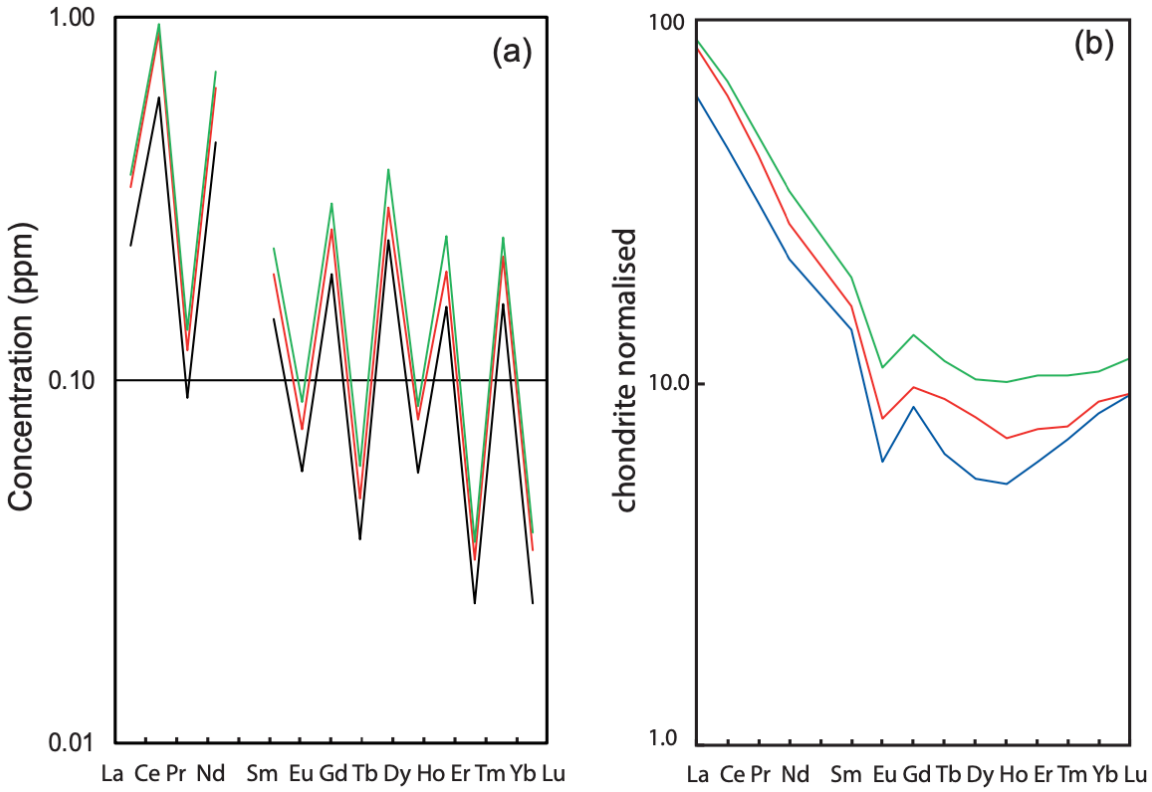

Figure 1.11. Plots of REE concentration. (a) REE concentrations in ppm for selected CI chondrites plotted against atomic number. REE with even atomic numbers have higher concentrations than those with odd atomic numbers. These values are used to normalise rock REE concentrations. (b) an example of a chondrite normalised plot showing the REE plotted by atomic number of the x-axis and CI chondrite normalised concentrations plotted on a log scale y-axis (from Rollinson and Pease, 2021).

The high field strength (HFSE) elements, like Zr, Hf, Ta and Nb, are all relatively small cations, with ionic radii between 64 and 76 pm, and high charge (valance state of Zr and Hf is +4 and Ta and Nb is +5) (Figure 1.8.); Rollison and Pease, 2019). These elements are less electropositive than the alkaline and rare earths and tend to form covalent bonds. Due to their high charge, substitutions in common minerals are energetically unfavorable, making them moderately to highly incompatible. Additionally, their high ionic potential (high ionic charge to radius ratio) makes them highly insoluble, and thus immobile during weathering and metamorphism (White, 2013).

The behaviour of first series transition elements is less predictable than other elements because many of these elements have two or more valence states in nature (White, 2013). Additionally, they are highly electronegative, so while they form ionic bonds with O in oxides and silicates, they form covalent bonds with other non-metals, such as S. Behaviour of these elements in magmas and in aqueous solutions is variable, but principally dependent on valence state. Nevertheless, a general trend in compatibility is recognized, with Ti, Cu, Zn generally being moderately incompatible, and Cr, Ni and Co being highly compatible (White, 2013).

Most suitable for the study of sediment provenance are the HFSE (Zr, Nb, Hf, Ta), certain first series transition metals (Sc, Cr, Co), REE, Y and Th. These elements are relatively immobile during weathering and diagenesis and thus have short residence times in seawater (Taylor and McLennan, 1985). This makes trace element contents of sediments robust tools to investigate sediment provenance, weathering intensity, and tectonic setting.

1.3.3 Application of Isotope Systematics to Provenance Studies

Provenance studies based on isotopic data have been extensively applied to the analysis of (meta)sedimentary successions deposited in different tectonic settings (Ali et al., 2014;

Boghossian et al., 1996; McLennan et al., 1990; Nie et al., 2012; Paravidini et al., 2021; Stevenson et al., 2000). Isotopes are ideal provenance tracers because isotopes of the same element have similar chemical properties, thus travel together through the sedimentary system, preserving their source-area characteristics (Potter et al., 2005). By revealing the major geochemical characteristics of the rocks providing sediment to ancient and modern sedimentary basins, provenance studies provide insight into the patterns and temporal changes in the sediment dispersal system, and ultimately tectonic setting of the source to sink sedimentary system. Since the evolution of syn-orogenic basins is controlled principally by orogenic-driven changes in the rates of accommodation and sediment supply (e.g., Catuneanu, 2006), provenance studies may also offer insight into the evolution of the adjacent orogen and changes of orogenic sediment sources and transport pathways. Two isotopic systems particularly useful in provenance studies are neodymium (Nd) and strontium (Sr). Neodymium isotopes are a powerful indicator of provenance due to a lack of significant fractionation during transport and diagenesis, whereas Sr isotopes are sensitive to secondary processes (Carter et al., 2020). Therefore, detrital zircon geochronology combined with Nd ($^{143}Nd/^{144}Nd$) and Sr ($^{87}Sr/^{86}Sr$) isotope geochemistry is effective for identifying provenance changes during sedimentary basin filling (Eriksson et al., 2004; Lan et al., 2014).

1.3.3.1 Strontium isotope geochemistry

Rubidium-strontium systematics are used both as a radiometric dating technique and a tracer of geochemical processes. There are four naturally occurring isotopes of strontium, the most abundant being ^{88}Sr (83%), followed by ^{86}Sr (10%), ^{87}Sr (7%), and ^{84}Sr (<1%). Only ^{87}Sr is a radiogenic by-product, produced by the beta (β) decay of ^{87}Rb, which has a half-life of 4.88×10^{10} years (Potter et al., 2005). Abundances of ^{87}Sr are expressed in reference to the stable

isotope ^{86}Sr. When the Earth formed, it incorporated Sr with an initial, or primordial $^{87}Sr/^{86}Sr$ ratio, which has since increased by the generation of radiogenic ^{87}Sr. Initial $^{87}Sr/^{86}Sr$ ratio of a mineral or rock is inherited from its parental reservoir, and continued decay of Rb causes $^{87}Sr/^{86}Sr$ to increase through geological time (Long, 1999).. There are two unknown values for a given geochemical reservoir: its age of crystallization, and its initial $^{87}Sr/^{86}Sr$ composition. $^{87}Sr/^{86}Sr$ ratio measured today for a rock derived *t* years ago from a source can be expressed as follows:

$$(3) \quad \frac{^{87}Sr}{^{86}Sr} = \left(\frac{^{87}Sr}{^{86}Sr}\right)_i + \left(\frac{^{87}Rb}{^{86}Sr}\right)(e^{\lambda t} - 1)$$

At magmatic temperatures there is no isotopic fractionation, so initial values of $^{87}Sr/^{86}Sr$ are uniform throughout a pluton (McCulloch and Wasserburg, 1978). However, during crystallization of a magma chamber differentiation results in variable mineral abundances throughout a rock, and thus local variations in the Sr isotopic signature. For example, Rb, which behaves like K, enters readily into biotite, less into K-feldspar, and even less into plagioclase. On the other hand, Sr is geochemically similar to Ca, so enters plagioclase more readily than K-feldspar and biotite (Long, 1999; McCulloch and Wasserburg, 1978). Quartz does not accommodate Rb and Sr. Therefore, a rock rich in biotite would have a higher Rb/Sr ratio, whereas one with abundant plagioclase would have a lower Rb/Sr ratio.

The application of the $^{87}Sr/^{86}Sr$ ratio was pioneered by Dasch (1969), who showed that deep-marine clays were not in isotopic equilibrium with seawater, but instead mirrored the composition of rocks found on adjacent landmasses (Potter et al., 2005). This was an important finding because it suggested that early burial diagenesis has little effect on the chemistry or mineralogy of clays, in contrast to the significant changes that take place under deeper burial (Potter et al., 2005). It was established that the Sr isotopic composition and abundance in fine-

grained marine sediments is controlled by a small number of factors, including: detrital minerals, whose Sr isotopic signature is inherited from predominantly young volcanic rocks ($^{87}Sr/^{86}Sr$ = 0.704 ± 0.002), or old continental, radiogenic crustal rocks ($^{87}Sr/^{86}Sr$ generally between 0.73-0.8); and authigenic minerals (carbonates, sulfides, silicates, etc.), whose $^{87}Sr/^{86}Sr$ is identical to that of the seawater from which they precipitated (Potter et al., 2005). Since then, the $^{87}Sr/^{86}Sr$ ratio has been widely applied in provenance studies (Ali et al., 2014; Cameron and Hattori, 1997; McCulloch and Wasserburg, 1978; McLennan et al., 1990; Singh et al., 2008).

$^{87}Sr/^{86}Sr$ is often combined with $^{143}Nd/^{144}Nd$ in provenance studies, because Sr provides insight into source rock composition, whereas Nd tells when the source igneous rocks separated from the mantle. However, it is important to point out that because fine-grained sediments often experience post-depositional K addition or Ca loss, the Sr isotopic system is more prone to being altered by diagenesis in mudstones (Potter et al., 2005).

It is often assumed when interpreting Rb-Sr data that a system is closed, i.e. there is neither gain nor loss of a parent or daughter except by radioactive decay (Long, 1999; Moorbath, 1964). However, whether this is true depends on geological conditions and physical scale. During solid-state metamorphism, recrystallization or neomorphism of metamorphic minerals, there is likely limited transport of Rb and Sr (McCulloch and Wasserburg, 1978). However, open system behaviour may have occurred if large amounts of diagenetic fluids had passed through the system, or with repeated metamorphic events. Another potential problem for interpretation of isotopic data could be a mild metamorphic above the blocking temperature, above which ions diffuse into or out of a mineral, for some minerals, and below the blocking temperature for others (Basu, 2017).

1.3.3.2 Neodymium isotope geochemistry

Neodymium isotopes are important as geochronological tools to date the timing of events such as magma crystallization and metamorphism, and geochemical tracers for understanding the compositional evolution of the continental crust and mantle (McCulloch and Wasserburg, 1978). Neodymium has seven natural isotopes, of which five are stable: ^{142}Nd (27.153 %), ^{144}Nd (23.798 %), ^{145}Nd (8.293 %), ^{146}Nd (17.189 %), and ^{148}Nd (5.756 %), and two are long-lived radioisotopes, ^{143}Nd (12.173 %) and ^{150}Nd (5.638 %) (Meija et al., 2016)) ^{143}Nd is commonly used as a geochemical tracer due to the predictable α-decay of ^{147}Sm to ^{143}Nd, with a half-life of 1.06×10^{11} years that corresponds to a decay constant ($\lambda_{Sm^{147}}$) of 6.54×10^{-12} year^{-1}. Sm is slightly more compatible than Nd in the Earth's mantle due to its smaller ionic radius. Therefore, the Sm–Nd isotopic system is sensitive to the fractionation of mantle-derived magmas at different times of continental crust formation. During fractional crystallization and partial melting of a reservoir, fractionation of Sm from Nd results in an altered Sm/Nd ratio, which will eventually change the relative abundance of ^{143}Nd (Bizimis and Scher, 2016; McCulloch and Wasserburg, 1978). The mechanisms behind these changes are essential for understanding the chemical evolution of different terrestrial reservoirs.

The Nd-isotope composition of a rock is a function of its initial ^{143}Nd/^{144}Nd ratio, its ^{147}Sm/^{144}Nd ratio, and its age. In general, since Nd is more incompatible than Sm, the continental crust has a lower ^{147}Sm/^{144}Nd ratio relative to the average whole-Earth ratio due to mantle fractionation (Bizimis and Scher, 2016). With ^{147}Sm isotope radioactive decay, the lower Sm/Nd will result in the low ^{143}Nd/^{144}Nd ratio of the continental crust relative to mantle sources. Therefore, the ^{143}Nd/^{144}Nd ratio measured today for a rock derived *t* years ago from a source can be expressed as follows:

$$(4)\quad \frac{^{143}Nd}{^{144}Nd} = \left(\frac{^{143}Nd}{^{144}Nd}\right)_i + \left(\frac{^{147}Sm}{^{144}Nd}\right)(e^{\lambda t} - 1)$$

Individual terranes may be fingerprinted by Nd isotopic ratio, whereby older continental crust displays low $^{143}Nd/^{144}Nd$ ratios, and more recently fractionated rocks, such as those from volcanic arcs, display higher $^{143}Nd/^{144}Nd$ ratios (Jenkyns et al., 2002). This can provide information on both provenance and tectonic evolution of sedimentary basins ((Bowring and Podosek, 1989; Burwash et al., 1988; Hauck et al., 2017; Johnson and Winter, 1999; McLennan et al., 1990; Murphy, 2000; Rainbird et al., 1997; Ross et al., 1992). The use of Sm-Nd isotopic studies to study sedimentary rocks also relies largely on the observation that earth-surface processes, like chemical weathering, transport, and diagenesis, generally have no significant effect on the fractionation of Sm and Nd (Taylor and McLennan, 1985). Although the redistribution of REE can rarely occur during or after sediment deposition, it is not a major concern since Sm and Nd are generally immobile in fluids and low-temperature alteration (e.g. Bock et al., 1994; McDaniel et al., 1994; Ehrenberg and Nadeau, 2002). In this regard, both the Sm/Nd and the initial $^{143}Nd/^{144}Nd$ will be similar to the average ratios in the source rocks (McCulloch and Wasserburg, 1978). The comparison of the $^{143}Nd/^{144}Nd$ ratio of a given rock compared to CHUR is typically expressed using the ε_{Nd} notation in parts per 10,000 and can be expressed as follows:

$$(5)\ \varepsilon Nd = \left(\frac{\left(\frac{^{143}Nd}{^{144}Nd}\right)_{rock}}{\left(\frac{^{143}Nd}{^{144}Nd}\right)_{CHUR}} - 1\right) * 10000$$

The Nd isotopes of fine-grained siliciclastic rocks have previously been used in foreland basins to assess tectonic evolution through changes in sediment provenance. Specifically, changes in the relative influence of the two adjacent source areas – advancing mountainous orogenic system on one side and the relatively stable craton on the other - can be quantified

based on the fact that juvenile volcanic rocks have a more radiogenic isotopic signal ($\varepsilon Nd>0$) whereas rocks with a cratonic origin have a less radiogenic isotopic signal ($\varepsilon Nd<-4$) (Nie et al., 2012; Paravidini et al., 2021; Stevenson et al., 2000).

1.4 Tectonic subdivisions of western Laurentia

The Nd isotopic signatures of North American Archean and Proterozoic sources are either well known or can be confidently predicted (e.g., Villeneuve et al. 1993; Chauvel et al. 1987). Figure 1.12. shows the areal distribution of basement domains in western Canada based on crustal chemical age (Gehrels and Ross, 1998; Hoffman, 1988). Previous studies of the

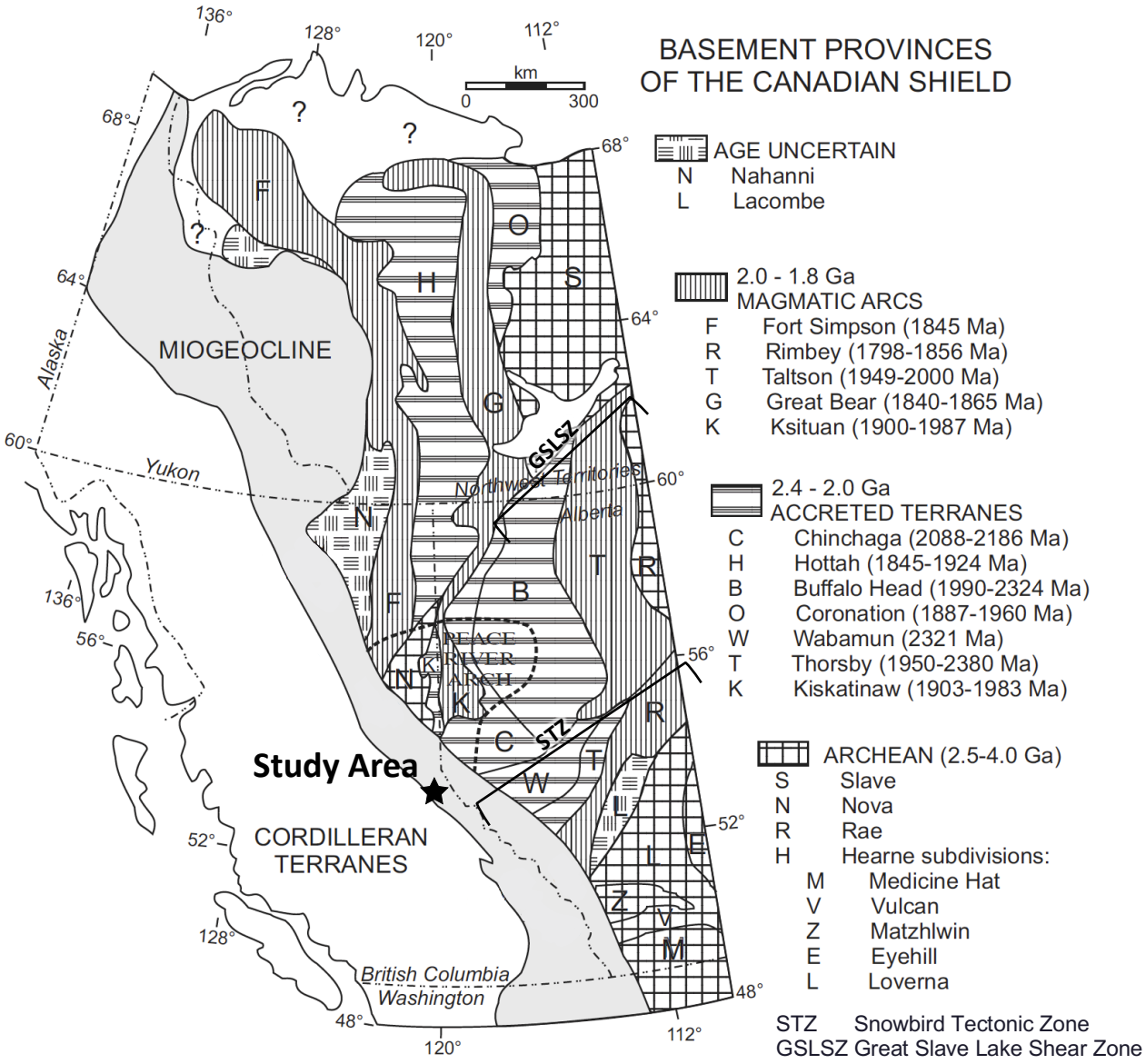

Figure 1.12. Schematic map of the Cordilleran miogeocline, showing basement domains of the western Canadian Shield, modified from Gehrels and Ross (1998). Ages are based on U-Pb dates. Except for limited regions in the Great Bear, Trans-Hudson, and Rimbey domains, all basement of western Canada has Archean Nd signature.

crystalline basement in western Canada consist of petrographic and petrological analysis (Burwash and Culbert, 1976), geophysical interpretation, K-Ar geochronology, and Sm-Nd analysis (Burwash and Culbert, 1976; Frost and Burwash, 1986). In addition, the exposed Shield in northeastern Alberta has been studied extensively (Baadsgaard and Godfrey, 1972; Nielsen et al., 1981; Langenberg, 1983; Goff et al., 1986; Sprenke et al., 1986; Wilson, 1986). The combination of geophysical interpretation with isotopic and lithological studies provides good constraint on the nature of the basement that underlies Alberta and British Columbia. For the most part, the geochronology confirms the location of domain boundaries by demonstrating consistency in the age of magmatic events within discrete domains. Models for the tectonic evolution of the Canadian Shield domains can also be carried into the buried basement, providing a tectonic framework for the domains in the interior of Alberta. Tectonic models for southern Alberta were initially presented by Hoffman (1988, 1989) and Ross et al. (1991) and for northern Alberta by Theriault and Ross (1991). The crystalline basement of western Laurentia can be subdivided into three broad regions: a) a southern domain dominated by Archean domains; b) a central domain consisting of domains that surround the Snowbird Tectonic Zone; c) a north-eastern domain comprising the Early Proterozoic domains that lie between the Snowbird Tectonic Zone and the Great Slave Lake shear zone, and d) northern domain comprising Paleoproterozoic domains located north of the Great Slake Lake Shear zone.

1.4.1 Southern Source Area (Southern Alberta and Northern Montana)

Crystalline basement rocks of southern Alberta, Saskatchewan, and the northwestern United States are part of the southern part of the Hearne Craton, the Medicine Hat Craton, and the Wyoming Craton (Thomas et. al 1987; Hoffman 1988). The Medicine Hat Block (MHB) is the oldest domain in the subsurface of Alberta and appears to continue southward into western

Montana where it is separated from the Wyoming province by the Great Falls tectonic zone (O'Neill and Lopez, 1985). The MHB has limited geochemical data available due to extensive cover. Drill core has provided U-Pb protolith crystallization ages from 3.28-2.50 Ga (Gifford et al., 2020). Villenueve et al. (1993) analyzed drill core samples from the Medicine Hat Block in southern Alberta for Sm-Nd isotopes that yielded εNd values of -31.2 and -39.7 (εNd(i) = +0.6 and -0.1) and crustal residence ages (T_{DM}) of 2.86 Ga and 3.48 Ga respectively. The $^{147}Sm/^{144}Nd$ ratios of approximately 0.10 are typical of enriched continental crust. The Sm-Nd isotopic data are consistent with the data of Frost and Burwash (1986). Buhlmann et al. (2000) suggested the Medicine Hat block might represent a northern extension of the Wyoming craton. They found that minette dykes and mica-clinopyroxenite xenoliths, representing mantle below the Medicine Hat Block in the Milk River area, yielded whole rock $^{87}Sr/^{86}Sr$ values of 0.70566-0.70747, and εNd values from -19.3 to -12.4, which plot in the same εNd – $^{87}Sr/^{86}Sr$ space as other samples from the Wyoming craton.

The southern Hearne Craton can be separated into two domains: the Eyehill High and the Loverna Block. Villenueve (1993) measured Nd isotopic ratios from the Eyehill High at -24.2 to -29.6 (εNd(i) = +1 to +1.4), with $^{147}Sm/^{144}Nd$ ratios ranging from 0.1051 to 0.1195, and T_{DM} ages from 2.85 to 2.83 Ga. The Loverna Block has an εNd value measured at -36.5 (εNd(i) = -12.9), a $^{147}Sm/^{144}Nd$ ratio of 0.0951, and a T_{DM} age of 3.05 Ga.

1.4.2 Eastern Source (Central to Northern Alberta and Saskatchewan)

The eastern source area comprises the 1.86-1.80 Rimbey magmatic arc domain, and the accreted Wabamun (2.32 Ga) and Thorsby (1.98-1.90 Ga) domains (Villenueve et al., 1993). These domains may be related to events along the Snowbird Tectonic Zone, a region of folded sedimentary cover and scattered igneous suites first described as a suture related to the Trans

Hudson orogeny, and later attributed to the 1.90-1.86 Ga Snowbird orogen (Hoffamn, 1988; Berman et al., 2007).

The Rimbey High extends from rocks exposed in the Virgin River shear zone in western Saskatchewan (MacDonald, 1987) to the Alberta Foothills, and probably represents a magmatic arc that was formed by southward subduction of oceanic lithosphere (Ross et al., 1991) during collision of the Hearne and Rae provinces. Most of the basement intersections in the Rimbey High consist of biotite granite (syenogranite to monzogranite) dated between 1.85 and 1.78 Ga (Villenueve et al., 1993). Sm-Nd isotopic analysis yielded εNd values of -32.8 and -24.6 (εNd(i) = -17.9 and -1.4), $^{147}Sm/^{144}Nd$ ratios of 0.1316 and 0.0992, and T_{DM} ages of 4.03 and 2.36 Ga (Villenueve et al., 1993). An elevated $^{147}Sm/^{144}Nd$ ratio of 0.1316 for the more negative εNd sample may indicate overestimation of the protolith age due to assimilation of ancient continental crust in the petrogenesis of this Rimbey Arc granitoid. Alternatively, the Rimbey granites may represent collisional anatectic granite bodies formed along the Snowbird Zone (Villenueve et al., 1993).

Located northeast of the Rimbey magmatic arc are the Thorsby and Wabamun domains. Tectonic and isotopic control is limited here due to sparse drill core control. The Thorsby Low is a narrow (ca. 30 km) aeromagnetic low that merges with the Snowbird Tectonic Zone to the northeast. Basement intersections in the Thorsby Low are few (three in total) and consist of two plutonic rocks dated at 2.40 and 2.29 Ga and a pegmatite dated at 1.91 Ga (Villenueve et al., 1993). εNd is measured at -17.3 (εNd(i) = +0.9) and $^{147}Sm/^{144}Nd$ at 0.1392, with a T_{DM} age of 2.79 Ga (Villenueve et al., 1993). The Wabamun High is a broad wedge-shaped domain of largely undeformed magmatic rocks Ross et al. (1991) suggested that the Wabumun High may

be a tectonic escape wedge related to late-stage convergence and transpression along the Snowbird Zone, similar to the Tantato Domain (Hanmer, 1987).

1.4.3 Northeastern Source (Northern Alberta, southern Northwest Territories)

The northeastern source area comprises the Paleoproterozoic domains located north of the Snowbird tectonic zone, and south of the Great Slave Lake Shear zone. This includes several 2.4-2.0 Ga accreted terranes, including the Chinchaga (2.19-2.09 Ga), Buffalo Head (2.32-1.99 Ga), and Kiskatinaw (1.98-1.90 Ga) terranes, 2.0-1.8 Ga magmatic arcs, Talston (2.00-1.95 Ga) and Ksituan terranes (1.99-1.90 Ga), and the Nova craton (Thériault and Ross, 1991).

The Taltson Arc is a 150-200 km wide magmatic zone, bounded to the east by the Rae province, and to the north by the Great Slave Lake shear zone, that can be traced into the subsurface of Alberta from extensive surface exposures. It comprises a 1986 Ma quartz diorite to granodiorite suite and 1966-1935 peraluminous granitoids, with most ages in the 1.98-1.94 Ga range (Thériault and Ross, 1991). Measured εNd values range from –42.1 to -34.3 (εNd(i) = -9.7 to -3.7), $^{147}Sm/^{144}Nd$ ratios vary from 0.798 to 0.0946, and T_{DM} ages vary from 2.68 to 2.57 Ga (Thériault and Ross, 1991). The Talston domain may reflect continental arc magmatism with pervasive melting of pre-existing crust following collision of the Rae province and Buffalo Head domain (Thériault and Ross, 1991).

The Buffalo Head and Chinchaga terranes are age-equivalent terranes, bounded to the east by the Talston domain, to the south by the Wabamun high and an inferred fault splay of the Snowbird Tectonic Zone, and to the north by the Great Slave Lake shear zone. Basement intersections consist of a wide range of rock types, but felsic to intermediate meta-plutonic rocks dominate. The Buffalo Head domain is 200-300 km wide and composed primarily of metaplutonic rocks ranging in composition from gabbro to leucogranite, with U-Pb

crystallization ages in the 2.32 to 1.99 Ga range. Measured εNd values in the Buffalo Head Terrane range from -35.4 to -18.2 (εNd(i) = -6.3 to +0.2), $^{147}Sm/^{144}Nd$ ratios vary from 0.0807 to 0.1358, and T_{DM} ages vary from 2.83 to 2.51 Ga (Thériault and Ross, 1991). Scattered εNd values may be a result of mixing various proportions of pre-existing, evolved crust with more primitive mantle-derived magmas (Thériault and Ross, 1991). The 20-80 km wide Chinchaga domain, situated west of the Buffalo Head Terrane, is composed mainly of metasedimentary and metaplutonic rocks, with U-Pb crystallization ages ranging from 2.19 to 2.09 Ga (Villenueve et al., 1993). εNd values for the Chinchaga terrane range from -23.4 to -20.8 (εNd(i) = -1.8 to +0.6), with T_{DM} ages from 2.68-2.57 Ga (Thériault and Ross, 1991). The $^{147}Sm/^{144}Nd$ ratios fall between 0.0943 and 0.1205, typical of LREE-enriched crust (Thériault and Ross, 1991). The Nd isotopic ratios suggest the Chinchaga domain has a greater proportion of juvenile material compared to the Buffalo Head Terrane, and that the two terranes are distinct entities.

The 10-130 km wide Ksituan domain is located immediately west of the Chinchaga domain. It is characterized by undeformed magmatic arcs, primarily granitic gneisses, with U-Pb crystallization ages between 1.99 to 1.90 Ga. Measured εNd values range from -21.6 to -20.3 (εNd(i) = -2.1 to -1.8), $^{147}Sm/^{144}Nd$ ratios vary from 0.1204 to 0.1237, and T_{DM} ages vary from 2.63 to 2.62 Ga (Thériault and Ross, 1991). This reflects a smaller Archean contribution compared to the Buffalo Head and Talston domains.

The Nova Domain is a 10 km wide Archean province located west of the Ksituan High. With a U-Pb crystallization age of 2.81 Ga, it is postulated to be a dislocated remnant of the Slave Province, or alternatively, Archean crust that underlies the Ksituan domain. εNd values range from -29.7 to -28.5 (εNd(i) = -2 to +5.6), with a T_{DM} age of 2.48 Ga. The $^{147}Sm/^{144}Nd$ ratios fall between 0.0934 to 0.0987. The variability in εNd suggests that the components of the

Nova domain include a strongly depleted mantle source from the late Archean, and assimilation of an older Archean component

1.4.4 Northern Source (Northern British Columbia, Northwest Territories)

The northern source area comprises the Paleoproterozoic domains located north of the Great Slave Lake Shear zone and consists of parts of the Wopmay Orogen, namely the 1.92-1.85 Hottah and Nahanni terranes, and two 2.0-1.8 Ga magmatic arcs, the Fort Simpson (1.85 Ga) and Great Bear (1.87-1.84 Ga) arcs. The Wopmay Orogen is a north-trending Proterozoic orogenic belt (1.95-1.84 Ga), exposed along the western margin of the Slave Craton, and comprises three major tectonic elements: Hottah Terrane (1.92-1.85), Coronation Margin (1.96-1.89 Ga), and the Great Bear Magmatic Zone (1.87-1.84), each of which preserve remnants of a magmatic arc. These elements can be traced westward from the exposed Canadian Shield until they become truncated to the south by the Great Slave Lake shear zone (Thériault and Ross, 1991).

The Hottah Terrane is the oldest component of the Wopmay Orogen, comprising amphibolite facies sedimentary and intermediate volcanic rocks intruded by 1.94-1.90 calc-alkaline plutons of the Hottah Arc. It is interpreted as the remnants of a continental magmatic arc that collided with the Slave Craton ca. 1.89 Ga (Bowring and Podosek, 1989). εNd values for the Hottah terrane range from -26.1 to -22.8 (εNd(i) = -1.67 to +0.25), with $^{147}Sm/^{144}Nd$ ratios from 0.0896 and 0.1109 and T_{DM} ages from 2.45 to 2.14 Ga (Bowring and Podosek, 1989; Villenueve et al., 1993). The Great Bear Magmatic Zone (GBMZ) is the youngest tectonic element exposed in the Wopmay Orogen, comprising calc-alkaline volcanic and plutonic rocks. The GBMZ has Nd values that range from -26.08 to -15.6 (εNd(i) = -1.63 to 0.09), and $^{147}Sm/^{144}Nd$ ratios between 0.0923 to 0.1361 (Bowring and Podosek, 1989).

The Fort Simpson domain lies to the west and sub-parallels the Hottah Terrane, and extends for over 100 km. It is suggested that the Fort Simpson domain represents a continental arc built on the eastern margin of the Nahanni Terrane by a west-dipping subduction zone prior to the collision of the Hottah and Nahanni terranes (Villenueve and Thériault, 1991). The age of the Nahanni Terrane is unconstrained. Measured isotopic ratios for the Fort Simpson terrane give εNd values ranging from -24.8 to -22.1 (εNd(i) = -2.1 to +1.3), with $^{147}Sm/^{144}Nd$ ratios ranging from 0.0871 to 0.1120, and T_{DM} ages from 2.45 to 2.14 Ga (Villenueve and Thériault, 1991).

1.5 Previous Geochemical Work in Proterozoic Passive Margin Western Laurentia Sediments

In the northwestern U.S.A. the lower part of the Windermere Supergroup consists of mafic metavolcanics of the Huckleberry Formation (correlative to the Irene Formation in southeast B.C.) and marks a Proterozoic rifting event that initiated the proto-Pacific Ocean along the western margin of Laurentia (Hadlari et al., 2021). The Huckleberry volcanics have an Sm-Nd whole rock extrusion age of 762 ± 44 Ma, suggesting a Neoproterozoic age for this rift event (Devlin et al., 1988). Devlin et al. (1985) reported $^{87}Sr/^{86}Sr$ values between 0.70460 and 0.70548, and εNd values between +2.4 and +3.4. However, they noted the Rb-Sr system has been disturbed following extrusion of the volcanics due to open-system behaviour, and the introduction of K and Rb into the system.

Burwash et al. (1988) studied Proterozoic sedimentary rocks in southern B.C., including quartz arenites of the Fort Steele Formation, the oldest exposed stratigraphic unit in the Purcell Supergroup, and the basal Toby conglomerate of the Windermere. They suggest that the Toby conglomerate was derived mostly from the underlying Purcell, based on similar detrital zircon ages between 2.60-2.63 Ga, and $^{143}Nd/^{144}Nd$ values between -14.2 and -12.6. Above the Toby, the upper Horsethief Creek Group contained a mixture of reworked Purcell and cratonic detritus. The hybrid sediment sources result in an expanded range of Nd isotope values between -25.9 and -21.5.

Boghossian et al. (1996) studied a suite of samples of Neoproterozoic to Late Cretaceous age from the Foothills and Fold and Thrust belt of southwestern Alberta and southeastern British Columbia. They found that shales from the Horsethief Creek and Miette formations have εNd values ranging from -29.5 to -27.7 (T_{DM} = 2.62 to 2.24 Ga). Additionally, detrital zircons were

similar in age to that of the Archean Medicine Hat Block (T_{DM} 3.48-2.86 Ga) and the 1.85-1.78 Ga Rimbey domain (T_{DM} = 4.03 to 2.36 Ga).

Garzione et al. (1997) reported Sm-Nd isotopic ratios and trace element composition of Neoproterozoic to Ordovician miogeoclinal sediments from the Canadian Cordillera in the Yukon Territory. They report that shales from the late Neoproterozoic to Cambrian Hyland Group have εNd values ranging from -27.5 to -22.0 (εNd(*600*) = -20.2 to -15.1), and therefore consistent with 2.0 Ga and older basement assemblages (Garzione et al., 1997)

Chapter 2: Methodology

2.1 Detrital Zircon Geochronology

Detrital zircon geochronology was completed at the University of Calgary, and details of analytical methods are described in Matthews and Guest (2016). Some of the detrital zircon ages were sourced from Hadlari et al. (2021). Detrital zircon was separated using standard separation techniques, and isotopic signal intensities were measured for 300 grains per sample by LA-ICP-MS. Preferred ages are $^{206}Pb/^{238}U$ for dates <1500 Ma and $^{207}Pb/^{206}Pb$ for dates >1500 Ma. A total of 2434 U-Pb analyses of detrital zircon grains yielded 1091 dates that passed filtering criteria. Measurements with <5% probability of concordance were filtered from the dataset. Poor analytical efficiency (average n = 121) is the result of widespread recent Pb-loss that affected most of the samples, and it is for this reason for the restrictive <5% probability of concordance filter.

2.2 Sample Collection and Preparation

Samples were collected in the field as fist-sized blocks. Initial sample preparation was done in the Marion Lab at the University of Ottawa. After removing extensively weathered material, samples were broken into small chips with a mallet. Approximately 100g of the broken sample was placed in an aluminum oxide ceramic puck mill and then pulverized for 3-4 minutes, with longer times for harder and more highly metamorphosed samples. Powdered samples were transferred to wide-mouth polypropylene jars. Between samples, the grinding mill was cleaned by pulverizing pure silica sand for four minutes. The mill was then rinsed with distilled water, dried with paper towels, and then rinsed with ethanol to ensure evaporation of water to complete dryness. About 50 mg of each sample was first dissolved carefully in Teflon vials using dilute HNO_3 to dissolve excess carbonate prior to the digestion process of the silicate fraction.

2.3 Whole Rock Geochemistry

Mudrock samples were analyzed by x-ray fluorescence (XRF) at the X-ray core facility at the University of Ottawa to determine their elemental composition. Before running the XRF analysis, loss on ignition (LOI) was obtained for each sample. Here, 1 g of sample was measured and placed in a ceramic crucible, which was then weighed and placed in a furnace for 1 hour at 1050° C. Samples were then removed, allowed to cool and re-weighed. The calculated difference in weight before and after heating represents the LOI. Powders from each rock sample was fused with a 50/50 lithium metaborate, lithium tetraborate flux. The resulting glass disk was then analysed on a Rigaku Supermini200 WDXRF Spectrometer, equipped with a 200 W Pd-anode X-ray tube. Concentrations of each element was calculated from pre-existing calibration curves, determined from previous analyses of reference materials and synthetic standards. Major elements analysed are presented as percentages in their oxide state (SiO_2, Al_2O_3, Fe_2O_3, MgO, CaO, Na_2O, K_2O, TiO_2, P_2O_5 and MnO), and minor elements analysed are presented as concentrations in parts per million (ppm) (V, Cr, Co, Zn, Rb, Sr, Zr, Y, Nb, Th and U).

2.4 Trace Element Geochemistry

The inductively coupled plasma – mass spectrometry (ICP-MS) in the Geochemistry Laboratory at the University of Ottawa was used to measure trace and rare earth elements. Approximately 50 mg of each powdered rock sample was subjected to a two-step digestion. For the first step, the sample was weighed and mixed with 3mL aqua regia (1:3 ratio of HNO_3:HCl) and heated on a hot plate at 110 °C for 24 hours, and subsequently centrifuged with deionized water. The resulting clear solution was brought to 10.0 g quantitatively with deionized water, and then further diluted by 10- and 100-fold for measurement on the ICP-MS. The residue from the first step was then again digested for 24 hours at 110 °C, but this time mixed with 0.5 ml of HF.

The solution was evaporated to near dryness, the residue heated with 0.5 ml of concentrated HNO_3 and re-dissolved, then centrifuged
with about 2 ml of deionized water, and the total volume of the solution was then brought to 10.0 g. It was further diluted by 10-fold for the measurement on the ICP-MS to obtain the elemental abundance for Ni, Cu, Y, Ba, La, Ce, Pr, Nd, Sm, Eu, Gd, Tb, Dy, Ho, Er, Tm, Yb, Lu, Pb, Th, and U. Elements were measured using the Agilent 8800QQQ Triple Quadrupole ICPMS Spectrometer. Samples were bracketed every 5 analyses by a calibration standard and a blank to measure and correct for sample drift. Detection limits range from .001 to 1 ppb for the elements measured, and all elemental abundances were on average greater than detection limits. To manage the range of concentrations in calibration standards, samples were run twice. Trace elements were analysed first at 10x dilution, and major and minor elements were subsequently analysed at 100x dilution.

2.5 Isotopic Analysis

Nd–Sr isotope measurements were carried out on a Multi-Collector ICP-MS (Neptune) at the Isotope Geochemistry and Geochronology Research Centre at Carleton University. Isotope analyses were performed on the second digestion following complete removal of the labile fraction by aqua regia in order to ensure only the detrital fraction remained.

The Sr and bulk REE were separated in 10 mL Bio-Rad polypropylene columns using Dowex AG50-X8 cation resin. The samples digested by the procedure described above (see 2.4) and then dried down on a hot plate at 90 °C. The dried residue was then redissolved overnight in 1.5 mL 2.5N HCl on a cool hotplate. Samples were added to the columns, which were then washed with ~1 mL 2.5N HCl. After letting 16 mL 2.5N HCl drain through the columns, Sr was collected in beakers with 7 mL 2.5N HCl. After letting 3.5 mL 6N HCl pass through the

columns, REEs were eluted in separate beakers using 9 mL 6N HCl. Sr and REE elutions were dried on a hotplate at 90 °C.

For Nd purification, the bulk REE residue was redissolved in 0.26N HCl and loaded into an Eichrom chromatographic column containing a 2 cm-thick bed of Teflon powder coated with HDEHP (di(2-ethylhexyl) orthophosphoric acid) (Richard et al., 1976). Nd was eluted using 0.26N HCl. Total procedural blanks for Nd are <50 pg and therefore insignificant. $^{143}Nd/^{144}Nd$ ratios were normalized to the JNdi-1 internal lab standard, for which the agreed-upon value is $^{143}Nd/^{144}Nd = 0.512115$ (Tanaka et al., 2000). The average $^{143}Nd/^{144}Nd$ measured for the internal lab Nd standard is 0.512089 ± 8, based on 7 runs between October 2021 and September 2022, for a total of 16 runs. All quoted uncertainties are 2-sigma standard deviations of the mean. Initial epsilon Nd values at 600 Ma are calculated using $(^{143}Nd/^{144}Nd)_{(CHUR,\ 0\ Ma)} = 0.512638$ and $(^{147}Sm/^{144}Nd)_{(CHUR,\ 0\ Ma)} = 0.1967$ (CHUR = chondritic uniform reservoir). Initial εNd values at 600 Ma were computed using values obtained from mass spectrometry.

Strontium was purified a second time with micro-columns using Eichrom Sr resin. Approximately 100 μL resin (50-100 microns thick) was added to the columns and allowed to settle. The resin was washed with 1200 μL water and conditioned with 400 μL 7N HNO_3. Sample was then added to the columns and washed with 1600 μL 7N HNO_3. Finally, strontium was collected in snap-top beakers with 1600 μL water. Measured Sr isotope ratios were mass bias corrected (using $^{86}Sr/^{87}Sr = 0.1194$, Steiger and Jäger, 1977) to correct for instrument fractionation. A Sr standard was analyzed every 12 or fewer samples. The average ratio measured for the Sr standard is $^{86}Sr/^{87}Sr = 0.708023 \pm 35$, based on 6 runs between August 2021 and August 2022, and a total of 19 standards run. The agreed-upon value is $^{86}Sr/^{87}Sr = 0.708000$. Total procedural blanks for Sr are < 250 pg. $^{86}Sr/^{87}Sr$ results were normalized to NIST NBS987

= 0.710245. Initial $^{86}Sr/^{87}Sr$ values were calculated using the Rb and Sr abundance obtained using mass spectrometry.

Chapter 3: Results

The purpose of this study is two-fold: use major element, trace element, and isotopic data to a) investigate the origin of the ICC4B sample with the anomalous detrital zircon population of 2.4-2.0 Ga, and b) to investigate broad scale provenance trends through a 2.5 km-thick succession in rocks of the Windermere Supergroup at Castle Creek study area (CC). As such, results will be presented, first, as broad scale trends in strata from basin-floor deposits in the upper Kaza Group (UKG) to upper continental slope deposits of the Isaac Formation, and second, as smaller scale trends, focusing on the stratigraphic level of ICC4B near the anomalous sample exhibiting lower Paleoproterozoic detrital zircon ages.

3.1 Detrital-Zircon U-Pb Type Populations

Representative CL images of zircons are shown in Figure 3.1. and U-Pb results are plotted in Tera-Wasserburg diagrams (Figure 3.2. ; Figure 3.3. ; Figure 3.4.). All analysed detrital zircons have Th/U > 0.1, with most being > 0.4. The detrital zircons from the eleven sandstone samples show variable grain size and morphology but exhibit similar age distributions. The zircons are typically 40-220 μm long with aspect ratios of 1:1 to 4:1 and are dominated by subangular to

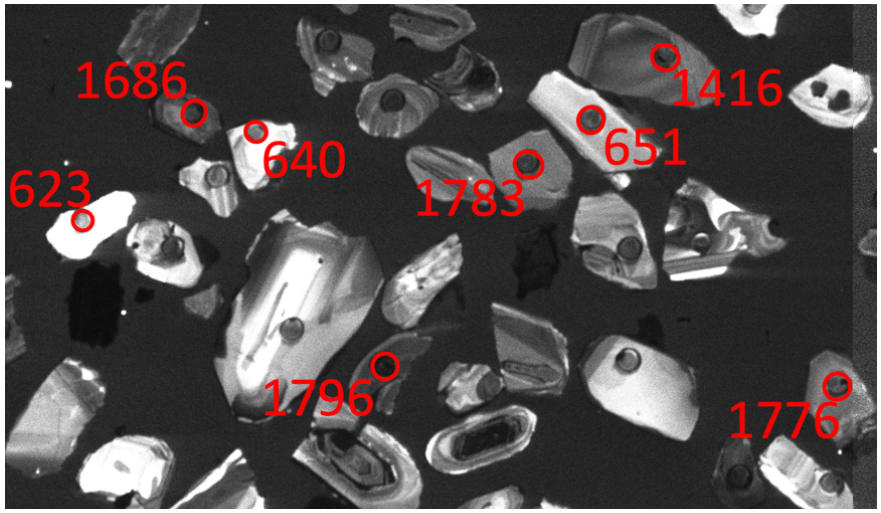

Figure 3.1. Example of cathodoluminescence (CL) images of zircons. The solid circles represent U-Pb analysis pits. U-Pb spot ages given here and elsewhere are $^{206}Pb/^{238}U$ ages for zircon components younger than 1.0 Ga and $^{207}Pb/^{206}Pb$ ages for those older than 1.0 Ga.

subrounded morphologies. In the CL images, many zircons exhibit oscillatory- or irregular concentric-zoning, whereas some show no internal structures and are structureless.

Many U-Pb ages were either > 5% discordant or showed disrupted Pb-U ratios but reproducible $^{207}Pb/^{206}Pb$ ratios during analyses. The results and interpretations presented here are based only on measurements showing < 5% discordant ages.

3.1.1 Type 1 Detrital Zircon Signature

This signature is observed in strata from the middle Kaza Group up to channel 1 of the Isaac Formation (ICC1). The age spectrum is distinctively bimodal, with a large number of Meso- to Neo-Archean ages scattered between 3.00-2.48 Ga, representing 33% of the total number of analyses, and a sharp Paleoproterozoic peak around 1.8 Ga, with 57% of the total number of analyses lying between 1.90 and 1.68 Ga (Figure 3.2.). Other ages include 12 grains with Paleoproterozoic ages between 2.06 to 1.92 Ga, 11 grains with Mesoproterozoic ages (1.59 to 1.13 Ga), 5 grains with Paleo- to Meso-Archean ages (3.31 to 3.10 Ga), and 1 grain dated at 2.22 Ga.

3.1.2 Type 2 Detrital Zircon Signature

The Type 2 signature is observed in strata from ICC3 up to ICC5 and consists of a large number of Meso- to Neo-Archean ages scattered between 3.00-2.50 Ga, representing 19% of the total number of analyses, and a sharp Paleoproterozoic peak around 1.8 Ga, with 57% of the total number of analyses lying between 1.98 and 1.57 Ga (Figure 3.3.). Additionally, there is a significant Neoproterozoic peak around 650 Ma, with 11% of the total number of analyses lying between 606 and 708 Ma. Note that this 650 Ma peak is absent in all other Windermere samples. The strength of the 650 Ma peak appears to increase stratigraphically upward from ICC3 (19-GC-1; although note low n=21 for this sample), where only 6 grains have the peak, to the base of

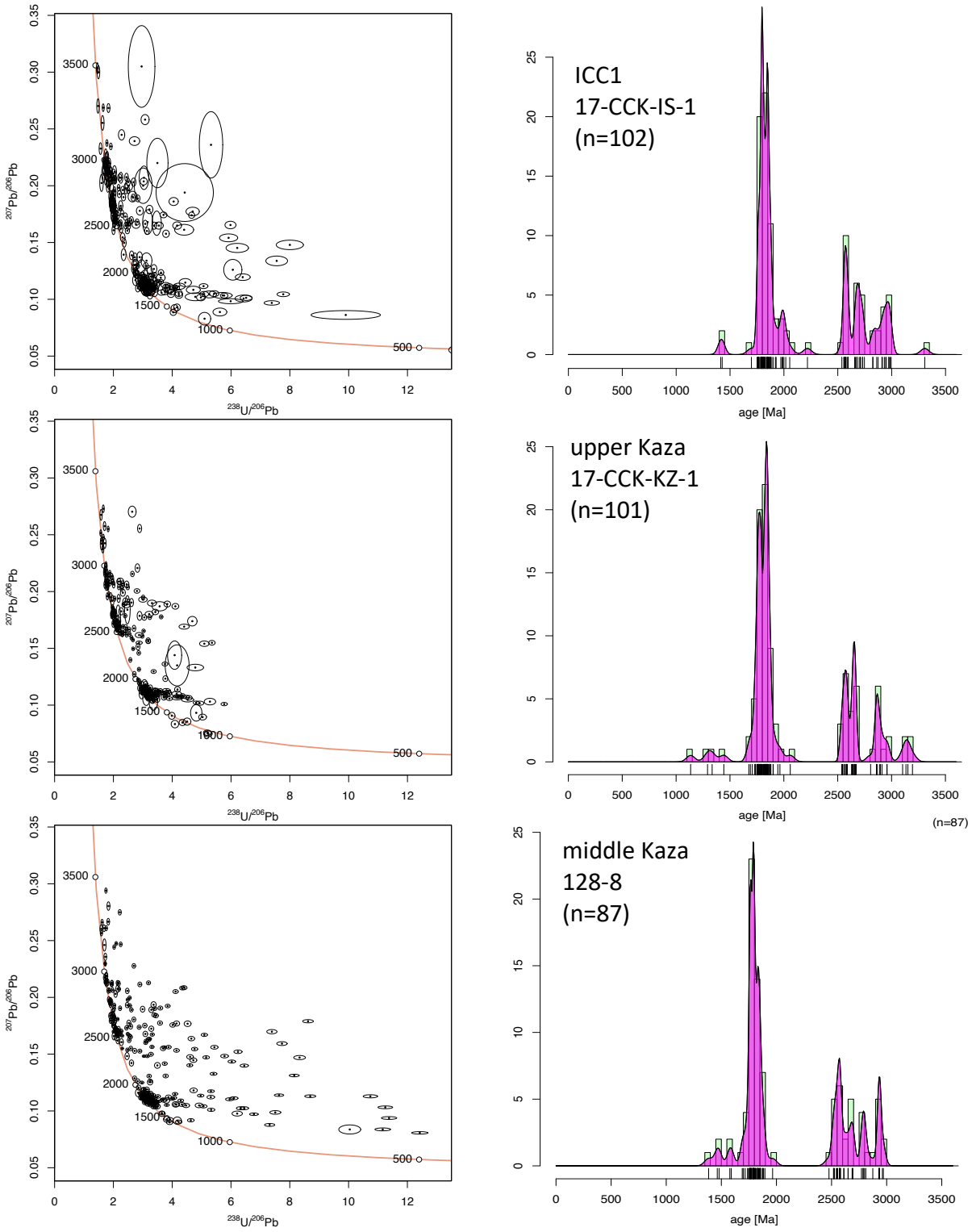

Figure 3.2. Tera-Wasserburg diagrams (left side) show U-Pb data for the middle Kaza Group, upper Kaza Group, and ICC1 (Type 1 signature). Each ellipse represents a single spot analysis and its 2σ standard error. Kernel density estimation (KDE) diagrams (right side) show distribution of ages.

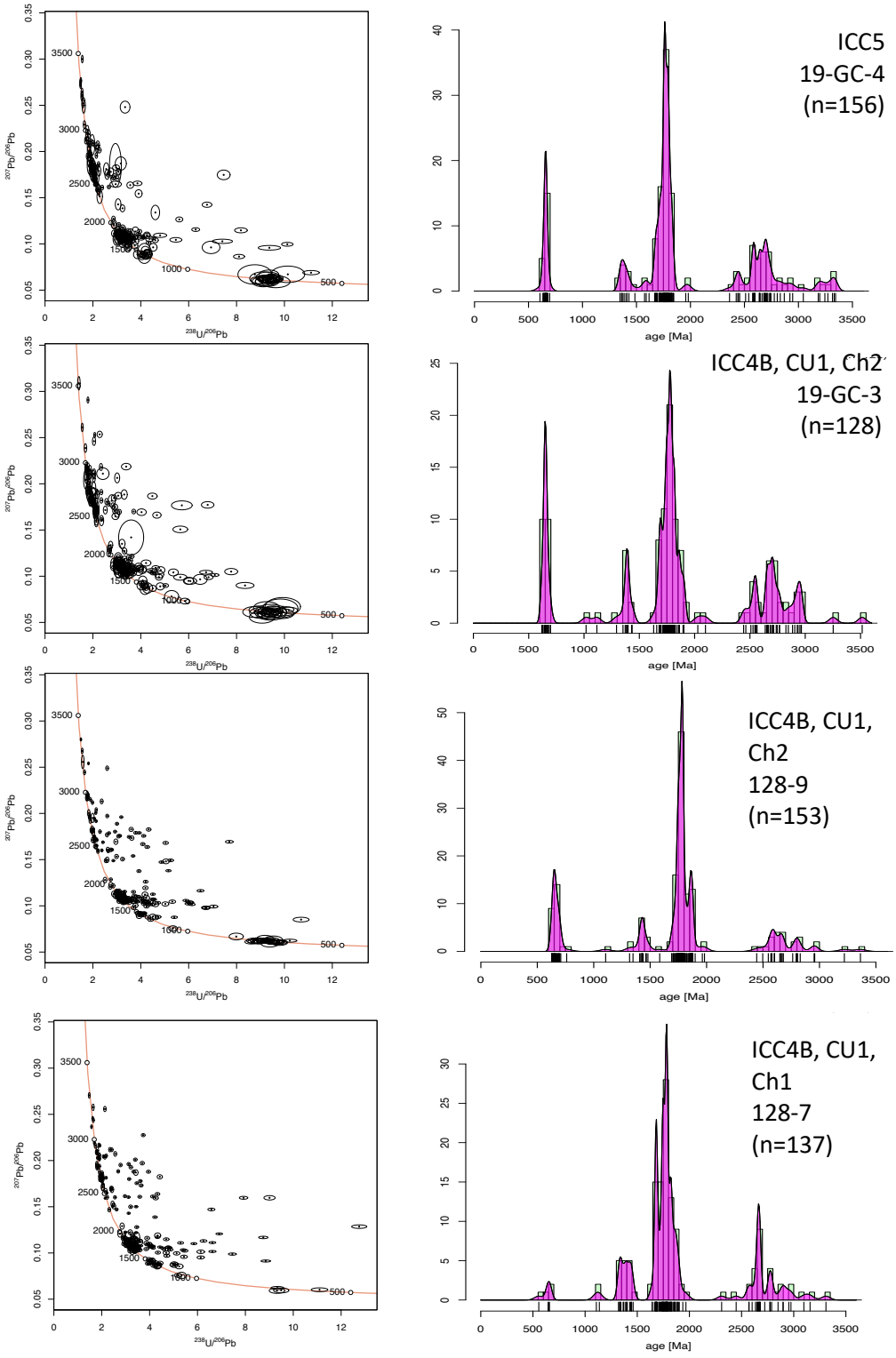
ICC5
19-GC-4
(n=156)
ICC4B, CU1, Ch2
19-GC-3
(n=128)
ICC4B, CU1,
Ch2
128-9
(n=153)
ICC4B, CU1,
Ch1
128-7
(n=137)
age [Ma]

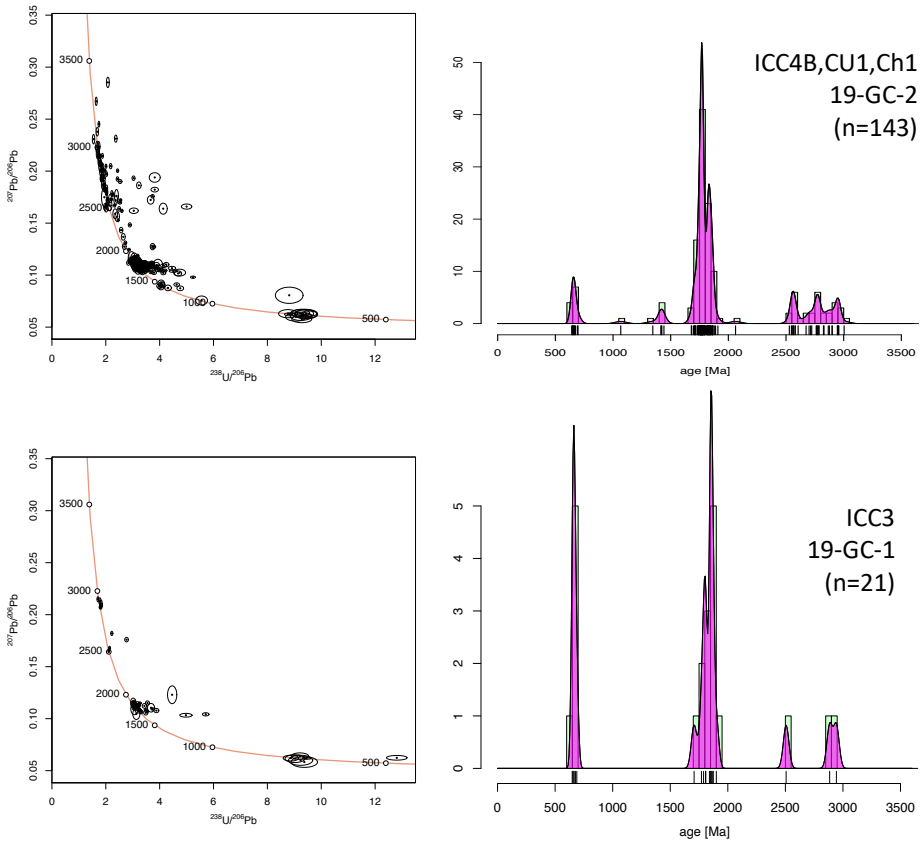

Figure 3.3. Tera-Wasserburg diagrams (left side) show U-Pb data for ICC3, ICC4, and ICC5 (Type 2 signature). Each ellipse represents a single spot analysis and its 2σ standard error. Kernel density estimation (KDE) diagrams (right side) show distribution of ages.

ICC4 (19-GC-2), where 11 grains have the peak, to the top of ICC4 and ICC5 (19-GC-3 and 19-GC-4), where each sample has 20 grains with the peak. Other ages include Mesoproterozoic ages, with 53 grains with between 1.49 and 1.29 Ga and 6 grains between 1.14 and 1.02 Ga, 15 grains with Paleo- to Meso-Archean ages (3.51 to 3.05 Ga), 13 grains with Paleoproterozoic ages between 2.46 and 2.03 Ga and 1 grain with a Neoproterozoic age of 760 Ma.

3.1.3 Anomalous detrital zircon populations in ICC4B

Two samples obtained from ICC4B, specifically channel unit 1, channel fill 2, exhibit signatures unlike those in any of the other samples analysed (Figure 3.4). Sample 128-10 has components of a typical Type 2 signature with 10% Meso to Neo-Archean ages (2.95 to 2.54

Ga), 42% Paleoproterozoic ages (1.92 to 1.61 Ga), as well as a sharp Neoproterozoic (Cryogenian) peak between 687 to 632 Ma, comprising 23% of total samples analysed. However, this sample contains 15 grains that exhibit younger Neoproterozoic (Ediacaran) ages, which uniquely range from 625 to 595 Ma.

Sample 17-CCK-IS-2 shows no evidence of the typical Archean and Paleoproterozoic bimodal signature. Instead, 92% of the total number of analyses have Paleoproterozoic ages scattered between 2.35 and 1.79 Ga, with more narrow groupings between 1.98 and 1.87 Ga, 2.12 and 2.05 Ga, and 2.35 and 2.27 Ga. Only 8 grains have Neo-Archean ages (2.65 to 2.55 Ga), and 1 grain has a Paleo-Archean age of 3.34 Ga. One single grain has a Mesoproterozoic age of 1.05 Ga.

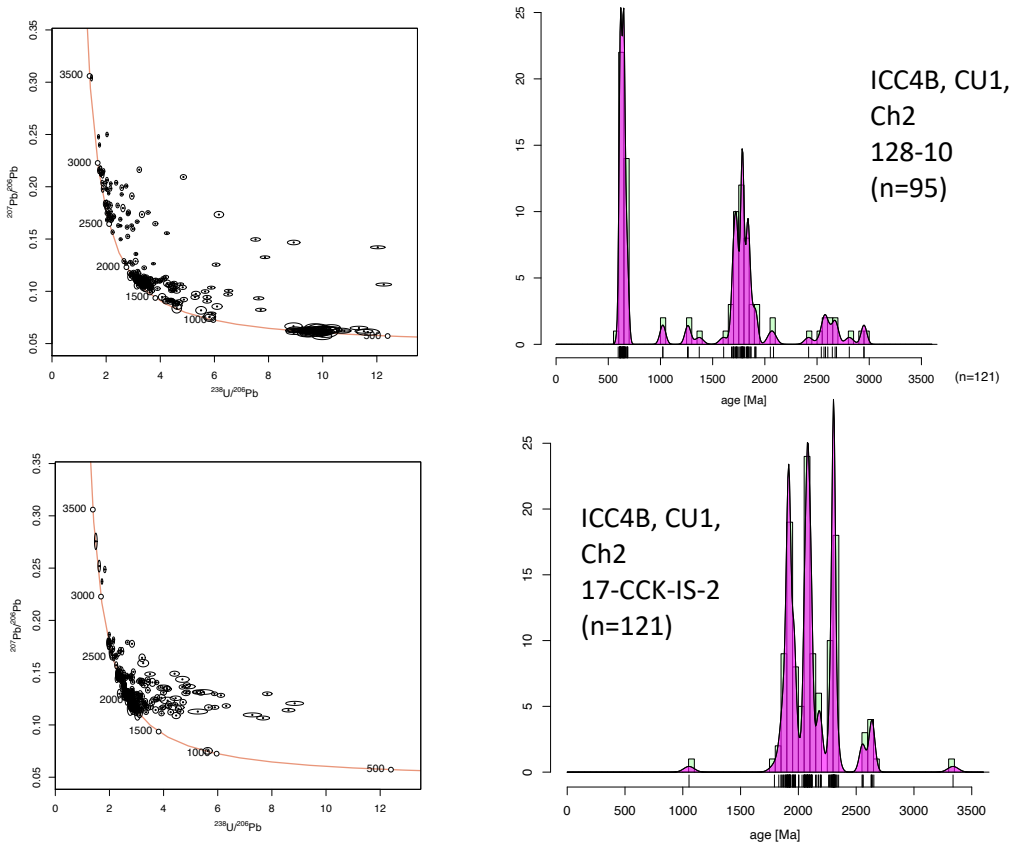

Figure 3.4. Tera-Wasserburg diagrams (left side) show U-Pb data for anomalous signatures in strata of ICC4B. Each ellipse represents a single spot analysis and its 2σ standard error. Kernel density estimation (KDE) diagrams (right side) show distribution of ages.

3.2 Major Element Geochemistry

XRF analyses on whole-rock samples from UKG stratigraphically upward to the top of the section above ICC6 show Al_2O_3 contents between 11.9 and 33.0 wt%, with an average of 21.3 wt%. Compared to the Upper Continental Crust (UCC) composition, represented by the Post-Archean Average Shale (PAAS) (McLennan, 2001), the studied samples have higher contents of total iron oxide (Fe_2O_3), between 2.2 and 13.6 wt% with an average of 7.0 wt% (PAAS = 5.0 wt%), MgO between 0.74 and 4.6 wt% with an average of 2.5 wt% (PAAS = 2.2 wt%), and TiO_2, between 0.5 and 2.0 wt% with an average of 0.9 wt% (PAAS = 0.7 wt%) (Figure 3.5.). The K_2O and Na_2O contents vary between 1.9 to 9.3 wt% and 0.2 to 2.4 wt% respectively. The mudstones have variable carbonate content, with CaO varying from 0.0 to 5.3 wt%, with an average of 0.5 wt%. There are some stratigraphic trends apparent from the major

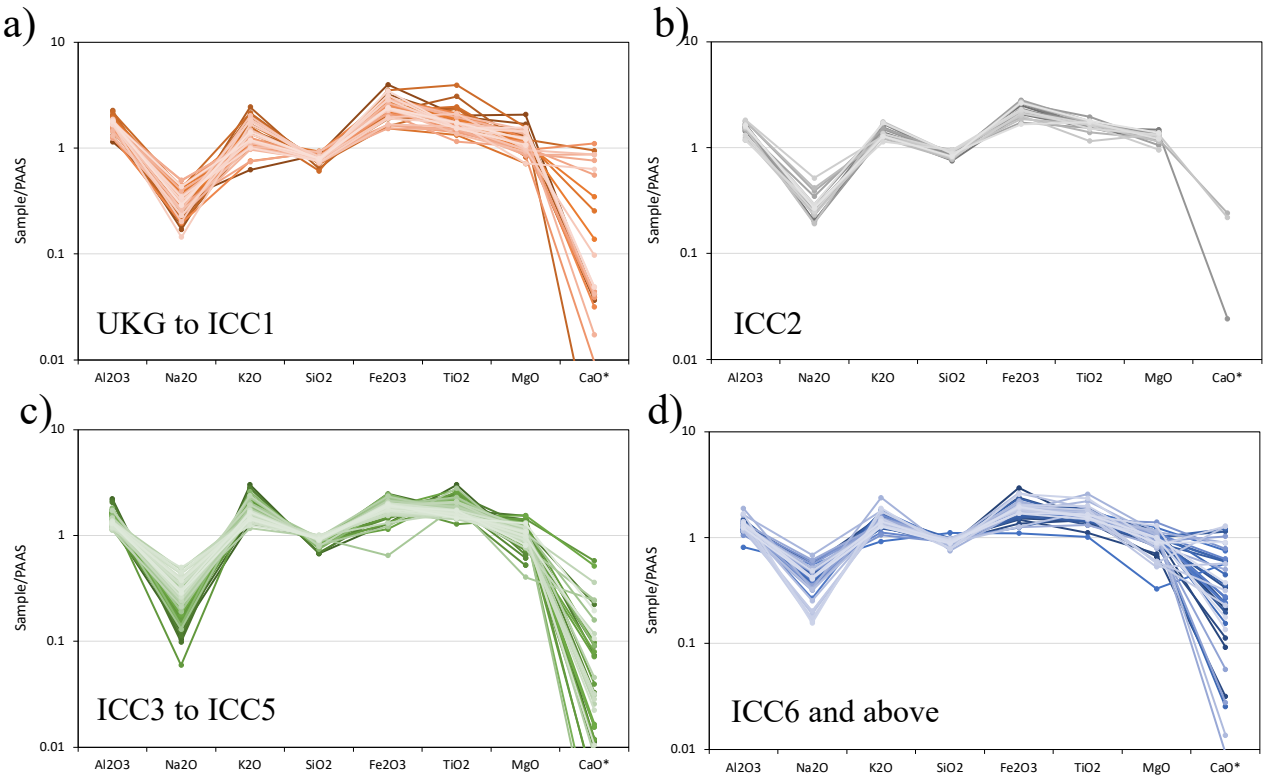

Figure 3.5. Major elemental oxides normalized to PAAS values for average shale, for: a) UKG to ICC1; b) ICC2; c) ICC3 to ICC5; d) ICC6 and above.

element geochemical data. Na_2O, MgO, TiO_2 and Fe_2O_3 tend to be highest between the UKG and ICC1, whereas SiO_2 is relatively low. Between ICC2 and ICC4, Na_2O, TiO_2 and Fe_2O_3 decrease whereas SiO_2 and K_2O increase. Above ICC6, Na_2O increases again, and Al_2O_3 decreases.

Bulk chemical variations in some major elements are plotted against Al_2O_3 on various diagrams (Figure 3.6.). Strong positive correlation between Al_2O_3 and K_2O in the studied samples shows that Al distribution is controlled by the abundance of K-bearing minerals (i.e., potassium feldspars, mica and clay minerals) (Figure 3.6a). TiO_2 also displays strong positive correlation with Al_2O_3 (Figure 3.6b). The absence of a significant correlation of Al_2O_3 with Na_2O suggests that Na is not associated with plagioclase feldspar. Weak positive correlation of Al_2O_3 with CaO but absence of a significant correlation with MgO (Figure 3.6c) suggests that Ca and Mg content are partially contained in clay minerals, but also probably in minor carbonate cements. Other oxides show no significant trends in the studied samples. The difference in Fe_2O_3+MgO content in the samples, which may be variable in mudstones of different tectonic settings, is not supported by differences in the intensity of weathering, which is estimated by the K_2O/Na_2O and Al_2O_3/SiO_2 ratios (Figure 3.7).

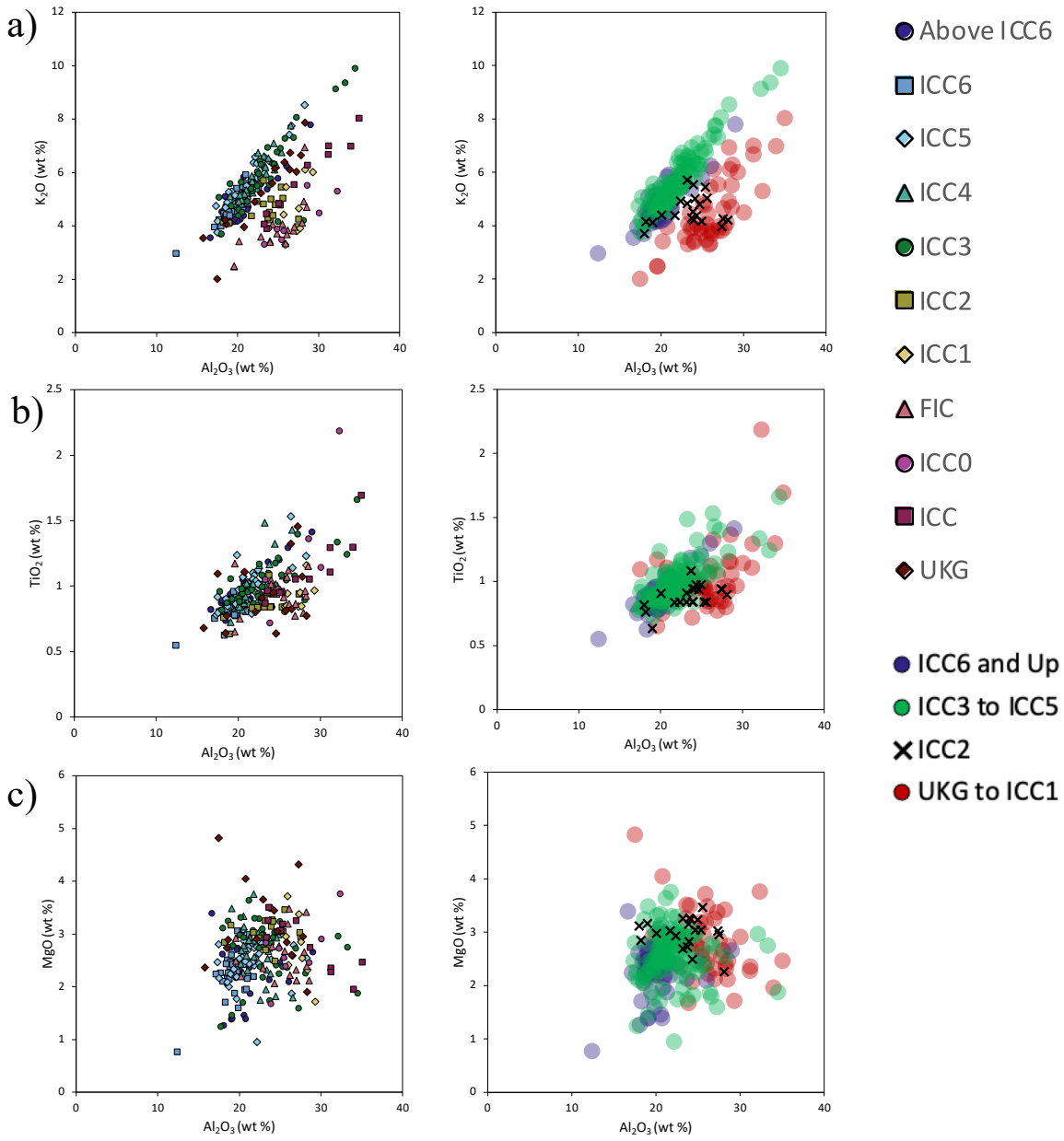

Figure 3.6. Distribution of samples for Al_2O_3 vs. other major oxides: a) K_2O, b) TiO2, c) MgO. Left side of page displays data by individual units; right side of page displays data as units categorized by similar characteristics into four separate groups.

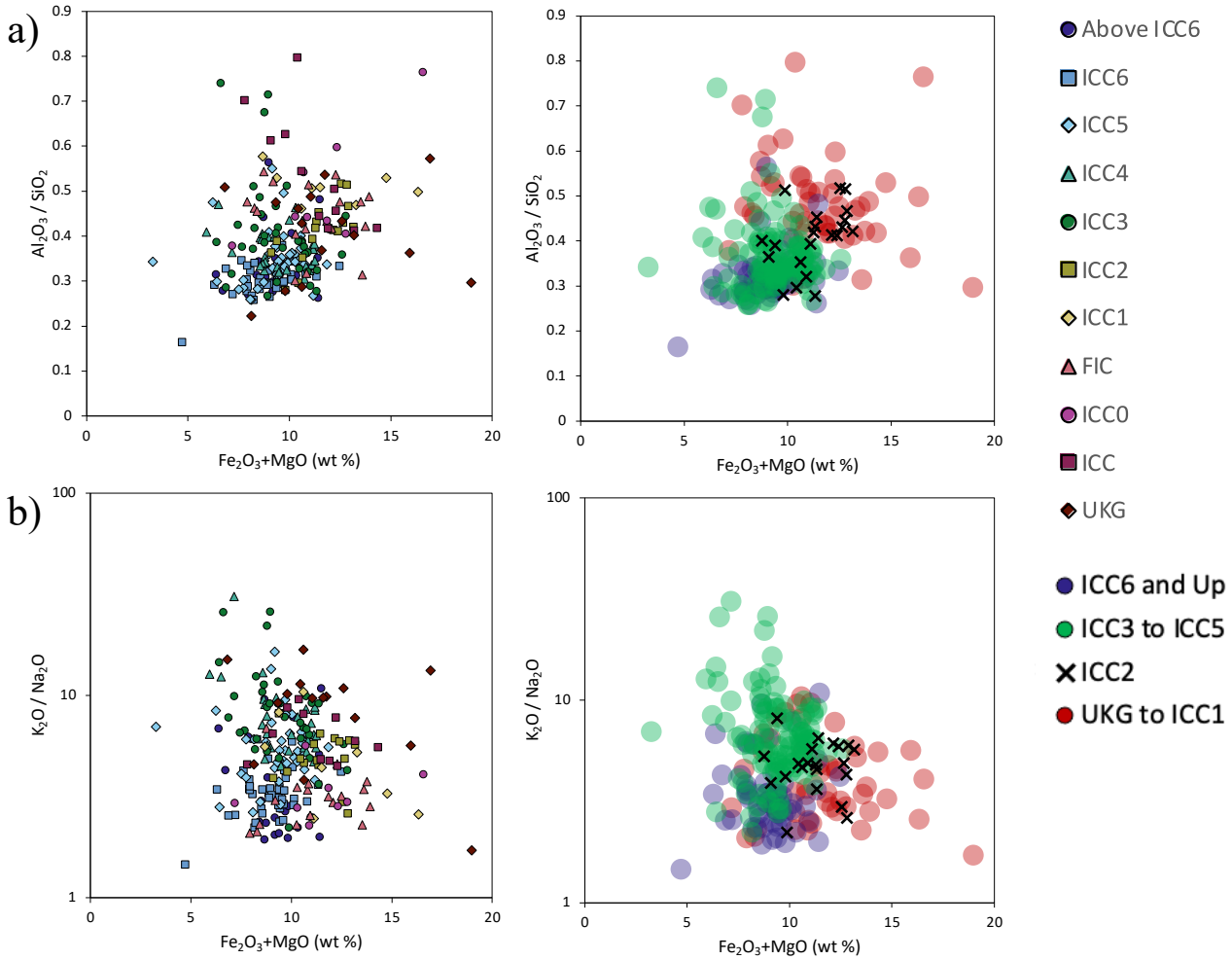

Figure 3.7. Distribution of samples for sum of major oxides Fe_2O_3 + MgO vs. ratios of other major oxies: a) Al_2O_3/SiO_2; B) K_2O/Na_2O. Left side of page displays data by individual units; right side of page displays data as units categorized by similar characteristics into four separate groups.

3.3 Trace Element Geochemistry

According to their typical behavior during fractional crystallization, weathering, and recycling, trace elements preserve characteristics of the source rocks in sedimentary rocks (Cox et al., 1995; McLennan et al., 1990; Taylor and McLennan, 1995; Wronkiewicz and Condie, 1989). In particular, the high field strength elements (e.g. Zr, Ta, Ti, Th, Nb), Sc, Al, Co, Hf, and certain REE (La, Yb), can provide useful information about provenance due to their stability and different affinities to either mafic or felsic rocks (Armstrong-Altrin et al., 2015; Bhatia and Crook, 1986; Crichton and Condie, 1993). Previous studies have shown that Th/Sc-Zr/Sc, Eu/Eu*, La/Sc-Co/Th, La/Co and La/Th-Hf diagrams can be used to identify sediment

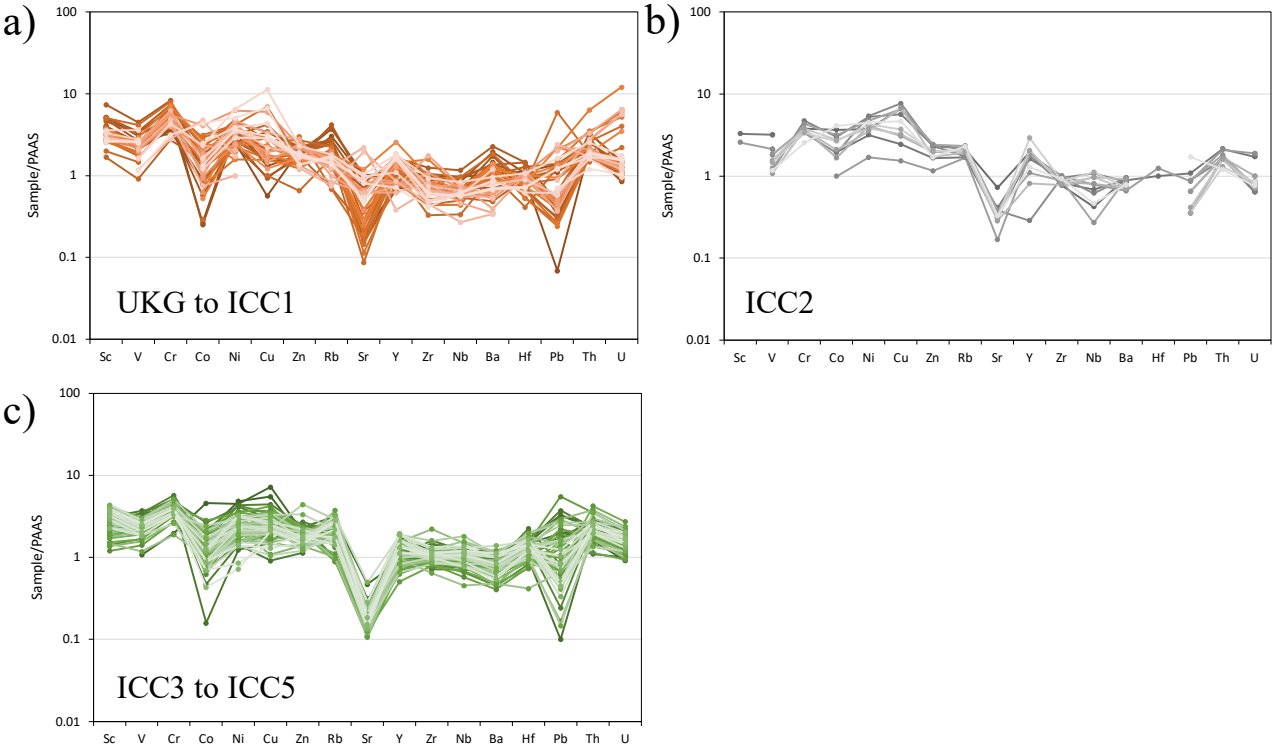

Figure 3.8. Distribution patterns of selected trace elements normalized by Post-Archean Average Shale (PAAS), for: a) UKG to ICC1; b) ICC2; c) ICC3 to ICC5.

provenance (Absar et al., 2009; Amedjoe et al., 2018; Bhatia and Crook, 1986; Condie and Wronkiewicz, 1990; McLennan et al., 1990; Paravidini et al., 2021; Tao et al., 2017). Eu/Eu* is defined as the anomaly of Eu relative to other REE, and can be calculated as follows:

(6) $Eu/Eu^* = Eu_N/[Sm_N)(Gd_N)]^{1/2}$

Trace element concentrations are typically displayed in normalized trace element spider diagrams, arranged in increasing atomic number (Figure 3.8). All the analyzed trace element concentrations have been normalized to the Post-Archean Average Shale (PAAS).

3.3.1 Large-ion lithophile elements (LILE, Rb, Cs, Ba, Sr), Th and U

For the samples analysed the alkali elements Rb and Ba have average concentrations ranging from 63 to 413 ppm, and 363 to 6510 ppm, respectively, and range from slightly depleted to strongly enriched compared to PAAS (Figure 3.8). The elements Sr and Cs tend to be depleted compared to PAAS, with average concentrations ranging from 27.5 to 2038 ppm, and 0 to 17.8 ppm, respectively. There are positive correlations between K_2O and Rb ($r = 0.936$), Cs ($r = 0.877$) and Ba ($r = 0.811$), indicating that clay minerals such as illite and muscovite are the main control on LILE abundance (McCulloch and Wasserburg, 1978). In contrast, Sr is only weakly correlated with K_2O ($r = 0.306$) and is moderately correlated with CaO ($r = 0.596$), indicating a significant contribution from carbonate minerals.

Stratigraphic trends in LILE show an enrichment in the UKG, and in the vicinity of ICC4. Near ICC4 the alkali elements Rb and Ba tend to be enriched compared to PAAS, with average concentrations of 221.14 ppm and 863.98 ppm, respectively (Figure 3.9), whereas Sr and Cs tend to be depleted compared to PAAS, with average concentrations of 57.98 ppm and 8.97 ppm, respectively. Sr is more depleted in ICC4 compared to ICC3 and the lower Isaac Formation

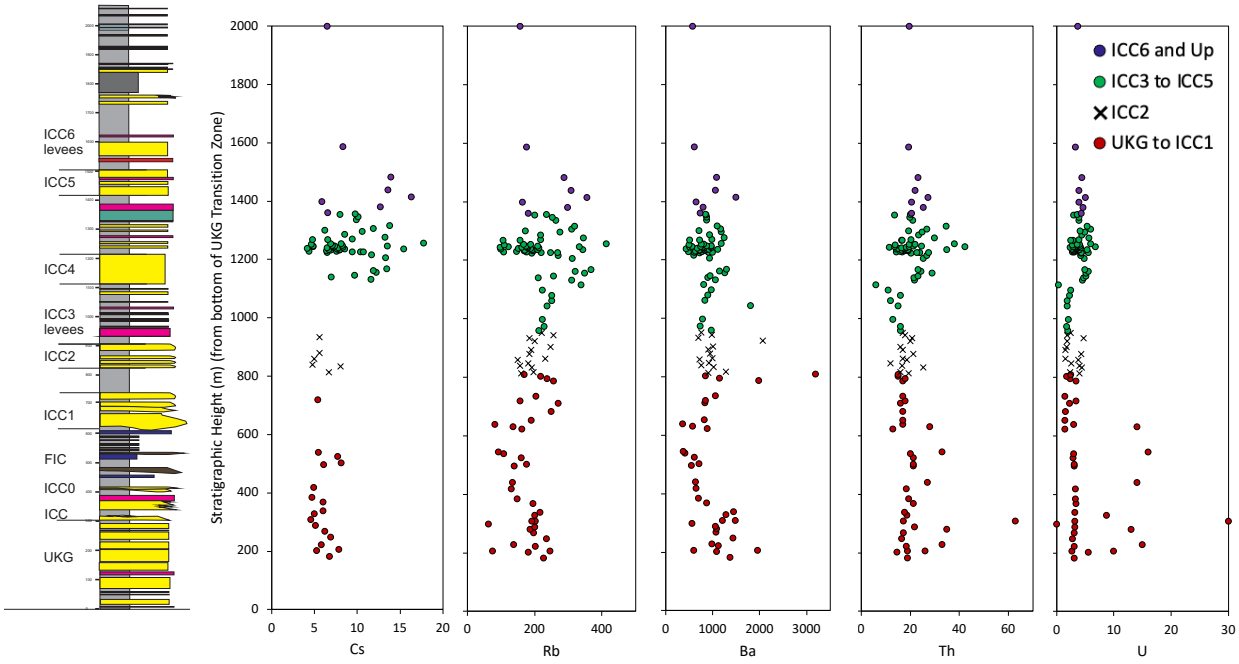

Figure 3.9. Stratigraphic trends for LILE, from UKG to ICC6.

(LIF), which includes ICC, ICC0, FIC. Th and U concentrations of ICC4 are also higher than in PAAS, as is the Th/U ratio at 5.30 (Figure 3.9).

3.3.2 High field strength elements (HFSE, Zr, Hf, Y, Nb and Ta)

HFSE are preferentially partitioned into the melt during partial melting and crystallization of magmas, thus are enriched in felsic rocks (Taylor and McLennan, 1995). Due to their immobile behaviour during post-depositional processes, like REE, these elements are robust provenance indicators. The average concentration of HFSE is depleted in the CC strata when compared with PAAS, except for some elements in a small number of samples (Figure 3.10). Average concentrations for Zr range from 78.8 to 531 ppm, Hf from 0 to 13 ppm, Ta from 0 to 4 ppm, and Nb from 1 to 47.1 ppm.

In general, concentrations of HFSE tend to be lowest in the UKG and highest around ICC4 (Figure 3.10.). ICC4 samples show average concentrations of Zr of 138.36 ppm and Hf of

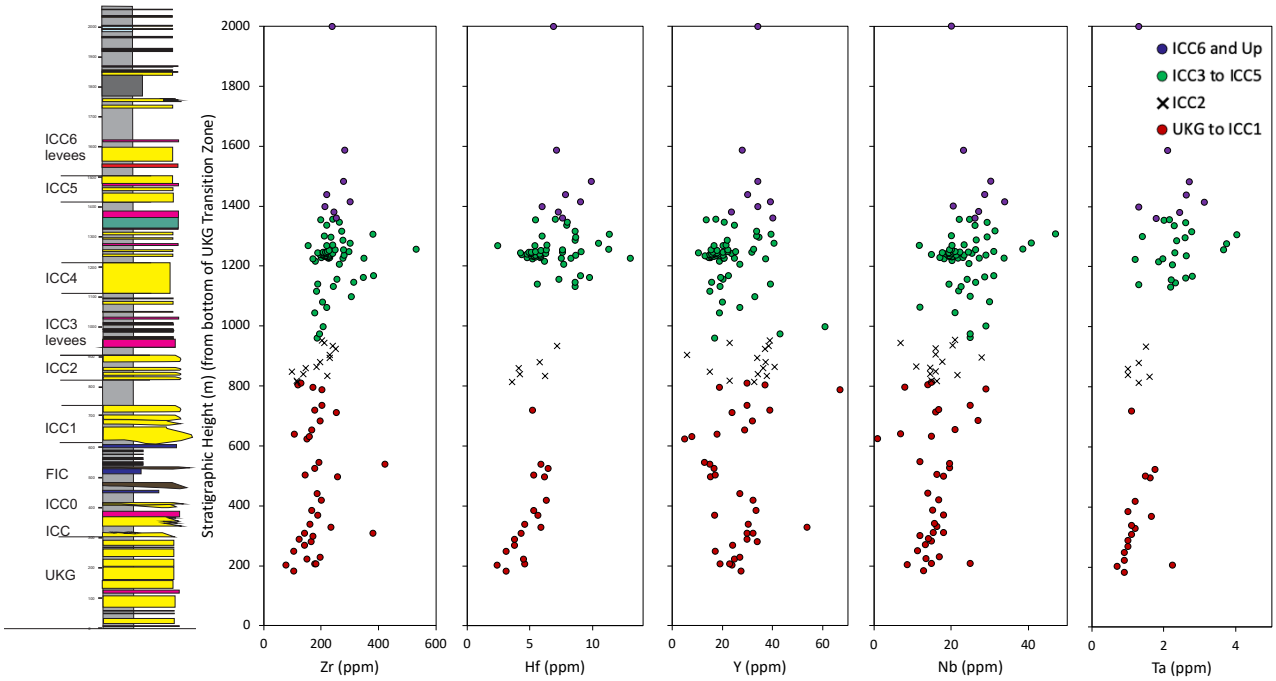

Figure 3.10. Stratigraphic trends for HFSE, from UKG to ICC6.

3.70 ppm. The average concentrations of Ta and Nb are 2.46 ppm and 24.41 ppm, respectively. The Zr/Hf ratios in all the analyzed samples range from 32.79 to 43.50 (average = 37.99) indicating that these elements are controlled by the abundance of zircons. Moreover, being higher than UCC (32.8, Taylor and McLennan, 1985), suggests that zircon abundance reflects sediment recycling.

3.3.3 Transition trace elements (TTE, Cr, V, Co, Ni and Sc)

The transition metals are highly compatible and tend to behave similarly during fractional crystallization of magmas, being incorporated into crystalline structures (Taylor and McLennan, 1995). Consequently, they are enriched in mafic to ultramafic rocks, but potentially mutually fractionated during later weathering. Mudrock samples in this study are typically depleted in Co, V and Ni, which may be attributed to the low levels of organic matter and secondary minerals. Only Cr and Sc show above average enrichment (Figure 3.11).

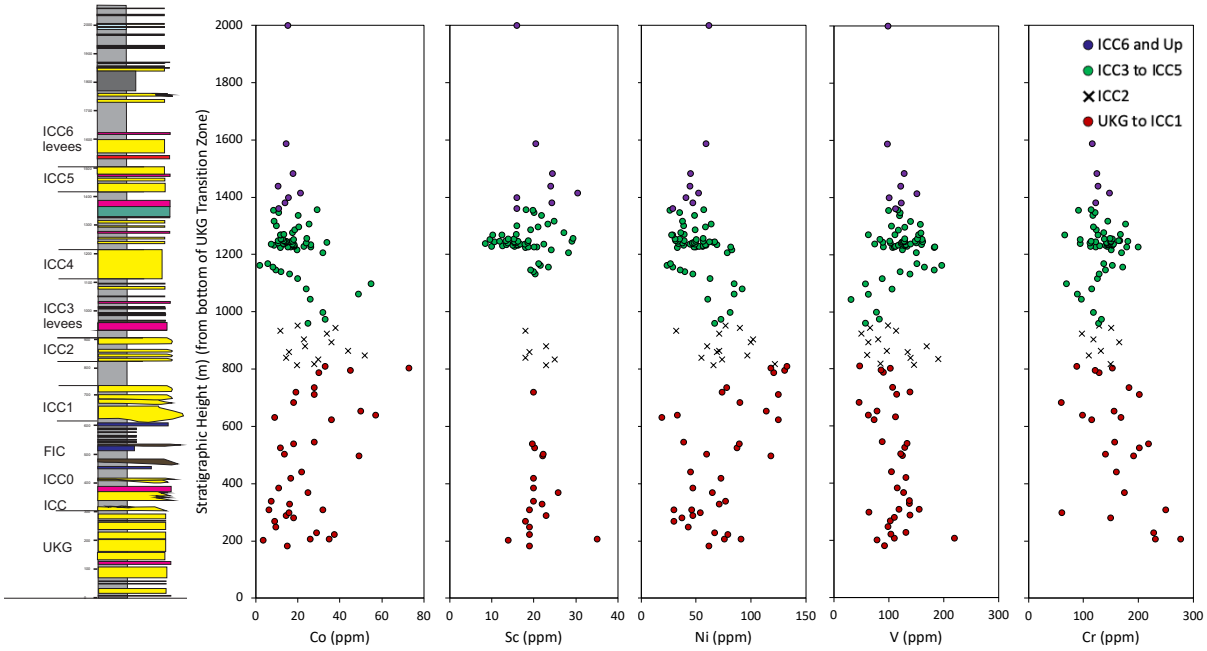

Figure 3.11. Stratigraphic trends for transition trace elements, from UKG to ICC6.

In terms of stratigraphic trends, total concentrations of transition trace elements tend to be highest in UKG to ICC1, lowest in ICC2 to ICC3, and again higher in ICC4. There are positive correlations between K_2O-Sc ($r = 0.81$), K_2O-V ($r = 0.77$), Al_2O_3-Sc ($r = 0.93$), Al_2O_3-Cr ($r = 0.72$) and Al_2O_3-V ($r = 0.77$) suggesting that the abundance of these elements is controlled by clay minerals. Co and Ni are more variable and more poorly correlated with K_2O and Al_2O_3 indicating factors other than weathering of clay minerals control the distribution of these elements, for example that they are contained in primary mafic minerals.

3.3.4 Rare earth elements (REE)

Chondrite-normalized REE patterns (McLennan, 1985) are shown in Figure 3.12. Despite variable concentrations, their distribution patterns are similar to PAAS. Overall, chondrite-normalized REE patterns for the studied samples appear similar to each other, with high ΣLREE/ΣHREE, flat HREE patterns, and generally negative Eu anomalies (Figure 3.12). The

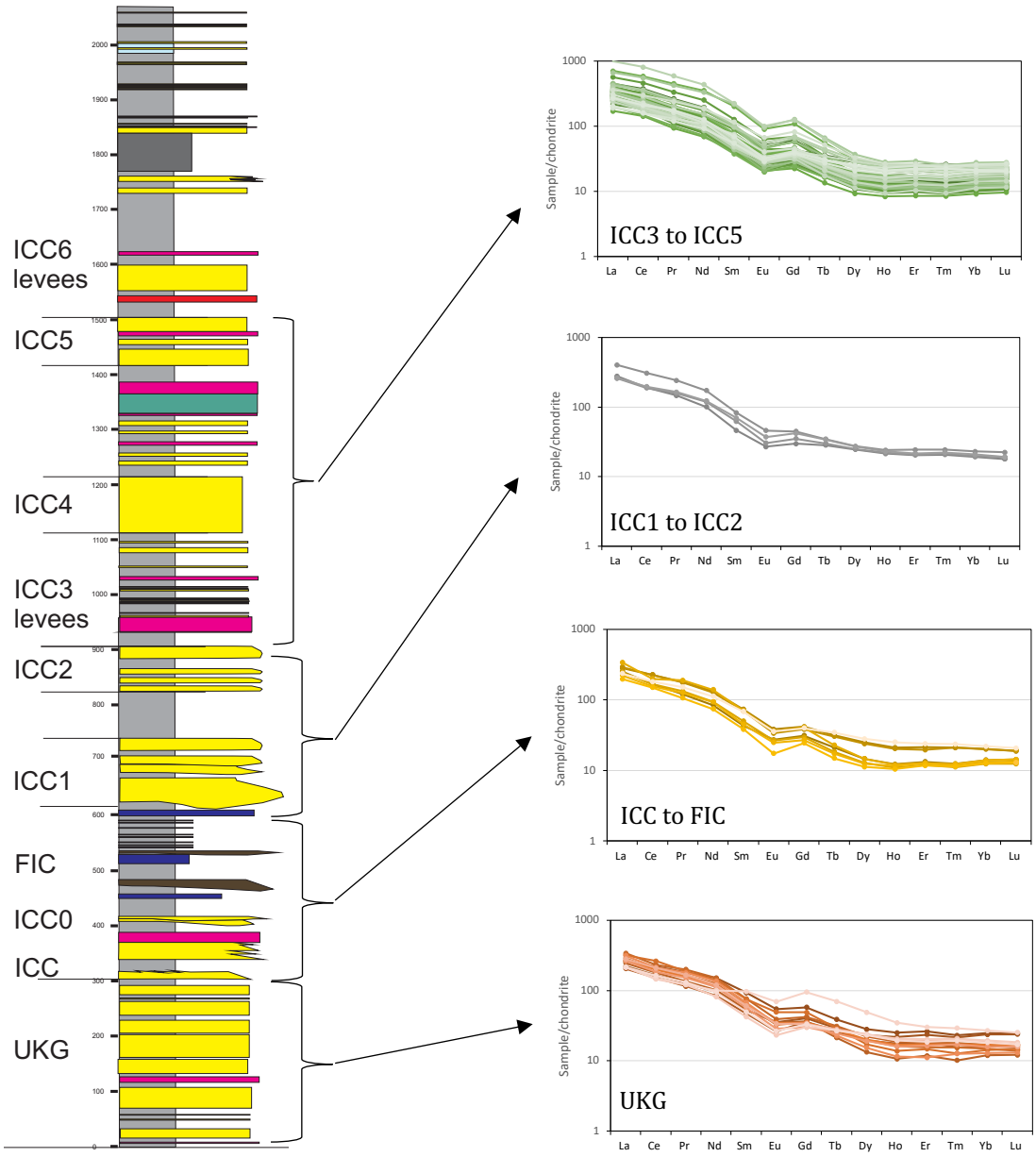

Figure 3.12. Chondrite-normalized REEs patterns for mudstone samples. The chondrite values are from (Boynton, 1984).

analyzed samples have Eu/Eu* values in the range of 0.79–1.03. The La/Sm Gd/Yb and La/Yb ratios range from 3.05 to 6.62, 1.69 to 5.56 and 12.70 to 45.02, respectively.

The analysis of REE of the ICC3 to ICC5 samples shows that the amount of total rare earth elements (ΣREE) is 186.76–1077.40 ppm (average 368.87 ppm), which is higher than the average value of ΣREE in the upper continental crust (146.4 ppm). Generally, the ΣREE content is comparatively low in the UKG and LIF. The ratio of ΣLREE/ΣHREE reflects the fractionation degree between the light rare earth elements (LREEs, including La, Ce, Pr, Nd, Sm, and Eu) and the heavy rare earth elements (HREEs, including Gd, Tb, Dy, Ho, Er, Tm, Yb, and Lu). The ratio of ΣLREE/ΣHREE in the study area is 10.95–24.20 (average 17.00), which is significantly higher than the ratio of PAAS (7.50). This indicates that the LREE is abundant, and the REE has a high degree of fractionation between light and heavy rare earth elements.

The ratio of La_N/Yb_N, La_N/Sm_N, and Gd_N/Yb_N represents the slope of the distribution curve in the chondrite-normalized REE diagram, and can be a measure of the fractionation of REE (Figure 3.13). The average ratio of La_N/Yb_N is 23.69 (ranging from 12.70 to 45.02) and La_N/Sm_N is 4.96 (ranging from 3.05 to 6.62), which collectively indicate enrichment of LREE. In contrast, Gd_N/Yb_N averages 2.93 (range: 1.69-5.56) suggesting a slight fractionation of HREE.

A moderate positive correlation between Zr-HREE (r = 0.499) suggests that HREE fractionation is only partly controlled by zircon abundance. There is a moderate positive correlation with LREE-Al_2O_3 (r = 0.406) and HREE- Al_2O_3 (r = 0.450) and with LREE-TiO_2 (r = 0.90) and HREE-TiO_2 (r = 0.87) but low correlation of P_2O_5 with LREE (r = 0.12) and HREE (r = 0.26), respectively. This indicates the variable influence of clay minerals and zircon, and minor influence of phosphate minerals, which tend to be enriched in REE.

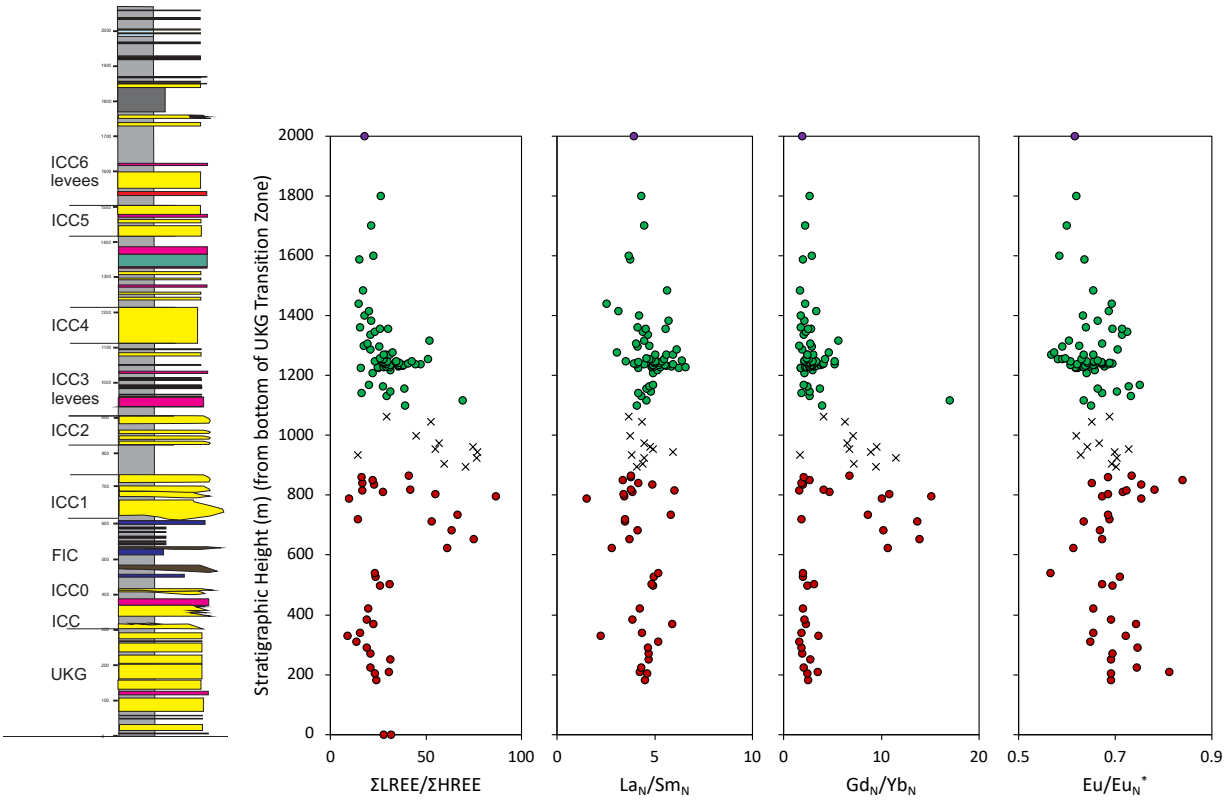

Figure 3.13. Stratigraphic trends for various ratios of REEs, from UKG to ICC6.

The Eu/Eu_N^* and Ce/Ce_N^* represent the magnitudes of the Eu and Ce anomalies, respectively (German & Elderfield, 1990). As Eu and Ce typically exist in different valence states depending on redox conditions, they are easily separated from other rare earth elements and exhibit an anomaly in the sediments, making it a good marker for tracking changes in the depositional environment (MacRae, Nesbitt, & Kronberg, 1992; Neal & Taylor, 1989). The Eu/Eu_N^* is 0.57–0.75 (average 0.65) indicating an obvious negative anomaly. Eu/Eu_N^* tends to be higher in the UKG and LIF and decreases through ICC3 to ICC6 (Figure 3.13). The Ce/Ce_N^* of 0.97–1.26 (average 1.05) suggests a slight positive anomaly. It is important to note that the Ce/Ce_N^* values in sedimentary rocks can be altered during post-depositional diagenesis, resulting in a good positive correlation between Ce/Ce_N^* and Eu/Eu_N^* and Ce/Ce_N^* and ΣREE, and a good negative correlation between Ce/Ce_N^* and Dy_N/Sm_N (Shields & Stille, 2001). Statistical results in

this study show no significant correlation between these elemental ratios, suggesting negligible post-depositional diagenetic alteration and the preservation of the primary detrital signature.

3.4 Isotope Geochemistry

3.4.1 Sm-Nd Isotopes

In this chapter Nd and Sr isotopic data are presented. Data are presented here by stratigraphic unit and compared with isotopic data from igneous units in western Laurentia as potential sediment sources (if any) in Chapter 4.

Neodymium isotopic data, specifically $^{143}Nd/^{144}Nd$ ratio of 28 samples, are presented in Table 3.1 and plotted against stratigraphic position in Figure 3.14. (note that labile rock fraction was removed prior to Nd and Sr isotope analysis). Sm (5.66 to 33.36 ppm) and Nd (33.82 to 201.33 ppm) values are somewhat higher than UCC and PAAS, and $^{147}Sm/^{144}Nd$ ratios (0.094–0.129) are similar but with a slightly wider range than typical terrigenous sediments (0.105–0.115; Taylor and McLennan, 1985). For the purpose of $\varepsilon Nd(T)$ calculation, a depositional age of 600 Ma was assumed.

Four samples from the lower Isaac Formation (LIF), which includes ICC, ICC0, and FIC, shows $\varepsilon_{Nd}(0)$ to range from -26.31 to -25.11 with an average value of -25.95; $^{147}Sm/^{144}Nd$ ratios range from 0.094 to 0.104; and T_{DM} ages range from 2.53 to 2.65 Ga. One sample from ICC3 exhibits an $\varepsilon_{Nd}(0)$ value of -21.57, $^{147}Sm/^{144}Nd$ ratio of 0.098, and a T_{DM} age of 2.24 Ga.

Twenty samples were analysed from ICC4; 15 from below the 'starry night debrite' (SND) regional marker, and 5 from immediately above. $\varepsilon_{Nd}(0)$ values range from -23.04 to -16.16 with an average of -20.64; $^{147}Sm/^{144}Nd$ ratios range from 0.0961 to 0.1288 with an average of 0.1060; and T_{DM} ages range from 1.96 to 2.44 Ga, with an average of 2.21 Ga (Figure 3.14.). Four samples from the lower part of ICC4 (below SND) yielded the most negative $\varepsilon_{Nd}(0)$ values from

Table 3.1. Nd isotopic data of sedimentary rocks from the Neoproterozoic Windermere Supergroup.

Sample	Nd (ppm)	Sm (ppm)	$^{143}Nd/^{144}Nd$	$^{147}Sm/^{144}Nd$	$^{143}Nd/^{144}Nd(T)$	εNd(0)	εNd(T)	T_{DM}
Upper Kaza Group								
KI-2	64.2	11.2						
Lower Isaac Formation								
KI-31	38.4	6.4						
KI-138	42.8	7.4	0.511298+-4	0.104100	0.510889	-26.1	-19.1	2.65
KI-139	63.5	10.4	0.511351+-3	0.098804	0.510962	-25.1	-17.6	2.53
KI-144	49.3	6.8						
KI-61	42.6	6.7	0.511292+-4	0.094321	0.510921	-26.3	-18.4	2.59
KI-64	33.8	5.7	0.511289+-5	0.101185	0.510891	-26.3	-19.0	2.64
ICC3								
J-16m	63.3	10.6						
J3-10m	55.9	9.1						
J5-20m	89.5	14.6	0.511532+-12	0.098386	0.511146	-21.6	-14.0	2.24
J6-27m	58.9	9.8						
J7-32m	44.7	7.5						
ICC4 (below SND)								
SI2-0m	50.0	8.3						
SI2-0m dup	72.3	12.0						
SI2-10m	61.0	10.0						
SI2-20m	51.7	8.9						
21-ICC4B-2m	35.9	6.1	0.511614+-13	0.102290	0.511212	-20.0	-12.8	2.13
21-ICC4B-6m	50.2	8.1	0.511598+-10	0.097288	0.511215	-20.3	-12.7	2.13
21-ICC4B-7m	59.4	10.0	0.511462+-4	0.101776	0.511062	-22.9	-15.7	2.37
21-ICC4B-9m	61.6	11.0	0.511546+-7	0.107475	0.511123	-21.3	-14.5	2.27
AS TOC 0m	115.8	19.1	0.511616+-7	0.099565	0.511225	-19.9	-12.5	2.11
21-ICC4B-11m	79.5	14.9	0.511531+-5	0.113598	0.511084	-21.6	-15.2	2.33
21-ICC4B-14m	70.1	13.3	0.511596+-6	0.114667	0.511146	-20.3	-14.0	2.24
21-ICC4B-16m	58.6	10.3	0.511544+-24	0.105874	0.511128	-21.3	-14.4	2.26
21-ICC4B-18m	31.7	6.2	0.511680+-52	0.117659	0.511217	-18.7	-12.6	2.12
21-ICC4B-19m	58.7	10.0						
21-ICC4B-20m	65.2	11.0	0.511481+-7	0.102342	0.511079	-22.6	-15.4	2.34
AS TOC 10m	162.6	30.1	0.511461+-8	0.111945	0.511020	-23.0	-16.5	2.43
21-ICC4B-21m	32.8	5.6	0.511762+-96	0.103029	0.511357	-17.1	-9.9	1.90
21-ICC4B-22m	68.6	11.6	0.51153+-33	0.102299	0.511128	-21.6	-14.4	2.26
21-ICC4B-22.7m	50.2	7.8	0.511578	0.093527	0.511210	-20.7	-12.8	2.13
21-ICC4B-UP1-0m	42.2	6.7	0.511697+-9	0.096150	0.511319	-18.4	-10.7	1.96
21-ICC4B-UP1-1m	59.1	10.2	0.511457+-6	0.103847	0.511049	-23.0	-15.9	2.39
21-ICC4B-UP1-2m	84.2	14.3	0.511569+-12	0.102835	0.511164	-20.9	-13.7	2.21

AS TOC 20m	83.4	14.6	0.511666+-9	0.106117	0.511249	-19.0	-12.0	2.07
ICC4 (above SND)								
21-ICC4B-SND-2m	57.6	9.9	0.511523+-15	0.103483	0.511116	-21.7	-14.6	2.28
21-ICC4B-SND-0m	53.4	8.5	0.511558+-11	0.096645	0.511178	-21.1	-13.4	2.18
AS TOC 40m	152.4	32.5	0.51181+-5	0.128751	0.511304	-16.2	-11.0	1.99
AS TOC 50m	39.4	6.5						
AS TOC 60m	87.7	15.4						
AS TOC 70m	70.6	14.3	0.511773+-7	0.122340	0.511292	-16.9	-11.2	2.01
AS TOC 80m	201.3	33.4	0.511563+-5	0.100139	0.511170	-21.0	-13.6	2.20
AS TOC 100m	52.0	8.8						
AS TOC 110m	51.9	8.8						
CCN 83	46.0	7.8						
AS TOC 120m	43.9	7.1						
ICC5								
CCN 81	45.3	7.5						
CCN 78	85.4	17.2						
CCN 75	49.4	11.1						
CCN 70	52.3	8.1						
CCN 65	42.4	8.1						
CCN 61	359.8	62.8						

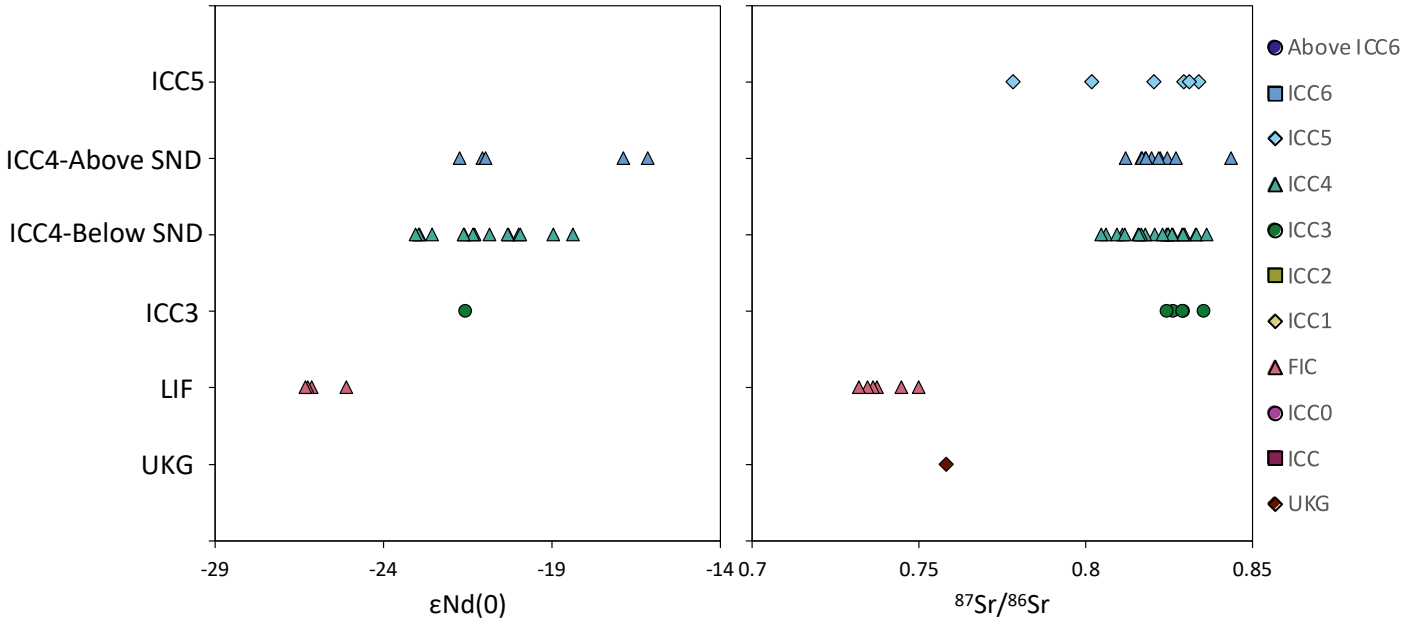

Figure 3.14. Provenance ages against stratigraphic position of Windermere Supergroup strata at Castle Creek.

ICC4, ranging from -23.04 to -22.57. These samples have $^{147}Sm/^{144}Nd$ ratios ranging from 0.1018 to 0.1119 (average = 0.1050). The T_{DM} ages calculated from these samples are among the oldest in the entire suite of studied samples, ranging from 2.43 to 2.34 Ga (average 2.38 Ga). Two samples from the lower part of ICC4 (below SND), and two samples from the upper part of ICC4 (above SND), yielded the most positive $\varepsilon_{Nd}(0)$ values from ICC4, ranging from -18.96 to -16.16. These samples have $^{147}Sm/^{144}Nd$ ratios ranging from 0.0961 to 0.1288 (average = 0.1133), and calculated T_{DM} ages are among the youngest in all the studied samples, ranging from 2.07 to 1.96 Ga (average 2.01 Ga), possibly reflecting contribution from other younger source areas. The wide spread of $\varepsilon_{Nd}(0)$ values in the vicinity of ICC4 suggests that sediment was sourced from an area with a combination of juvenile and evolved crust, or two isotopically different sources areas.

3.4.2 Rb-Sr isotopes

Fifty-two samples from various positions in the upper Kaza to Isaac succession at Castle Creek were analyzed for Sr isotope composition of the silicate fraction (Table 3.2). Sr isotope ratios are plotted against stratigraphic position in Figure 3.14.. In the basal part of the succession (UKG to LIF) $^{86}Sr/^{87}Sr$ values range from 0.7320 to 0.7582. In ICC3, however, $^{86}Sr/^{87}Sr$ ratio are notably higher and range from 0.8242 to 0.8355 (average 0.8289). Within ICC4, samples from below the SND give variable $^{86}Sr/^{87}Sr(0)$ values ranging from 0.8047 to 0.8364 (average 0.8215) whereas those above are equally variable but have slightly higher $^{87}Sr/^{86}Sr(0)$ values that range from 0.8119 to 0.8438 (average 0.8220). Six samples from ICC5 give slightly lower, yet still highly variable $^{87}Sr/^{86}Sr(0)$ values ranging from 0.7783 to 0.8339 (average 0.8159). Six samples from ICC5 give slightly lower, yet still highly variable $^{87}Sr/^{86}Sr(0)$ values ranging from 0.7783 to 0.8339 (average 0.8159).

Table 3.2. Sr isotopic data from Windermere mudrocks at the Castle Creek study area.

Sample	Rb (ppm)	Sr (ppm)	$^{87}Rb/^{86}Sr$	$^{87}Sr/^{86}Sr$	$^{87}Sr/^{86}Sr(T)$
Upper Kaza Group					
KI-2	246.8	114.1	6.29	0.758237+-6	0.705296
Lower Isaac Formation					
KI-31	195.5	180.0	3.16	0.749924+-8	0.723359
KI-138	140.6	261.0	1.56	0.737443+-7	0.724285
KI-139	177.0	312.7	1.64	0.736314+-6	0.722487
KI-144	156.4	125.8	3.61	0.74473+-6	0.714335
KI-61	160.7	267.0	1.75	0.734625+-7	0.719930
KI-64	108.2	186.3	1.68	0.732031+-7	0.717847
ICC3					
J-16m	311.2	148.7	6.13	0.826298+-9	0.774721
J3-10m	257.2	42.2	17.82	0.824245+-11	0.674197
J5-20m	348.3	74.6	13.67	0.829314+-8	0.714222
J6-27m	320.9	45.5	20.64	0.828936+-9	0.655188
J7-32m	367.6	74.5	14.45	0.835503+-6	0.713855
ICC4 (below SND)					
SI2-0m	286.7	59.0	14.23	0.824853+-7	0.705098
SI2-0m dup	305.1	63.2	14.12	0.82479+-6	0.705942
SI2-10m	271.3	65.9	12.04	0.824197+-7	0.722816
SI2-20m	268.2	58.6	13.39	0.824833+-5	0.712081
21-ICC4B-2m	107.6	44.6	7.05	0.811004+-9	0.751692
21-ICC4B-6m	197.4	50.0	11.56	0.833016+-9	0.735667
21-ICC4B-7m	169.6	58.6	8.48	0.82982+-6	0.758451
21-ICC4B-9m	191.6	70.4	7.97	0.829092+-9	0.761997
AS TOC 0m	342.9	54.7	18.36	0.8261+-7	0.671543
21-ICC4B-11m	209.0	80.6	7.60	0.833161+-8	0.769209
21-ICC4B-14m	187.8	54.4	10.11	0.829328+-6	0.744180
21-ICC4B-16m	212.6	61.8	10.08	0.825858+-29	0.741030
21-ICC4B-18m	98.2	39.2	7.31	0.806051+-16	0.744521
21-ICC4B-19m	162.8	50.0	9.52	0.809358+-23	0.729203
21-ICC4B-20m	177.3	62.3	8.33	0.820685+-6	0.750548
AS TOC 10m	332.5	77.2	12.60	0.82303+-8	0.716983
21-ICC4B-21m	122.1	45.4	7.86	0.811808+-18	0.745621
21-ICC4B-22m	209.0	51.2	11.93	0.81792+-15	0.717524
21-ICC4B-22.7m	173.9	47.7	10.66	0.815899+-17	0.726132
21-ICC4B-UP1-0m	110.4	35.9	8.99	0.804724+-6	0.729068
21-ICC4B-UP1-1m	187.7	47.5	11.56	0.816763+-13	0.719428
21-ICC4B-UP1-2m	167.7	40.9	11.98	0.816047+-34	0.715177

AS TOC 20m	412.7	64.3	18.79	0.836377+-7	0.678189
ICC4 (above SND)					
21-ICC4B-SND-2m	105.9	33.7	9.19	0.822529+-35	0.745157
21-ICC4B-SND-0m	218.0	48.8	13.07	0.811914+-12	0.701899
AS TOC 40m	345.8	91.3	11.11	0.843772+-11	0.750235
AS TOC 50m	217.7	39.6	16.08	0.824636+-15	0.689260
AS TOC 60m	276.5	64.0	12.63	0.817866+-12	0.711544
AS TOC 70m	310.3	87.3	10.40	0.827253+-6	0.739697
AS TOC 80m	319.0	72.4	12.89	0.816808+-11	0.708312
AS TOC 100m	263.8	59.7	12.91	0.819837+-6	0.711115
AS TOC 110m	253.8	68.5	10.84	0.821909+-6	0.730688
CCN 83	201.1	48.1	12.24	0.816939+-9	0.713923
AS TOC 120m	235.7	66.7	10.34	0.818164+-13	0.731105
ICC5					
CCN 81	297.9	66.7	13.06	0.820637+-6	0.710730
CCN 78	355.8	157.3	6.62	0.833934+-6	0.778162
CCN 75	308.8	64.5	14.01	0.829448+-7	0.711530
CCN 70	288.7	50.3	16.79	0.831179+-8	0.689796
CCN 65	177.0	53.7	9.62	0.801945+-7	0.720979
CCN 61	440.0	347.1	3.69	0.778289+-7	0.747202

3.4.3 Nd-Sr isotope fractionation

$f^{Sm/Nd}$ is the fractional deviation of the $^{147}Sm/^{144}Nd$ ratio from that in chondritic meteorites ($f^{Sm/Nd} = (^{147}Sm/^{144}Nd_{\ sample} / {}^{147}Sm/^{144}Nd_{\ chondrite})-1$; where $^{147}Sm/^{144}Nd_{\ chondrite} = 0.1967$), and is a measure of the degree of differentiation of the depleted mantle source (McLennan et al., 1990). Mudstones in this study show a relatively narrow range of $f^{Sm/Nd}$ from -0.52 to -0.35. Additionally, the lack of correlation between $^{147}Sm/^{144}Nd$ ratios and $\varepsilon_{Nd}(0)$ ($R^2 = 0.09$) (Figure 3.15.) suggests that Sm–Nd compositions have not been altered by sedimentary and post-depositional processes (McCulloch and Wasserburg, 1978; McLennan et al., 1990). On the other hand, the wide range of $^{87}Rb/^{86}Sr$ ratios (1.56 to 20.64) is possibly a consequence of grain size sorting and Rb–Sr redistribution during post-depositional processes (Evans et al., 2009).

Accordingly, provenance reconstructions based on the Sm–Nd isotope system are considered more robust and thus used here to constrain sediment provenance.

To consider which minerals may be controlling the distribution of isotopic values in the samples, εNd (0) and $^{87}Sr/^{86}Sr(0)$ were plotted against major elements. SiO_2 shows no correlation with εNd (0) and $^{87}Sr/^{86}Sr$ (0), suggesting silica abundance has little or no effect on the isotopic ratio (Figure 3.16.). However, both $^{87}Sr/^{86}Sr$ (0) and εNd (0) show a slight positive correlation with K_2O, and a slight negative correlation with Fe_2O_3 + MgO. The correlation between the whole rock chemistry and isotopic ratios may suggest that several distinct sources contributed sediment to these units, which affected isotopic ratios.

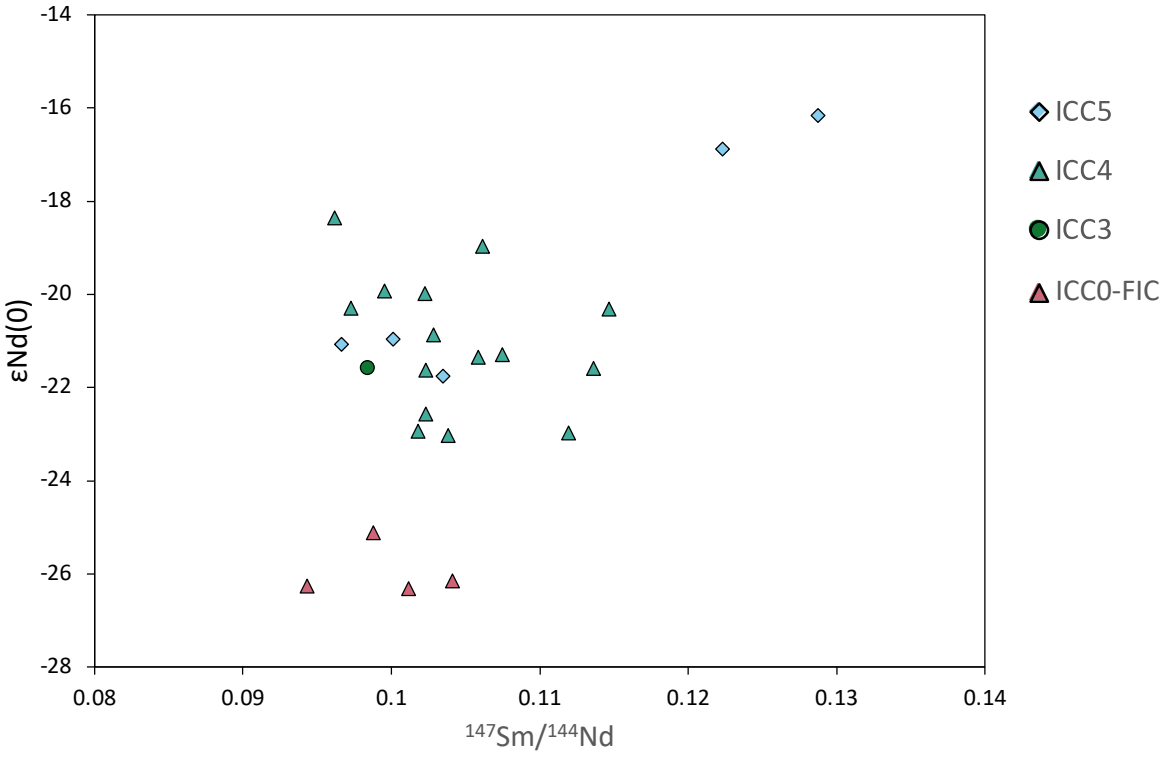

Figure 3.15. $^{147}Sm/^{144}Nd$ vs. **εNd (0)** plot for the Castle Creek samples

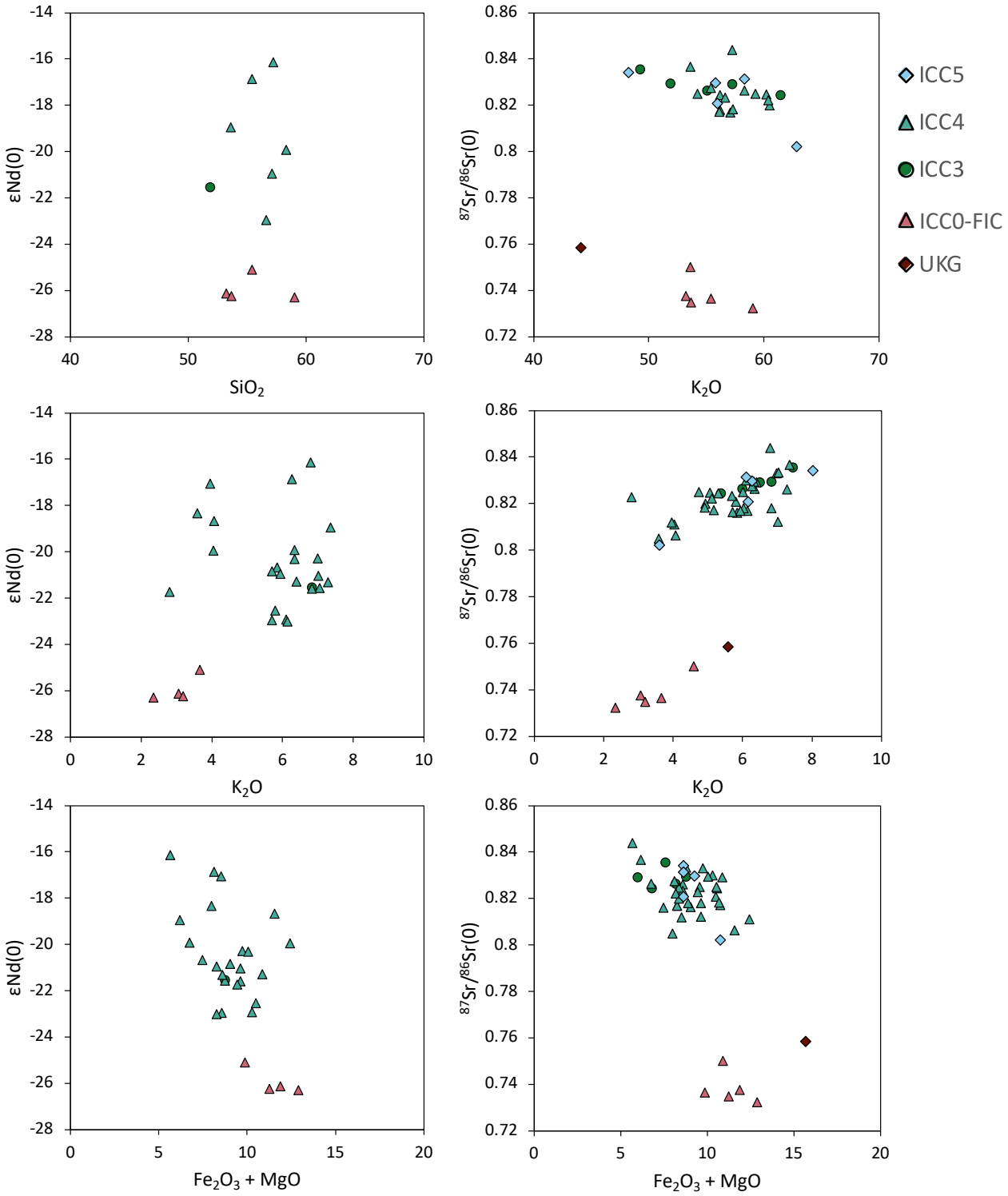

Figure 3.16. Plots of $^{87}Sr/^{86}Sr$ (0) and εNd (0) versus (a) SiO_2, (b) K_2O, (c) Fe_2O_3 + MgO for samples from the UKG and IF.

Chapter 4: Discussion

4.1 Source rock composition

The major and trace element geochemical compositions of sedimentary rocks have been used extensively to discriminate tectonic settings of sedimentary basins. Based on their geochemical characteristics, strata at the Castle Creek (CC) study area have been subdivided into three distinct, compositionally unique groups: Assemblage 1, comprising UKG up to ICC1, Transitional Assemblage, comprising ICC2, Assemblage 2, comprising ICC3, ICC4 and ICC5, and Assemblage 3, comprising ICC6 and all strata above to the base of the Cunningham Formation. This chapter discusses composition of the source rocks of these assemblages based on geochemical proxies for weathering, provenance, and tectonic setting.

4.1.1 Weathering

The major element composition of sedimentary rocks can be significantly affected by the intensity of weathering in the source region, which is controlled by composition of the rock, duration of weathering, climatic conditions, and tectonic setting (Fedo et al., 1996; Nesbitt and Muehlenbachs, 1997; Nesbitt and Young, 1984). Several chemical indices have been proposed to quantify weathering effects on the major elements, including the Chemical Index of Alteration (CIA) (Nesbitt and Young, 1982). CIA value of unweathered igneous rock is about 50, whereas CIA values for average shales range from 70 to 75 and reflect a composition of muscovite, illite and smectite. As source rocks become more intensely weathered, mineral content becomes dominated by kaolinite and gibbsite, resulting in CIA values close to 100 ((Nesbitt and Young, 1982). In this study CIA ranges from 55.6 to 82.7 (average = 74.1) and is therefore similar to that of the average shale, although lower values may indicate more moderate chemical weathering in the source area. CIA values are highest in Assemblage 1 (average = 77.6) and Transitional

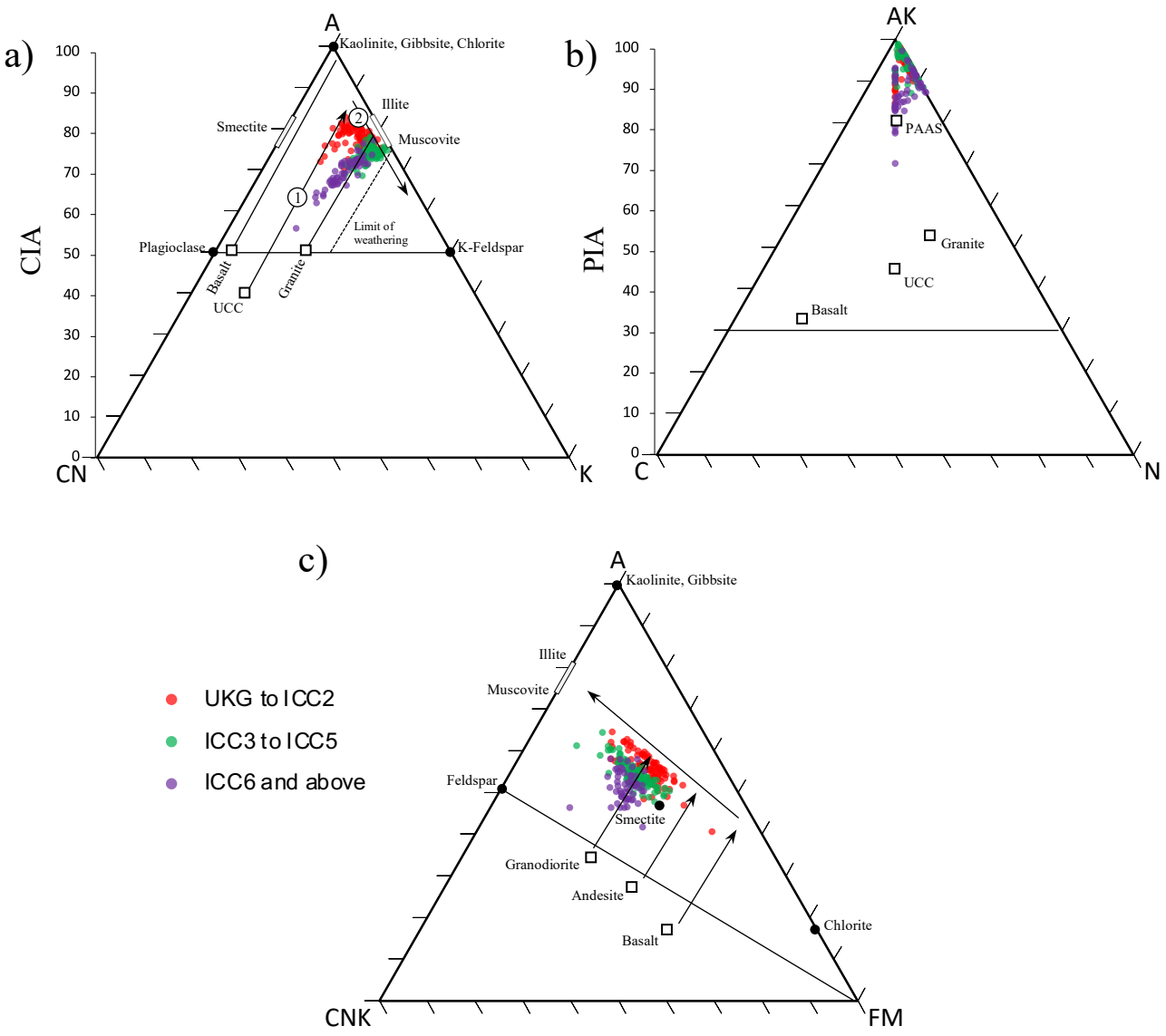

Figure 4.1. Major element ternary diagrams showing the weathering control on the composition of the Windermere supergroup siliciclastic samples. Various unweathered igneous rocks are represented by hollow squares, and unweathered rock-forming minerals are represented by black circles. Reference values of source rocks from McLennan et al., (1993) after Nesbitt and Young (1984, 1989). Arrows indicate weathering trends for different source rocks. The solid line separates the non-weathered and the weathered fields. a) Al_2O_3–$CaO+Na_2O$–K_2O (A-CN-K) diagram; also a measure of CIA. (1) represents the weathering trend of UCC; (2) represents effects of K metasomatism. B) $Al_2O_3+K_2O$–CaO–Na_2O (A-C-N) diagram; also a measure of PIA. c) Al_2O_3 –Fe_2O_3+MgO–$CaO+Na_2O+K_2O$ diagram. The samples indicate a trend that is interpreted as a variation of the composition of the source rocks.

Assemblage (average = 77.9) indicating higher chemical weathering, which decreases through to Assemblage 2 (average = 74.5). Assemblage 3 has the lowest CIA values (average = 70.9).

Another way to evaluate control of chemical weathering on composition is by plotting the data in Al_2O_3-CaO+Na_2O-K_2O (A-CN-K) compositional space (molar fraction; Figure 4.1a). More intense weathering of bedrock tends to yield Al-rich sediments that move along a weathering trend from the unweathered parent rock, sub-parallel to A-CN. Also shown are positions of idealized minerals, possible source rocks like basalt, granite and granodiorite, and UCC, estimated from PAAS. In Figure 4.1a, the arrow extending from UCC towards the field for illite represents the predicted weathering trend for an average source rock, which would produce Al-rich sediments due to loss of Na and Ca. A second arrow pointing towards K-feldspar represents the approximate trend of K-enrichment, with the dashed line representing the limit of weathering. Assemblage 1 plots near the weathering trend derived from UCC, whereas assemblages 2 and 3 plot closer to the weathering line for granite. Assemblage 2 data plot furthest from the average shale composition and are clustered near muscovite. Many of the samples are clustered toward the A-K line, indicating that much Na_2O and CaO have been removed from bulk composition due to chemical weathering. All samples plot to the left of the "limit of weathering" line, suggesting the CIA values have not been affected by severe post-depositional K-metasomatism and may still be used as a reliable weathering indicator.

The obvious limitation of the CIA parameter is the common post-depositional addition of K in older clastic rocks (K-metasomatism). Accordingly, some workers have preferred K-free indices, such as the Plagioclase Index of Alteration (PIA) (Fedo et al., 1996)), or the Chemical Index of Weathering (CIW) (Harnois, 1988):

$$PIA = [(Al_2O_3 – K_2O)/(Al_2O_3 + CaO^* + Na_2O – K_2O)] \times 100$$

$$CIW = Al_2O_3/(Al_2O_3+CaO^*+ Na_2O) \times 100 \text{ (elements in molecular proportions)}$$

The PIA describes the weathering of feldspars, whereas the CIW index estimates overall weathering in addition to eliminating the possible effect of K-metasomatism. PIA can be visualized by plotting in (Al_2O_3–K_2O)–CaO*–Na_2O (A-C-N) compositional space (Figure 4.1b). PIA values may range from 50 for unweathered plagioclase to a maximum value of 100 for kaolinite and gibbsite. Both assemblages 1 and 2 show very high PIA, indicating intense chemical weathering as shown by depletion in CaO and Na_2O and the strong correlation of Al_2O_3 and TiO_2 (Figure 3.6.). Nonetheless, Assemblage 2 has slightly higher PIA values (average = 92.3) compared to Assemblage 1 (average = 91.1) and Transitional Assemblage (average = 92.1). Assemblage 3 has significantly lower PIA values compared to the other assemblages (average = 83.9). CIW varies from 65.0 to 98.4 (average = 90.8) indicating generally high chemical weathering of the source, with higher values in Assemblage 2 (average = 94.3) and lower values in Assemblage 1 (average = 92.7). Assemblage 3 has the lowest CIW values (average = 87.5). However, CIW can also be affected by source rock composition, and therefore is suspect where composition in the source area varies (Fedo et al., 1995).

The CIA and the CIW indices are primarily measures of unweathered feldspar versus clay mineral content, and while they can be affected by source rock composition neither are strong indicators of provenance. ICV includes Fe and Mg in its calculation and may be used to assess the original composition of shales and siltstones. ICV values of the CC samples range from 0.52 to 1.34 (average = 0.79). The Al_2O_3 –Fe_2O_3+MgO–CaO+Na_2O+K_2O ternary diagram shows that samples plot away from smectite and towards muscovite, and that the variation of these elements does not correlate with a weathering trend (Figure 4.1c). Figure 4.2 displays the relationship between CIA and ICV values. Assemblage 1 has the highest CIA values, (average =

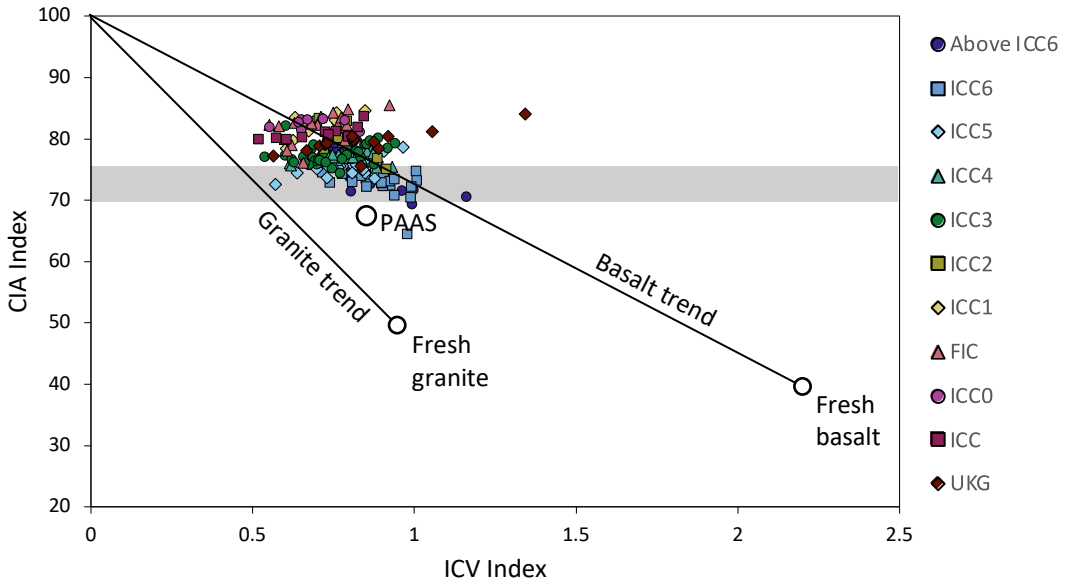

Figure 4.2. Two indicators of weathering, Chemical Index of Alteration (CIA) and Index of Chemical Variation (ICV) in samples from Castle Creek (reference data from Lee 2002). The grey area represents the range of CIA values of Neoproterozoic shale.

77.6) and variable ICV values (average = 0.73). Starting at the transitional assemblage upward to Assemblage 2, CIA values decrease (average = 74.5), and ICV values increase (average = 0.76). Assemblage 3 has the lowest CIA values (average = 70.9) and the highest ICV values (average = 0.83). Overall, the trends for CIA, CIW and PIA values suggest intense continental weathering at the base of the Assemblage 1. Weathering intensity decreases in Assemblage 2 to reach its lowest intensity in Assemblage 3. Nearly all ICV values are < 1, suggesting presence of mudstones with abundant clay minerals associated with high sediment recycling and chemical weathering. However, there is some variability between samples. The higher ICV values in Assemblage 2 and 3 suggest greater input of first cycle deposits with higher feldspar, pyroxene, amphibole, or biotite.

4.1.2 Major Element Discriminant Function

The provenance discriminant function diagram of major elements proposed by Roser and Korsch (1988) is used to predict the provenance of sedimentary rocks and comprises four

provenance groups (mafic igneous; intermediate igneous; felsic igneous; and quartzose sedimentary). The provenance groups are defined by a global database of fine-grained clastic sediments derived from identified tectonic settings. Two different discriminant functions are applied to our dataset and are shown in Figure 4.3. The first diagram (Figure 4.3a) uses variable function coefficients for the absolute values of each of the major oxides, calculated as follows:

(7) Discriminant Function 1 = $(-1.773TiO_2) + (0.607Al_2O_3) + (0.760Fe_2O_3) + (1.500MgO) + (0.616CaO) + (0.509Na_2O) + (-1.224K_2O) + (-9.090)$

(8) Discriminant Function 2 = $(0.445TiO_2) + (0.070Al_2O_3) + (-0.250Fe_2O_3) + (-1.142MgO) + (0.438CaO) + (1.475Na_2O) + (-1.426K_2O) + (-6.861)$

However, this does not account for the addition of carbonate sediments, which in the Precambrian would have been formed by a variety of abiotic and microbial processes. The effect of carbonate dilution is to push composition, as defined by the discriminant function diagram, towards a more mafic/intermediate source. The second diagram (Figure 4.3b) takes this into account by normalizing the major oxide values to Al_2O_3, calculated as follows:

(9) Discriminant Function 3 = $(30.638\ TiO_2/Al_2O_3) + (-12.541\ Fe_2O_3/Al_2O_3) + (7.329\ MgO/Al_2O_3) + (12.031\ Na_2O/Al_2O_3) + (35.402\ K_2O/Al_2O_3) - 6.382.$

(10) Discriminant Function 4 = $(56.500\ TiO_2/Al_2O_3) + (-10.879\ Fe_2O_3/Al_2O_3) + (30.875\ MgO/Al_2O_3) + (-5.404\ Na_2O/Al_2O_3) + (11.112\ K_2O/Al_2O_3) - 3.890.$

Samples from Assemblage 1 plot in the quadrant for mafic and intermediate igneous provenance, whereas assemblages 2 and 3 plot in the quadrants for quartzose sedimentary and felsic provenance, suggesting high sediment maturity due to progressive loss of feldspar and increase in quartz, most probably related to source rock weathering or recycling. The transitional assemblage appears to link Assemblage 1 and 2, starting with a mafic igneous provenance at its

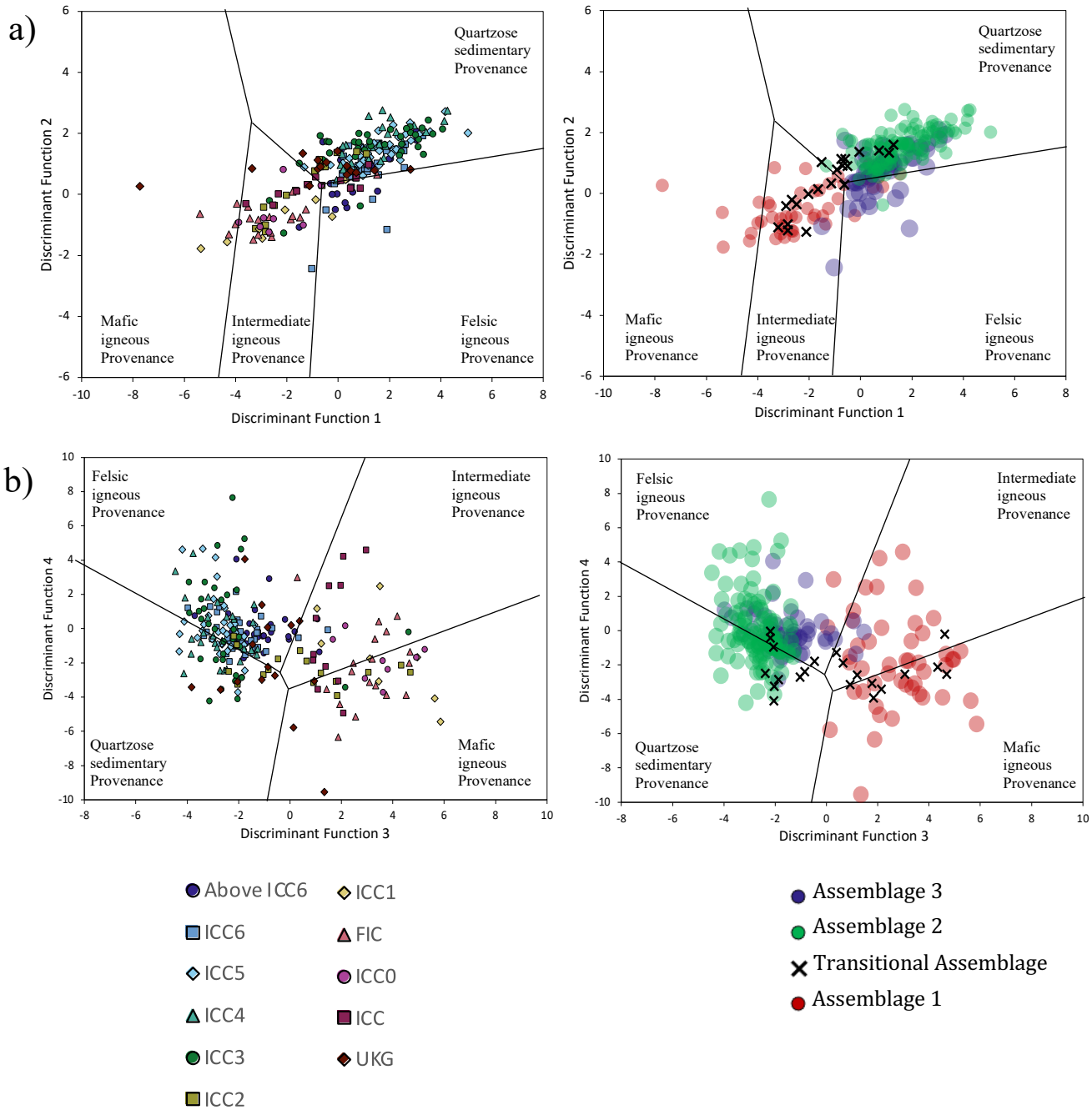

Figure 4.3. Two discriminant function diagrams for the provenance signatures of Castle Creek samples using major elements (after Roser and Korsch, 1988), using: a) oxide/Al_2O_3 ratios. Discriminant Function 3 = (30.638 TiO_2/Al_2O_3) + (-12.541 Fe_2O_3/Al_2O_3) + (7.329 MgO/Al_2O_3) + (12.031 Na_2O/Al_2O_3) + (35.402 K_2O/Al_2O_3) – 6.382. Discriminant Function 4 = (56.500 TiO_2/Al_2O_3) + (-10.879 Fe_2O_3/Al_2O_3) + (30.875 MgO/Al_2O_3) + (-5.404 Na_2O/Al_2O_3) + (11.112 K_2O/Al_2O_3) – 3.890. b) oxide abundances. Discriminant Function 1 = (-1.773TiO_2) + (0.607Al_2O_3) + (0.760Fe_2O_3) + (-1.500MgO) + (0.616CaO) + (0.509Na_2O) + (-1.224K_2O) + (-9.090); Discriminant Function 2 = (0.445TiO_2) + (0.070Al_2O_3) + (-0.250Fe_2O_3) + (-1.142MgO) + (0.438CaO) + (1.475Na_2O) + (-1.426K_2O) + (-6.861).

base and transitioning stratigraphically upward to a more quartzose sedimentary provenance that continues into Assemblage 3. Roser and Korsch (1988) stated that sediments derived from passive continental margins, intracratonic sedimentary basins, and recycled orogenic provinces will plot in the quartzose sedimentary provenance field. This suggests a more recycled provenance for Assemblage 2 and 3, and the possibility of a more mafic or intermediate source for Assemblage 1. Roser and Korsch (1988) noted that even relatively high metamorphic grade should not affect bulk major element geochemical signatures, and therefore the application of discriminant functions are considered reliable provenance indicators for this study.

4.1.3 Tectonic Setting Discrimination

Previous studies on the chemical composition of siliciclastic sedimentary rocks demonstrate that composition is controlled primarily by the plate tectonic setting of the source areas and depositional basins, for which several discrimination diagrams have been proposed (Bhatia, 1983; Bhatia and Crook, 1986; Floyd and Leveridge, 1987; McLennan et al., 1990; Murphy, 2000; Roser and Korsch, 1986). Many trace elements are well-established as indicators of source area and tectonic setting. This is based on the observation that more incompatible elements Th, Zr, Nb, Y, and U have an affinity with felsic rocks, whereas the more compatible elements such as Cr, Ni, V, Sc and Ti have an affinity with mafic components (Armstrong-Altrin et al., 2012; Basu, 2016; Cullers, 2000).

Floyd and Leveridge (1987) defined a discrimination diagram using La/Th vs. Hf to characterize different arc compositions and provenance (Figure 4.4a). Assemblage 1 tends to have low La/Th (0.8-5.9) and Hf (2.4-8.4 ppm) concentration, and plots mostly in the acidic arc and mixed felsic/basic source areas. Assemblage 2 has similarly low La/Th (1.4-6.9), but higher Hf (5.2-11.3 ppm), following the trend towards a passive margin source, and therefore an

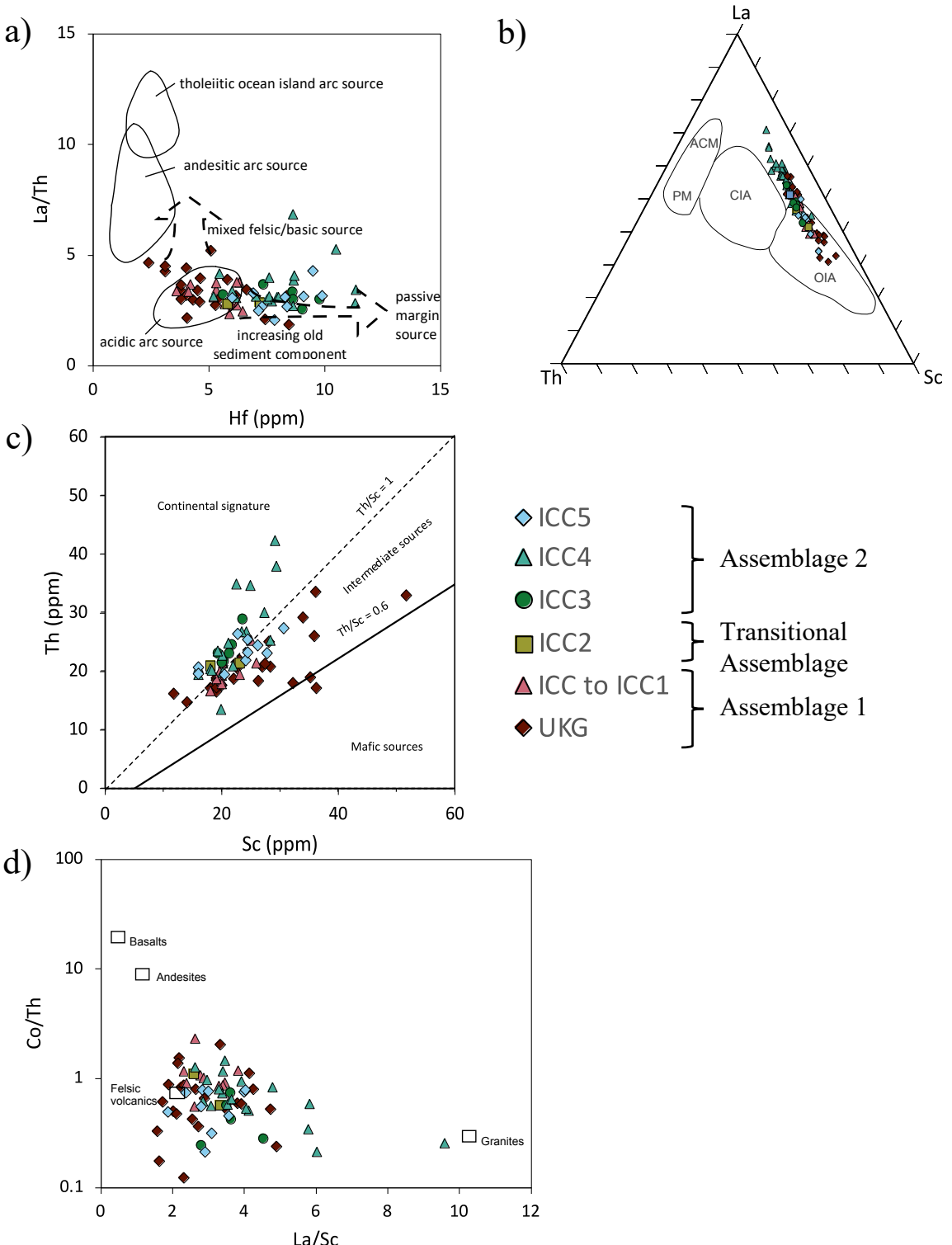

Figure 4.4. A) La/Th vs. Hf diagram (after Floyd and Leveridge, 1987). B) La-Th-Sc discrimination diagram differentiating ocean island arc (OIA), continental island arc (CIA), passive margin (PM), and active continental margin (ACM) (after Bhatia and Crook, 1986), d) Th/Sc discrimination diagram illustrating acidic to intermediate compositions for the studied samples. D) Discrimination diagram illustrating continental sedimentary provenance of the studied samples. E) Co/Th vs. La/Sc diagram (after McLennan et al., 1995).

increasingly more recycled sediment component. Transitional Assemblage values are intermediate between the two with average La/Th and Hf values of 2.2 and 6.5 ppm, respectively. Similarly, on the La–Th–Sc diagram, Assemblage 2 samples plot close to the continental island arc (CIA) field, whereas Assemblage 1 samples plot in the oceanic island arc (OIA) field, suggesting a more mafic component (Figure 4.4b). The Th versus Sc and Th/Sc vs. Cr/Th plots are also used to evaluate differences in source rock composition. The scatter plot for Th vs. Sc indicates a predominantly intermediate composition for Assemblage 1 due to the relatively high Sc (11.7-51.6 ppm) compared to Th, and a continental signature for Assemblage 2 and 3 with lower Sc (16.0-30.5 ppm) relative to Th (Figure 4.4c). The bivariate cross-plot of Co/Th vs. La/Sc is also commonly used to evaluate sediment provenance (Figure 4.4d) (Bai et al., 2015; Wronkiewicz & Condie, 1987). Assemblage 1 plots closer to a felsic volcanic to andesite source due to lower La/Sc ratios, whereas Assemblage 2 plots towards a granitic source.

4.1.4 Th/Sc, Th/U, and Zr/Sc Ratios (Sediment Sorting and Recycling)

Th, Zr and Sc are sensitive to igneous fractionation processes, with Th and Zr concentrated in felsic igneous rocks and Sc in mafic igneous rocks (Taylor and McLennan, 1985). Zr can also track sedimentary fractionation processes, as heavy minerals like zircon, apatite and monazite commonly accumulate with quartz during sedimentation. Therefore, Zr/Sc ratios can be used to assess the enrichment of zircon, which is a measure of sedimentary recycling, and Th/Sc ratios can be an indicator of relative proportions of felsic and mafic rocks (McLennan et al., 1995). Th/Sc ratios higher than ~ 1, if coupled with high values of Zr/Sc (> 10), indicate input from recycled sources. Therefore, a Zr/Sc versus Th/Sc bivariate plot

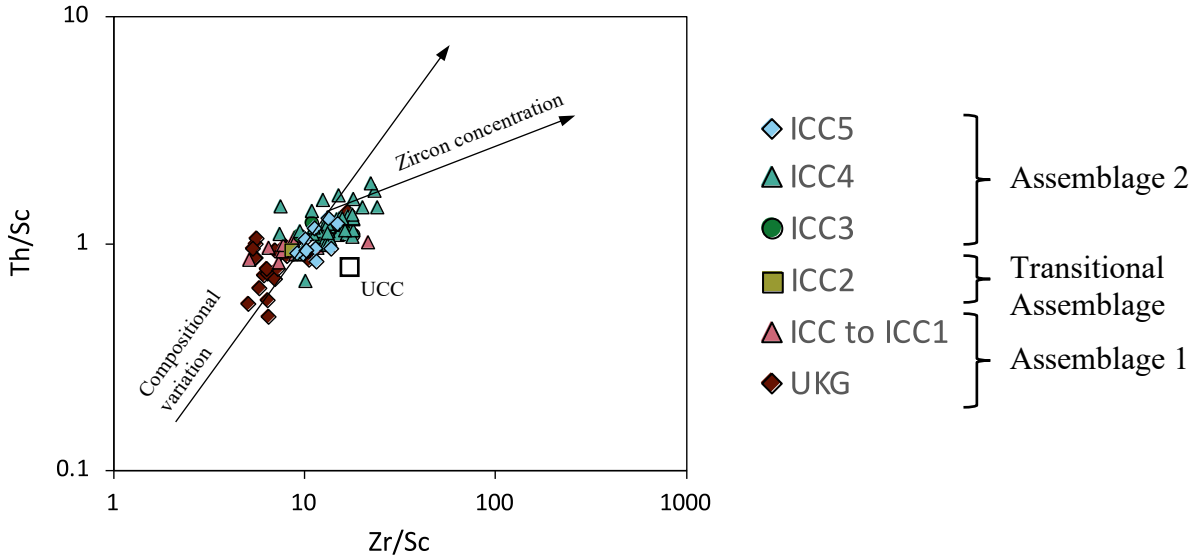

Figure 4.5. a) Th/Sc vs. Zr/Sc discrimination diagram (after McLennan et al., 1993) illustrating compositional variations and sediment recycling of sediments in the shales and sandstones. B) Th vs. Th/U discrimination diagram illustrating moderate weathering and sediment recycling (after McLennan et al., 1993).

(McLennan, 1993) can be used to evaluate the relationship between the degree of sediment reworking (Zr enrichment during sediment sorting) and source rock compositional variation.

Th/Sc and Zr/Sc values are lowest in Assemblage 1, averaging 0.9 and 8.0, respectively, slightly outside the range expected for an evolved continental source (Figure 4.5.). Th/Sc and Zr/Sc increase stratigraphically upward, with average values of 1.2 and 14.1 for Assemblage 2, and 1.0 and 12.2 for Assemblage 3. The lower Th/Sc ratios in Assemblage 1 compared to Assemblage 2, suggests that strata in Assemblage 1 were derived from source rocks with more significant and/or additional input from mafic/intermediate rocks. Furthermore, Zr/Sc ratios tend to be higher in Assemblage 2 compared to Assemblage 1, indicating more abundant zircon, and in turn, a more recycled component (Figure 4.5.).

4.1.5 Transition Metals (Derivation from Ultramafic/Mafic Sources)

The enrichment of certain transition metals such as Cr, Ni, and V in sedimentary rocks suggests a mafic provenance (Armstrong-Altrin et al, 2004). Therefore, if Assemblage 1 has a

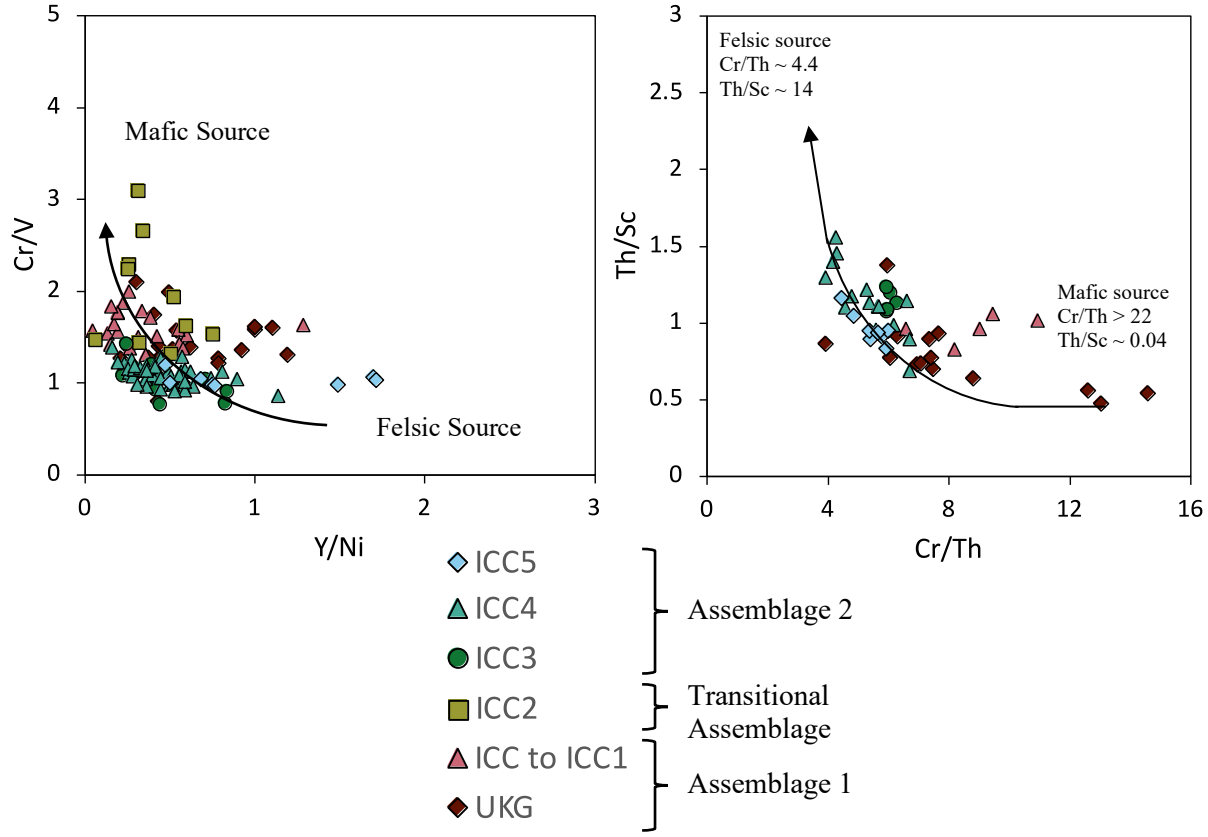

Figure 4.6. Cross-plot of: a) Y/Ni vs Cr/V; b) Cr/Th vs Th/Sc.

mafic/intermediate source rock component, it should also display enrichment in certain trace elements. A robust proxy for derivation of clastic sediments from mafic and ultramafic rocks is abundant Cr and Ni (Cr > 150 ppm and Ni > 100 ppm), low Cr/Ni ratios (1.3–1.5) and a high correlation coefficient between these two elements (Garver et al., 1996). Conversely, low abundances and correlations of these elements indicate a felsic provenance (Wrafter and Graham, 1989; Garver et al., 1996; Armstrong- Altrin et al., 2004). Assemblage 1 has the highest Cr (60–289 ppm) and Ni (14-133 ppm) abundance in most of the studied samples, with weak correlation ($R^2 = 0.16$) and variable Cr/Ni ratios (0.7–8.9). Assemblage 2 and 3 have slightly lower Cr (66 to 200 ppm) and Ni (24 to 92 ppm) abundance, with negligible correlation ($R^2 = 0.04$) and variable Cr/Ni ratios (0.8-6.5). Presence of higher concentrations of Cr and Ni in

Assemblage 1 compared to Assemblage 2 and 3 may suggest presence of mafic rocks in the source region, which slowly diminished stratigraphically upwards.

One method that has been used to identify ultramafic and mafic source areas is a binary diagram (Figure 4.6a) of Cr/V versus Y/Ni ratios (McLennan et al., 1990). Mafic to ultramafic sources tend to have higher Cr/V, a measure of Cr enrichment compared to other ferromagnesian trace elements, and lower Y/Ni, a measure of enrichment of HREE compared to ferromagnesian trace element content (Ni) (Ali et al., 2014; Hiscott, 1984). Samples in this study have a low to moderate Cr/V ratio and low Y/Ni suggesting a mostly felsic source. However, the higher Cr/V ratio in strata of Assemblage 1 may indicate possible input of sediment derived from a mafic or intermediate source.

According to Culvers (1996), clastic rocks with Cr/Th values in the range 2.5 to 17.5 originate mostly from felsic sources, and the UCC has an average value of 7.76 (McLennan et al., 2006). While both assemblages fall within this range, we note that Cr/Th values are higher in Assemblage 1 (3.5-14.6) compared to Assemblage 2 (3.9-7.2), and as illustrated in a Th/Sc versus Cr/Th cross-plot (Figure 4.6b), suggests a comparatively larger mafic component in Assemblage 1.

4.1.6 Rare Earth Elements

REEs represent reliable provenance indicators, as they are not significantly affected by weathering, diagenesis, or metamorphism, and principally reflect source rock composition and tectonic setting (Bhatia, 1985, 1986). Sediments with a felsic igneous provenance generally have elevated LREE/HREE ratios, whereas sediments derived from mafic igneous rocks have low LREE/HREE ratios (Armstrong-Altrin et al., 2013; Cullers, 2000). Additionally, those derived from felsic source rocks show a negative Eu anomaly (Eu/Eu* = < 1) compared to mafic rocks

that have a small or no Eu anomaly (Eu/Eu* = 1) — signatures that are preserved in clastic sediments (Taylor and McLennan, 1995). Therefore, LREE/HREE ratios and size of the Eu anomaly are considered to be reliable tools for unraveling sediment provenance (McLennan et al., 1990; 1993; McLennan, 2001).

Figure 3.12. displays the chondrite-normalized REE patterns for the studied sediments. All the studied samples are enriched in LREE with nearly flat HREE patterns. Assemblage 2 tends to have higher LREE/HREE ratios (14.6-51.9) compared to Assemblage 1 (8.8-41.8). Moreover, the Gd/Yb, and La/Yb ratios average 3.0 and 25.3, respectively, for Assemblage 1, and 3.2 and 26.5, respectively, for Assemblage 2, also suggesting greater LREE enrichment in Assemblage 2. All samples have a strong to moderate negative Eu anomaly ranging from 0.57 to 0.84. Assemblage 1 tends to have a less negative anomaly (average 0.70), compared to Assemblage 2 (average 0.66), and the Transitional Assemblage has intermediate values (average 0.68). Collectively, these results suggest derivation from felsic source rocks, although the lower LREE/HREE, less negative Eu anomaly, and lower ratios of Gd/Yb and La/Yb suggest a larger mafic component in Assemblage 1.

4.2 Comparison to Isotope Data

Isotopic differences are noted between Assemblage 1 (lower UKG and LIF), and Assemblage 2 (upper part of IF), and are especially evident in ε_{Nd} and $^{87}Sr/^{86}Sr$ data. The isotopic signatures change from highly negative $\varepsilon_{Nd}(T)$ values (-19.1 to -17.6) and low $^{87}Sr/^{86}Sr$ values (0.7320 to 0.7582) in Assemblage 1, to less negative $\varepsilon_{Nd}(T)$ values (-16.5 to -10.7) and higher $^{87}Sr/^{86}Sr$ values (0.7783 to 0.8438) in the overlying strata of Assemblage 2 (Figure 4.7). Isotope data are unavailable for Assemblage 3, so only assemblages 1 and 2 will be discussed here. The linear trend between ε_{Nd} and $^{87}Sr/^{86}Sr$ suggests that both isotope systems have retained a signature that is primarily representative of their source rocks. However, as discussed in Chapter 3.4.3, the wide range of $^{87}Rb/^{86}Sr$ ratios (1.56 to 20.64) is possibly a consequence Rb–Sr redistribution during weathering and/or post-depositional processes. Accordingly, the Sm–Nd isotopic system is considered more robust and better for evaluating sediment provenance in this study area.

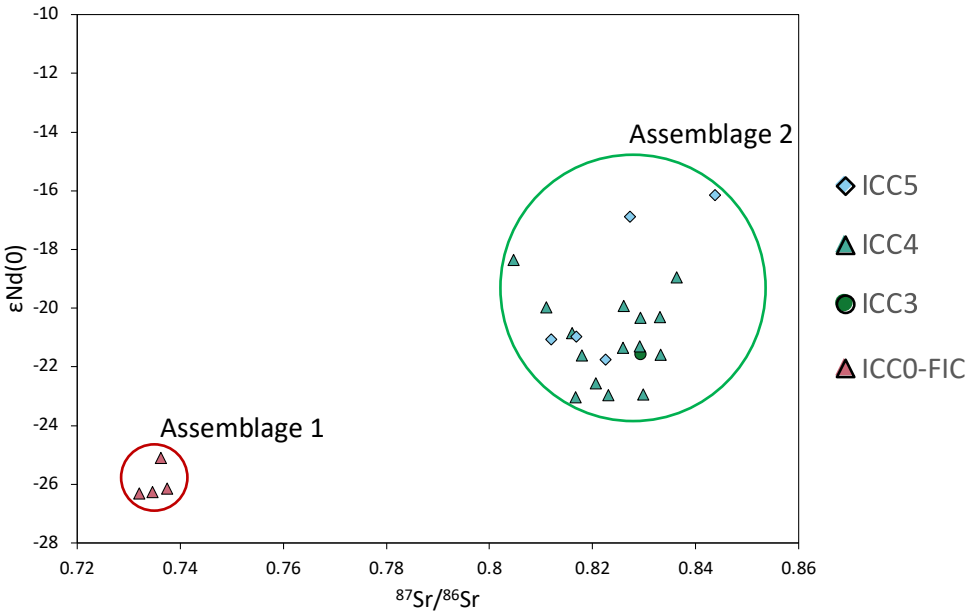

Figure 4.7. Cross-plot of $^{87}Sr/^{86}Sr$ vs. eNd(0), showing distribution of samples in Assemblage 1 and Assemblage 2.

The ε_{Nd} vs $^{147}Sm/^{144}Nd$ diagram can be used to compare the isotopic signature of sedimentary units with potential source rocks with known isotopic ratios. Furthermore, alignments of data in the diagram can be associated with mixing lines, representing different proportions of mixing between two isotopic reservoirs. Figure 4.8 compares isotopic data measured in this study with several possible sedimentary source terranes that make up the basement of western Laurentia (which may overlap), as well as similar data extracted from the literature. Also shown are fields for felsic and mafic igneous rocks with crystallization ages of 700-650 Ma, which represent potential juvenile sources.

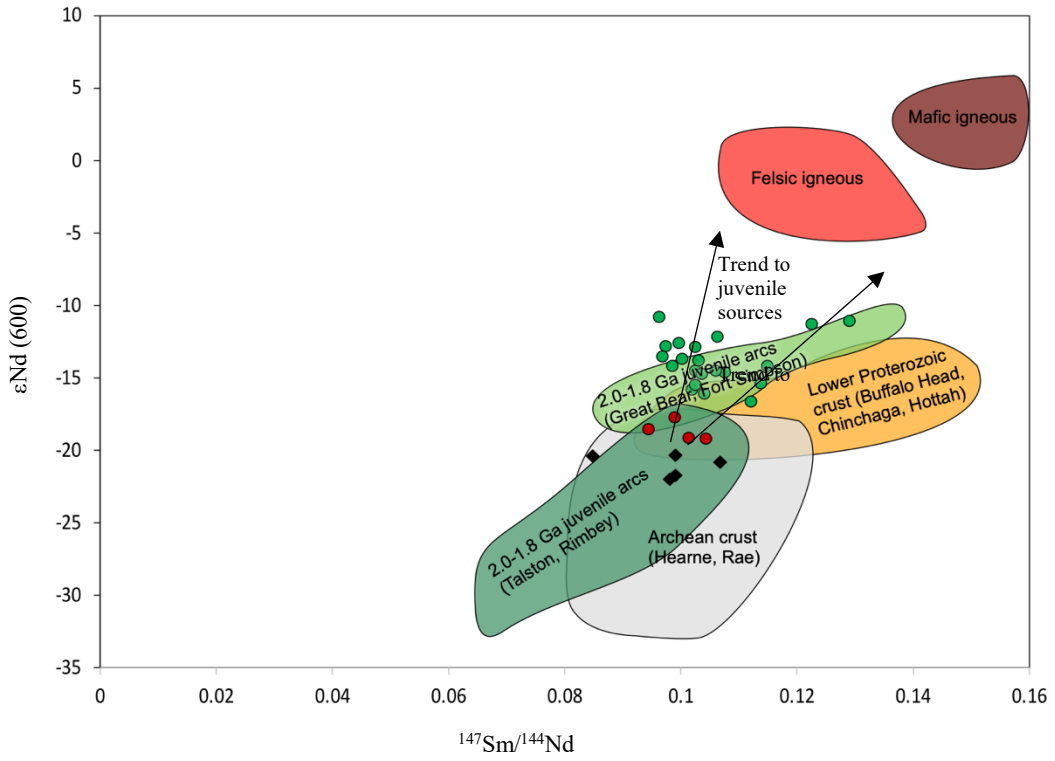

Figure 4.8. ε_{Nd} vs $^{147}Sm/^{144}Nd$ diagram. Also shown are western Laurentia basement source terranes. Red circles indicate Assemblage 1 samples; green circles indicate Assemblage 2 samples. Black diamonds represent literature values for correlative units from the Horsethief Creek Formation (Boghossian et al., 1996). Isotopic data for Laurentian basement rocks taken from Canadian Geochronology Knowledgebase (https://atlas.gc.ca/geochron/en/). Also shown are potential felsic and mafic igneous sources approximated from similar igneous sources with crystallization ages ca. 700-650 Ma.

Assemblage 1 yields $^{147}Sm/^{144}Nd$ values varying between 0.1041 and 0.0943 (f = -0.52 to -0.47), relatively homogeneous $\varepsilon_{Nd}(T)$ values (-19.1 to -17.6), and Archean T_{DM} crustal residence ages between 2.65-2.53 Ga. Calculated Sm-Nd depleted mantle (DM) crustal residence times (T_{DM}) of sedimentary rocks are considered as a weighted average of the age and provenance of the eroded rock units in the source area (McLennan and Hemming, 1992). These data correlate with Archean crust and 2.0-1.8 Ga juvenile arcs that make up the basement of western Laurentia (Figure 4.8).

A change in the isotope signal begins in the IF at ICC3. Assemblage 2 yields $^{147}Sm/^{144}Nd$ values varying between 0.1288 and 0.0961 (f = -0.51 to -0.35), less negative $\varepsilon_{Nd}(T)$ values relative to Assemblage 1, ranging from -16.5 to -10.7, and Paleoproterozoic T_{DM} crustal residence ages (2.43-1.96 Ga). There appears to be no stratigraphic trend associated with $\varepsilon_{Nd}(T)$ values within Assemblage 2, and values appear to vary randomly. Most data overlap between Archean crust and 2.0-1.8 Ga juvenile arcs of the Wopmay Orogen (Great Bear, Fort Simpson magmatic arcs), but several samples are located outside of the fields for the Laurentian basement (Figure 4.8). None of the Precambrian basement domains of western Laurentia correspond to the >-15 $\varepsilon_{Nd}(T)$ values, which suggests that the less negative $\varepsilon_{Nd}(T)$ samples have secondary input from a more juvenile source with higher Nd isotopic ratios. Figure 4.8 shows potential mixing trends of basement domains with these juvenile sources, although it is unclear from Nd data alone whether these sources are felsic or mafic.

Interpreting Rb-Sr isotope data in sedimentary rocks is highly speculative due to the mobility of Rb and Sr during diagenesis, and potential for altering and even resetting isotopic ratios. The large amount of scatter within the $^{87}Sr/^{86}Sr$ ratios may indicate that the initial $^{87}Sr/^{86}Sr$ ratio has been somewhat altered by diagenesis or metamorphism. Nonetheless, several observations are

clear. All samples have elevated $^{87}Sr/^{86}Sr$ ratios, which is consistent with results of Nd analyses suggesting varying proportions of Archean crust. However, Assemblage 1 has a relatively low $^{87}Sr/^{86}Sr$ (0.7320 to 0.7582) and $^{87}Rb/^{86}Sr$ (1.56 to 6.29), whereas Assemblage 2 has higher and wider range of $^{87}Sr/^{86}Sr$ (0.7783 to 0.8438) and $^{87}Rb/^{86}Sr$ (3.69 to 20.64) ratios (Figure 4.7). The lower $^{87}Sr/^{86}Sr$ and $^{87}Rb/^{86}Sr$ ratios in Assemblage 1 may indicate the presence of a more mafic source with characteristically low Rb abundance, and accordingly low radiogenic Sr (i.e. lower $^{87}Sr/^{86}Sr$). In the case of Assemblage 2, the higher $^{87}Sr/^{86}Sr$ and $^{87}Rb/^{86}Sr$ ratios suggests little mafic input. Combined with the Nd isotopic data, which suggests secondary input from a more juvenile source for Assemblage 2, Sr isotopic data suggests that the juvenile source was felsic.

4.3 Provenance and tectonic setting discriminations

Both trace-element analysis and Sr-Nd isotopic composition of strata of the Neoproterozoic Windermere Supergroup at the Castle Creek study area indicate derivation primarily from upper continental crust. This is reflected in the enriched LILE and LREE, negative Eu anomalies, $^{87}Sr/^{86}Sr > 0.71$, $\varepsilon Nd < -10$, and negative $f^{Sm/Nd}$ values. However, examination of data at a finer scale shows that the geochemical characteristics of these strata are not uniformly similar. εNd results suggest that strata in the UKG to ICC1 interval are distinctively different compared to those in stratigraphically higher strata in the IF. Hence, the calculated depleted mantle model ages (T_{DM}) of these mudstones show significant variations in provenance ages as a function of variation in the source area. Despite previous interpretations based on U-Pb dating of detrital zircons suggesting that late Neoproterozoic sediment pathways to the deep-water Windermere basin in the SCC were stable and from a catchment in the west Laurentia craton (Hadlari et al., 2021; Matthews et al., 2017; Ross, 1991), the Nd and Sr isotopic composition of the studied samples, in addition to major and trace element composition, reveal two distinct clusters suggesting at least two different sources areas over time (Figure 4.7), and are discussed next.

4.3.1 Assemblage 1: UKG, LIF, ICC1

Assemblage 1 consists of the samples from mudstones in the UKG to ICC1 interval and are characterized by T_{DM} = 2.65 to 2.53 Ga provenance age and measured Nd-isotopic ratios ranging from -26.3 to -25.1 ($\varepsilon Nd(T)$ = -19.1 to -17.6), the most negative of any group sampled. Strata from Assemblage 1 also have variable $^{87}Sr/^{86}Sr(0)$ values ranging from 0.7320 to 0.7582 with an average of 0.7392. Notably, these results are consistent with previous studies, such as Boghossian et al. (1996), who analysed five samples from Windermere strata of the Horsethief Creek and Miette formations in southeastern B.C., and reported $\varepsilon_{Nd}(0)$ values between -29.51 and -27.66, and T_{DM} ages between 2.62 and 2.24 Ga. Also, the Sr isotopic ratios and strong correlation with Nd isotopic ratios negates possible fractionation during transport.

The detrital zircon ages of samples from Assemblage 1 have a characteristic northwestern Laurentia bimodal distribution with major populations between 3.0 to 2.5 Ga and 1.9-1.75 Ga, and an absence of grains between 2.5 and 2.0 Ga (Figure 4.9.). This zircon age distribution, in addition to low $\varepsilon_{Nd}(0)$ values, are consistent with derivation from nearby Precambrian basement domains in the subsurface of western Canada. The 3.0 to 2.5 Ga age population matches that of multiple Archean terranes in western Laurentia. This age population has peaks at 2.94 Ga, 2.66 Ga, and 2.57 Ga, which correspond well with the Medicine Hat Block (ca. 3.28-2.50 Ga), as well as subdivisions of the southern Hearne province, specifically the Matzhiwin domain (ca. 2.59 Ga), Vulcan domain (ca. 2.75-2.63 Ga), Eyehill domain (ca. 2.84-2.56 Ga) and Loverna domain (ca. 3.04-2.71 Ga). The 1.9-1.75 Ga age population, with peaks at 1.85 Ga and 1.79 Ga, is like that of the Rimbey domain (1.85-1.79 Ga). If the craton beneath southern Alberta had been the sediment source, the notable absence of zircons between 2.00 and 2.40 Ga suggests that

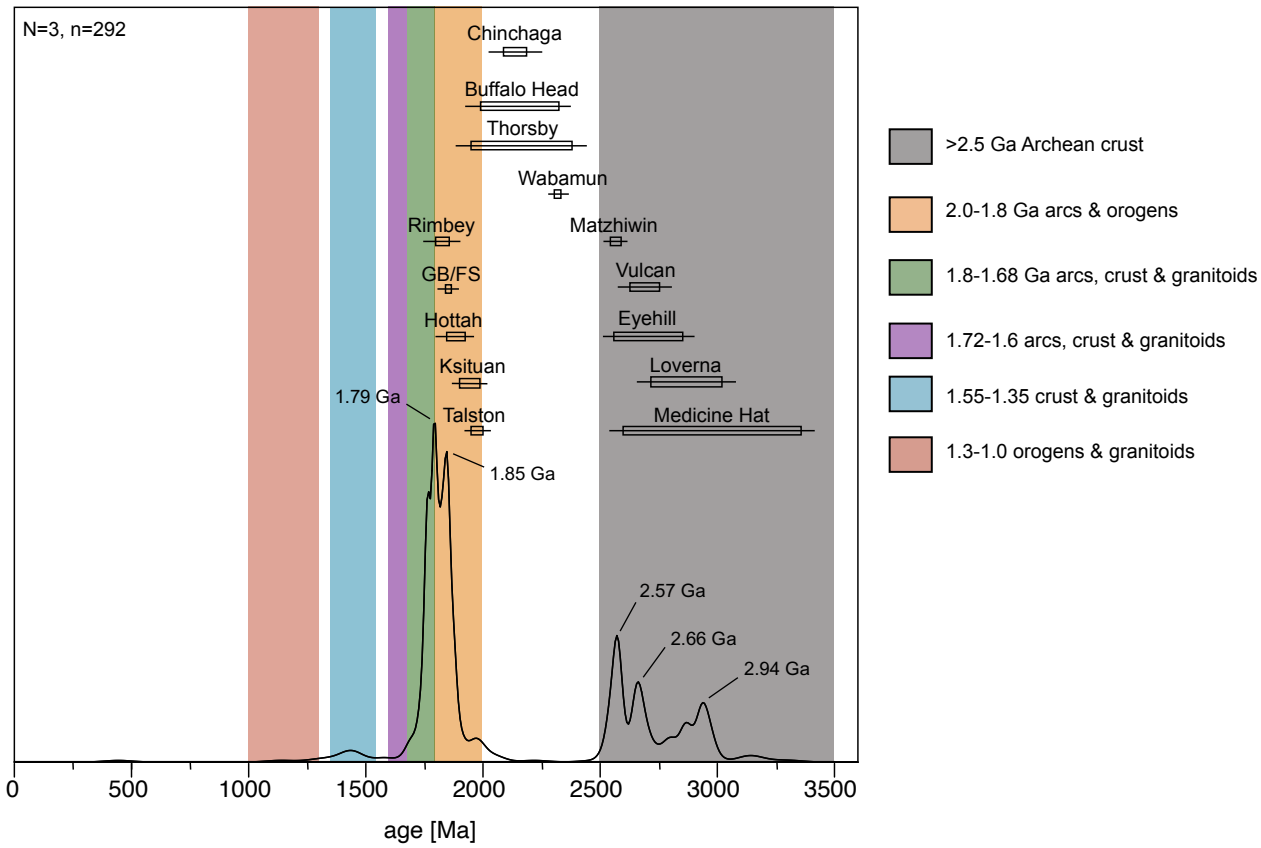

Figure 4.9. Composite kernel density estimation for all U-Pb zircon data for Assemblage 1 UKG, LIF, ICC1. Dates are $^{206}Pb/^{238}U$ for dates <1500 Ma, and $^{207}Pb/^{206}Pb$ for dates >1500 Ma. Samples with <1% probability of concordance were filtered from the data set. N is the number of samples; n is the number of measurements. Coloured regions correspond to major crystalline provenances of the Laurentian craton. Significant proximal sources are noted on the diagram with age ranges.

the 2.38-1.91 Ga Thorsby domain and the 2.32 Wabamun domain were not exposed and therefore not part of the sediment supply. Also, the low abundance of zircon age populations between 1.7 and 1.4 Ga suggests only limited input of recycled sediments from the Mesoproterozoic Belt Basin to the south.

Despite the $\varepsilon_{Nd}(0)$ and detrital zircon data suggesting derivation from an old continental rather than juvenile source for Assemblage 1, data plot in the intermediate igneous to mafic igneous provenance, due to their relatively high MgO, Fe_2O_3 and TiO_2 content (Figure 4.10. a). This is supported by trace element data (Figure 4.4. ; Figure 4.10. b), including low Th/Sc and

Zr/Sc, high Co/Th, high Cr abundance, and a more poorly developed Eu/Eu_N*, that collectively suggest an intermediate or mixed felsic/mafic source. This appears to conflict with the absence of a juvenile source in the detrital zircon and Nd isotope data. Two possible provenance models are proposed to explain the geochemical data in Assemblage 1. The first model uses the low abundance of incompatible trace elements and high transition trace metals to suggest a juvenile arc-derived component. It has been observed that passive margin turbidites (i.e. trailing edge, continental collision) generally have high levels of incompatible element enrichment (high Th/Sc, La/Sc, La/Yb), evolved major element compositions (high Si/Al, K/Na), lower ε_{Nd} (-26 to -1), high $^{87}Sr/^{86}Sr$ (0.709 to 0.734) and negative Eu-anomalies (McLennan et al., 1990). In comparison, active margin settings (i.e. forearc, continental arc, back arc, strike slip) have a mixture of old upper crust and young arc-derived material with less evolved major element composition , abundance of incompatible trace elements (Th/Sc = 0 to 1.8), higher ε_{Nd} (-13.8 to +8.3), lower $^{87}Sr/^{87}Sr$ (0.703 to 0.713) and less negative Eu anomalies ranging from 0.65 to 1.0 (McLennan et al., 1990). It is important to note that, unlike other types of strata, turbidites often

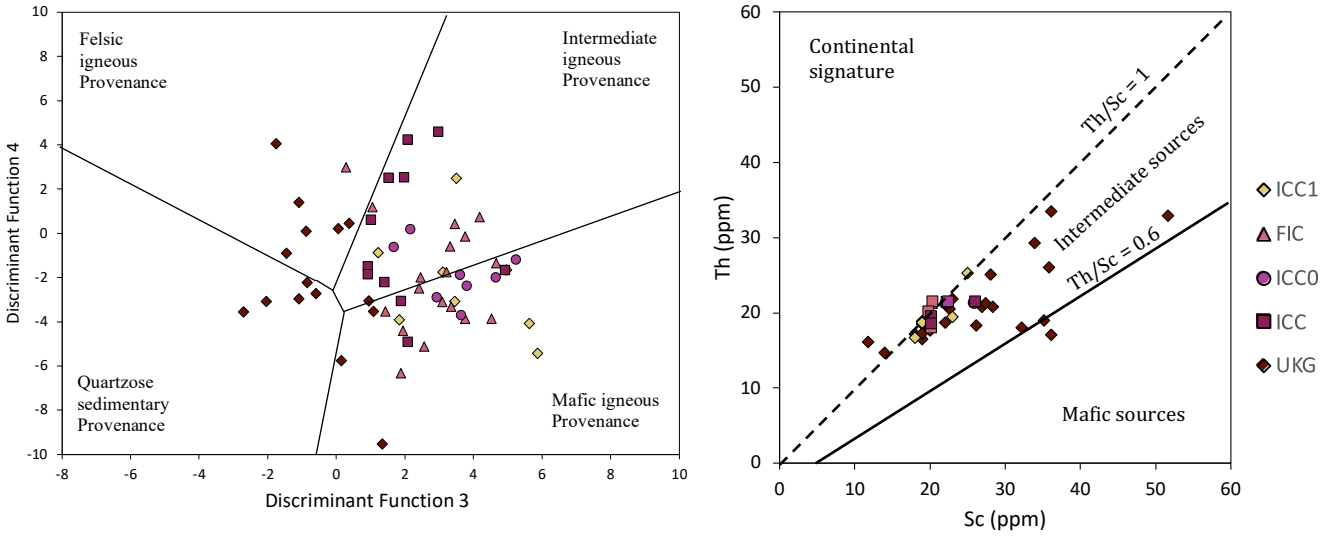

Figure 4.10. Bivariate plots for the interval between the UKG and ICC1 (Assemblage 1): a) Discriminant function diagram based on normalized major element oxides b) Bivariate Th versus Sc diagram.

exhibit considerable variability in composition. That being said, four provenance components may be recognized on the basis of these geochemical proxies: 1) old upper continental crust comprising old igneous/metamorphic terranes and recycled sediments, 2) young undifferentiated arc composed of young volcanic/plutonic sources that has undergone limited plagioclase fractionation, 3) young differentiated arc that has experienced plagioclase fractionation, and 4) mid-ocean ridge basalt (MORB) (McLennan et al., 1990).

Table 4.1. Turbidite provenance associations showing averages for selected geochemical proxies

	Major Element Compositions		Incompatible Trace Element Ratios							
	Si/Al	K/Na	Th/Sc	La/Sc	La/Yb	Eu/Eu*	Cr (ppm)	εNd	$^{87}Sr/^{86}Sr$	LREE/ HREE
Assemblage 1	2.4	6.1	0.9	2.9	25.3	0.70	142.8	-26	0.7414	22.1
Transitional Assemblage	2.4	4.7	1.2	3.3	14.9	0.63	144.1	N/A	N/A	14.3
Assemblage 2	2.7	8.3	1.2	4.5	32.3	0.65	114.9	-20.5	0.8233	29.0
Assemblage 3	3.2	4.0	1.0	3.2	20.3	0.62	82.2	N/A	0.8166	19.9

Geochemical data from Assemblage 1 (Table 4.1) suggest a mafic component in some of the strata, specifically: a flatter REE pattern (La/Yb_N = 25.3), a low Th/Sc ratio, and smaller negative Eu anomaly that is higher than that in UCC (Eu/Eu* = 0.7). Additionally, Assemblage 1 has a higher Cr/Th ratio (Cr/Th = 7.5) compared to other assemblages. This is also supported by the relatively lower $^{87}Sr/^{86}Sr(0)$ values ranging from 0.7320 to 0.7582 compared to other assemblages.

Volcanism associated with Neoproterozoic rifting is documented at several locations along the western margin of Laurentia (Goodfellow et al. 1995) and include the Gataga volcanics (alkalic mafic to felsic composition) in the northern Canadian Cordillera (ca. 696-690 Ma), Idaho rift volcanics (ca. 700-680 Ma), and the Huckleberry-Irene Formation volcanics (E-MORB composition) in the southern Canadian Cordillera (ca. 762 Ma) (Devlin and Bond, 1988). Detrital

zircon age peaks recycled into Cambrian strata suggest that rift-related volcanism in the SCC spanned an approximate age range of 700-640 Ma (Matthews et al., 2017). Problematic then is the lack of similar-aged detrital zircons in Assemblage 1. Furthermore, alkali basalts have high REE, which should be reflected in an altered Nd isotopic signature. For example, mafic volcanics of the Huckleberry Formation in northeastern Washington have an extrusion date of ca. 762 Ma and a measured $\varepsilon_{Nd}(0)$ from -3.9 to +3.0, which corresponds to a value for ε_{Nd}^{600} of +2.9 to +6.4 (Mackinder et al., 2019). If these rift-related volcanics were the source, which might account for the trace element signature observed in Assemblage 1, ε_{Nd}^{600} should be more positive than the measured values of -19.1 to -17.6.

Alternatively, the volcanic source could be a more ancient arc-related source, for example the Paleoproterozoic Great Bear magmatic zone of the northwest Canadian shield. The Great Bear Magmatic Zone is a subduction-related convergent margin igneous complex composed mostly of K-rich, calc-alkaline rocks (Badham, 1973), but also many mafic volcanic phases (Ootes et al., 2017). The age range of these volcanic rocks corresponds well with the well-developed 1.85 Ga peak in Assemblage 1. Nd isotopic data shows that even for these rocks, while initial ε_{Nd} values would have been positive, measured $\varepsilon_{Nd}(0)$ ranges from -23.6 to -15.6, corresponding to values for ε_{Nd}^{600} of -15.8 to -10.8 (Ootes et al., 2017). Furthermore, mixing of parental magma with older crust could result in an even more evolved Nd isotopic ratio. It is possible that volcanic rocks of this age could have contributed to the geochemical signature of Assemblage 1 without significantly affecting the Nd isotopic ratios.

The second possible provenance is Archean greenstone belts and their constituent metamorphosed mafic and ultramafic rocks. Some workers have documented elevated Cr and Ni abundances in Archean sedimentary rocks (Taylor and McLennan, 1984). The cause of this

enrichment is not well understood but may reflect a significant ultramafic source component. Elevated Cr and Ni is accompanied by an enrichment in MgO. The nearest potential source exhibiting these characteristics is the Slave craton, which has extensive 2.69-2.66 Ga granitoid-greenstone belts (Cousens et al., 2002). Rocks of the Banting Group and West Yellowknife Bay suite range in composition from basalt through rhyolite and plot in the subalkaline field, whereas the older Kam Group comprises tholeiitic volcanic rocks with abundant pillow lavas that are basalt to basaltic andesite in composition (Cousens et al., 2002). Alternatively, sediment of intermediate-mafic composition may have been derived from Archean mafic and ultramafic suites in the central Hearne province supracrustal belt of northern Saskatchewan, Manitoba and Nunavut – one of the most laterally extensive Neoarchean "greenstone" terranes in the Canadian shield. These rocks tend to have moderate LREE enrichment with negative Nb anomalies, enrichment in Th, and enrichment in ferromagnesian trace elements. These rocks are interpreted to have formed from depleted upper mantle melts, although many exhibit crustal contamination. Measured $\varepsilon_{Nd}(0)$ for the late Archean Banting Group range from -35.3 to -13.6, which corresponds to ε_{Nd}^{600} of -27.3 to -10.4 (Cousens et al., 2002). These highly negative Nd isotopic ratios could explain the Nd isotopic ratios and major and trace element geochemistry of rocks of Assemblage 1.

4.3.2 Assemblage 2 (ICC3, ICC4, ICC5)

Assemblage 2 consists of mudstones from ICC3 to ICC5 with variable Nd-isotopic ratios ranging from -23.0 to -16.2 corresponding to εNd(*T*) values ranging from -16.5 to -10.7, T_{DM} = 2.43 to 1.96 Ga provenance age, and $^{87}Sr/^{86}Sr$ ranging from 0.8438 to 0.7783 (average 0.8232).

Detrital zircon ages from Assemblage 2 are consistent with a northwestern Laurentia provenance, but rather than being bimodal are trimodal. This includes major populations between 3.0 to 2.5 Ga, 1.9-1.8 Ga, and a third at 655 Ma (Figure 4.11.). Like Assemblage 1, this zircon age distribution is consistent with derivation from nearby Precambrian basement domains in the subsurface of western Canada but uniquely has a major juvenile population. The 3.0 to 2.5 Ga age population matches that of multiple Archean terranes that make up the basement of western Laurentia. This age population has a similar signature to Assemblage 1, with a scattering of ages between 3.0 and 2.4 Ga, and peaks at 2.95 Ga, 2.77 Ga, 2.67 Ga, 2.57 Ga. These correspond well with the Medicine Hat Block (ca. 3.28-2.50 Ga), in addition to subdivisions of the southern Hearne province, specifically the Matzhiwin domain (ca. 2.59 Ga), Vulcan domain (ca. 2.75-2.63 Ga), Eyehill domain (ca. 2.84-2.56 Ga) and Loverna domain (ca. 3.04-2.71 Ga). The Paleoproterozoic age population is slightly younger skewed compared to Assemblage 1, with an age range of 1.92-1.64 Ga compared to 2.02-1.68 for Assemblage 1. The Assemblage 2 age population has a major peak at 1.78 Ga that closely matches the Rimbey domain (1.85-1.79 Ga). The lack of ages between 2.0-1.92 Ga suggests no major contribution from the Ksituan or Talston domains, whereas the minor peak between 1.43-1.31 Ga has no readily identifiable source. However, igneous rocks of ~ 1.37 Ga have been reported from the Salmon River arch area of Idaho (Evans and Zartman, 1990). It is possible that these grains originated from an

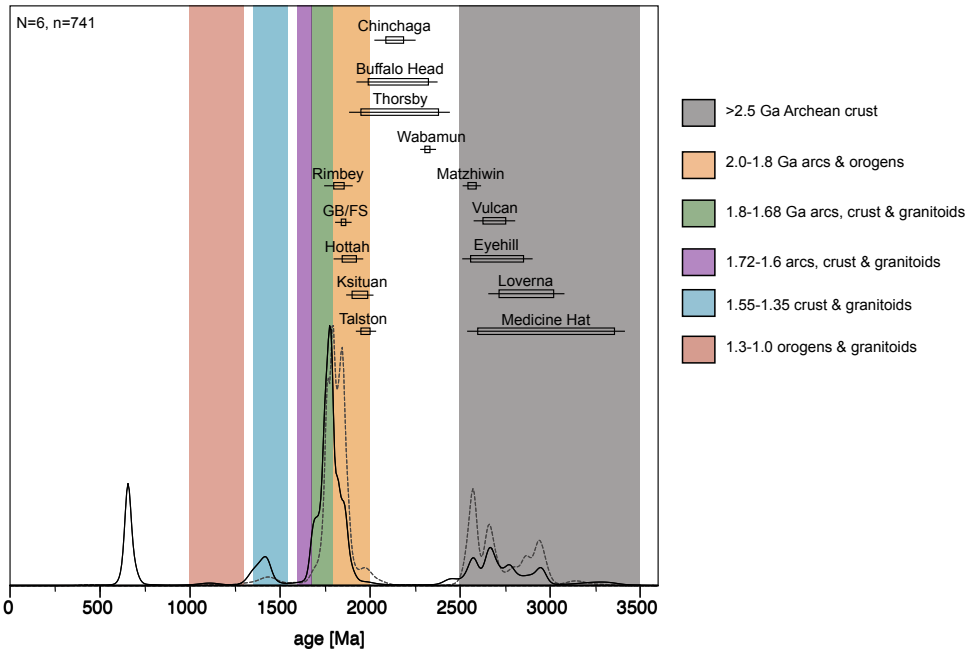

Figure 4.11. Composite kernel density estimation for all U-Pb zircon data for Assemblage 2 ICC3 to ICC5. Dates are $^{206}Pb/^{238}U$ for dates <1500 Ma, and $^{207}Pb/^{206}Pb$ for dates >1500 Ma. Samples with <1% probability of concordance were filtered from the data set. N is the number of samples; n is the number of measurements. Coloured regions correspond to major crystalline provenances of the Laurentian craton. Significant proximal sources are noted on the diagram with age ranges.

unknown pluton in the SCC with a similar age, or instead recycled from older Neoproterozoic clastic strata of northwestern Canada containing zircons that initially were derived from the Grenville province of east-central Canada (Rainbird et al., 1992; Gehrels and Ross, 1998).

The presence of Neoproterozoic ages in sedimentary rocks has been documented at several areas in the Cordillera. Matthews et al. (2017) reported ca. 650 Ma detrital zircon age populations in sandstones from the Latest Neoproterozoic middle Hamill Group (Purcell Mountains, B.C.), and the Three Sisters Formation in Kootenay Pass, B.C. Hadlari et al. (2021) reported a 665 Ma age peak in the Miette Group near Jasper, B.C. (Hadlari et al., 2021; Matthews et al., 2017). Additionally, Ross & Parrish (1991) reported 650 ± 15 Ma zircon grains from the Grand Forks complex, a metamorphic culmination in southern B.C. composed of

paragneiss, amphibolite gneiss, and pegmatite and forming part of the Shuswap Complex. These age populations were inferred to have been derived from magmatic rocks, though no obvious source in basement rocks of western North America was noted.

The observed 655 Ma peak is likely related to Neoproterozoic rift-related magmatism. There is broad consensus that the western passive margin of Laurentia formed after a protracted tectonic history involving two main episodes of extension (Bond and Kominz, 1984; Colpron et al., 2002; Moynihan et al., 2019; Ross and Parrish, 1991; Stewart, 1972). The initiation of Rodinian rifting along western Laurentia during the Tonian is thought to be linked to mantle plumes and marked by intrusion of the ca. 780 Ma Gunbarrel dikes that are exposed from northwestern Canada to Wyoming, and the Franklin dikes of northern Canada at ca. 720 Ma (Harlan et al., 2003; Li et al., 2008). Between 720 to 650 Ma, early rifting and volcanism occurred and intracratonic basins were formed, followed by deposition of glaciogenic deposits (e.g. Vreeland Formation) associated with sedimentation during the Sturtian Glaciation (Brennan et al., 2020; Yonkee et al., 2014). These strata are then overlain by siliciclastic rocks of the Windermere Supergroup and its correlatives throughout western North America, associated with subsidence from 650 to 580 Ma (Link et al., 1987). Lund et al. (2003) suggested that a major rifting event from Idaho to northern B.C. occurred around 690 Ma, associated with extrusion of felsic tuff in the Gataga Volcanics of northeastern B.C. (689 ± 4.6 Ma) (Fanning and Link, 2004; Lund et al., 2003). However, more recent work suggests a younger, short-lived pulse of igneous activity in the Windermere Basin ca. 680-650 Ma (Hadlari et al., 2021). The mechanisms driving Cryogenian (680-650 Ma) magmatism remain enigmatic due to the limited record of Neoproterozoic igneous rift-related strata in the North American Cordillera. Records of Cryogenian magmatic activity is restricted to a volcanic and intrusive alkalic suite in Idaho and

Utah (665-650 Ma) (Fanning and Link, 2004), and the Pool Creek syenite and associated dykes in southeast Yukon Territory (650-640 Ma) (Pigage and Mortensen, 2004). It is also possible that 660-650 Ma magmatism was derived from local sources that have no counterparts in previously dated Precambrian basement in the North American Cordillera.

Assemblage 2 exhibits a range of εNd(*T*) values from -16.5 to -9.9, and T_{DM} ages from 2.38 to 1.74 Ga, which is broader than in Assemblage 1 (-19.1 to -17.6 and 2.65 to 2.53 Ga, respectively), and significantly lower than lithostratigraphically equivalent strata in the Horsethief Creek and Miette groups (-22.0 to -20.3 and 2.61 to 2.24 Ga, respectively; Boghossian et al., 1996). This would suggest input from a more juvenile source, which is consistent with the prominent 655 Ma detrital zircon age population.

On the provenance discrimination diagram, most of these samples plot in fields for felsic igneous and quartzose sedimentary provenance (Figure 4.12.), reflecting their relatively low MgO, Fe_2O_3 and TiO_2 content. Furthermore, trace element ratios, such as high Th/Sc (0.68-1.85) and Zr/Sc (7.4-24), and low concentrations of Cr and Ni suggest a mostly continental source. REE patterns are similar to PAAS with LREE enrichment and negative Eu anomalies ranging from 0.57 to 0.74 (average = 0.68). The geochemical proxies for Assemblage 2 appear to

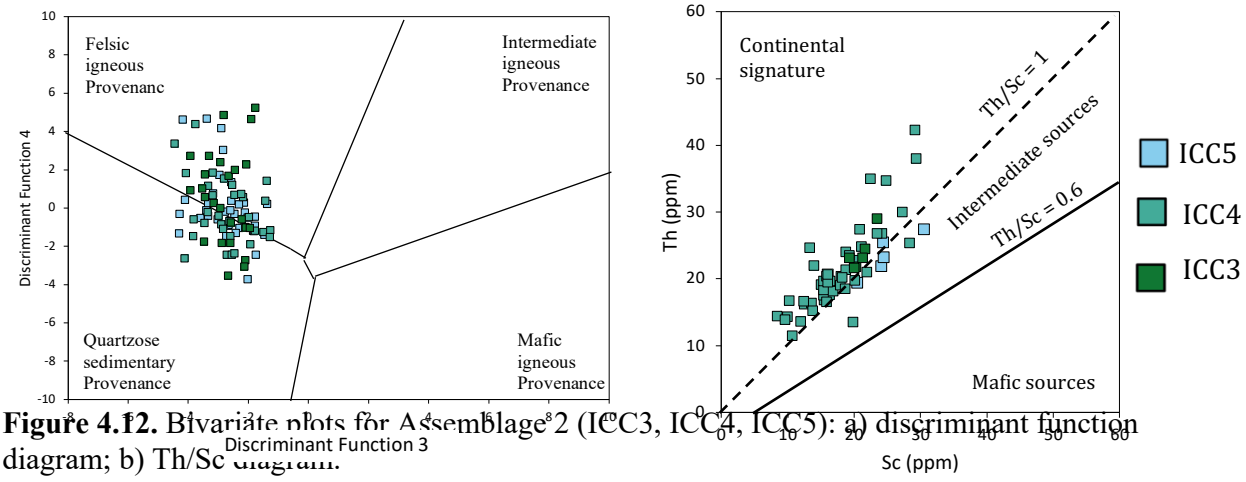

Figure 4.12. Bivariate plots for Assemblage 2 (ICC3, ICC4, ICC5): a) discriminant function diagram; b) Th/Sc diagram.

indicate a highly recycled continental source, with little to no mafic input. Furthermore, according to the turbidite tectonic classification scheme outlined in Table 4.1 geochemical data from Assemblage 2 are consistent with a mostly recycled or felsic component. They show an enriched LREE pattern (La/Yb_N = 32.3), high Th/Sc ratio, and a negative Eu anomaly like in UCC (Eu/Eu* = 0.65). Assemblage 2 has lower Cr and Ni compared to Assemblage 1.

These geochemical data, in addition to the 655 Ma detrital zircon age population and the more positive Nd isotopic ratios, are suggestive of a significant Neoproterozoic igneous rift-related source for Assemblage 2. The provenance discrimination diagram and trace element ratios appear to preclude the presence of a mafic source, and instead indicate a felsic igneous source. Nonetheless, Neoproterozoic rift-related igneous rocks have not been reported from the SCC but 665-651 Ma alkalic plutonic suites have been reported from exposures in Ramey Ridge, Acorn Butte, Rush Creek Point in central Idaho (Lund et al., 2009). These plutons are composite intrusive bodies with a felsic (syenite, quartz syenite, and syenogranite) composition, and since alkali felsic suites have abundant REEs, as source rocks, these suites could potentially alter the Nd isotopic ratio and contribute to the other observed trends in trace element composition.

4.3.3 Assemblage 3 (ICC6 to base of Cunningham)

Assemblage 3 consists of mudstones between ICC6 to the base of the Cunningham Formation. Compared to assemblages 1 and 2, data are much more limited, being confined to two measured $^{87}Sr/^{86}Sr$ ratios at 0.8019 and 0.778 and no Nd isotopic data, and therefore only ages derived from detrital zircons and major element composition are discussed.

The detrital zircons in Assemblage 3 have the characteristic Laurentia bimodal age distribution. This includes major populations between 3.0 to 2.5 Ga and 1.9-1.8 Ga (Figure 4.13.). This distribution resembles that in Assemblage 1, and accordingly is consistent with derivation from adjacent Precambrian basement domains in the subsurface of western Canada. However, the Paleoproterozoic age population in Assemblage 3 is skewed slightly younger, with an age range of 1.86-1.63 Ga compared with 2.02-1.68 Ga in Assemblage 1. Also, the major peak at

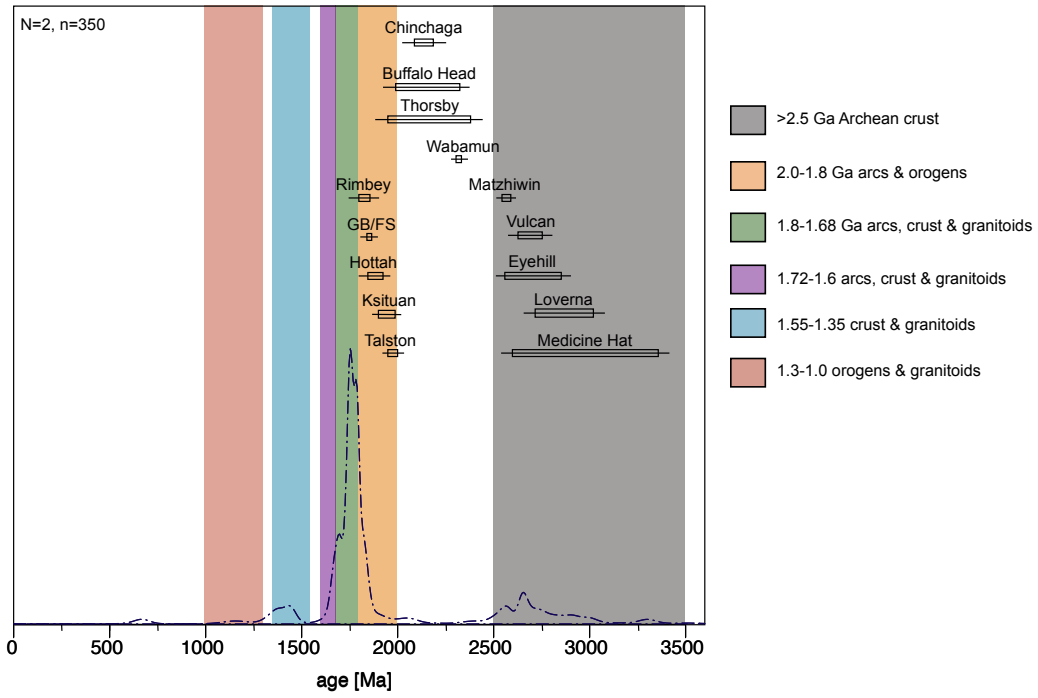

Figure 4.13. Composite kernel density estimation for all U-Pb zircon data for Assemblage 3 ICC6 to the base of the Cunningham Fm. Dates are $^{206}Pb/^{238}U$ for dates <1500 Ma, and $^{207}Pb/^{206}Pb$ for dates >1500 Ma. Samples with <1% probability of concordance were filtered from the data set. N is the number of samples; n is the number of measurements. Coloured regions correspond to major crystalline provenances of the Laurentian craton. Significant proximal sources are noted on the diagram with age ranges.

1.75 Ga is slightly lower than the one reported from the Rimbey domain (1.85-1.79 Ga). Local sources for the 1.79-1.63 Ga grains have not been recognized, suggesting there may be unrecognized plutons of this age in the area, or that they were transported from a distant region, which may include the southwestern U.S.A., where igneous rocks of these ages have been reported (Hoffman, 1989).

In the provenance discrimination diagram, samples from Assemblage 3 plot in the felsic igneous provenance field, with some in the quartzose sedimentary provenance field, but stratigraphically upward trend towards a more intermediate/mafic igneous composition, which is consistent with the upward increase in MgO, Fe_2O_3 and TiO_2 (Figure 4.14.).

Assemblage 3 is interpreted to mark the end of the input of juvenile ca. 655 Ma sources, and a return to the characteristic bimodal detrital zircon Laurentian signature. In the upper part of Assemblage 3 the increasing input of mafic/intermediate source material (Figure 4.14.) appears to suggest the return of the source that contributed to Assemblage 1. However, further study of the trace and minor element composition in Assemblage 3 is needed to develop this potential trend more fully.

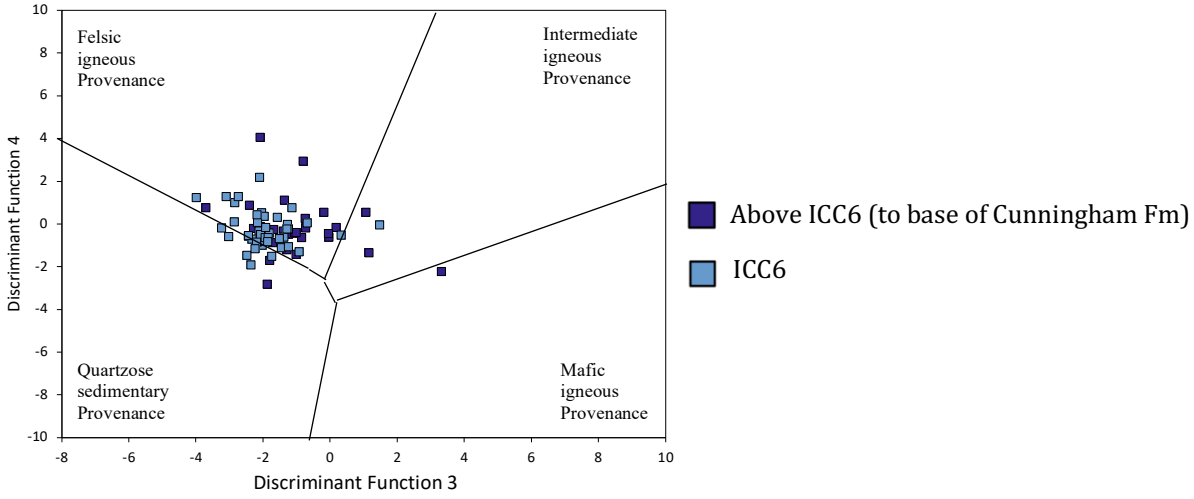

Figure 4.14. Bivariate plots for Assemblage 3 (ICC6 and above) showing discriminant functions.

4.3.4 Anomalous Signatures within Assemblage 2

The original objective of this thesis was to investigate and characterize the anomalous detrital zircon signature observed in ICC4B (17-CCK-IS-2), specifically the presence of a significant 2.4-2.0 Ga age population. This sample was one of only three samples originally collected from the 1.5 km-thick part of the Isaac Formation at the Castle Creek study area – the ICC4B sample from about the middle of the succession (Figure 4.15.). However, later, a much more closely spaced suite of samples was collected and showed the ICC4B sample to be a singularity and therefore the objectives of the research changed to a broader understanding of the larger Windermere turbidite system at the Castle Creek study area. Notably also, a sample collected ~ 1 m above the original 17-CCK-IS-2 sample was intended to be a duplicate of the original sample, and like the 17-CCK-IS-2 sample was different compared to all other samples, but interestingly also unique compared to the 17-CCK-IS-2 sample.

The age distribution of the 17-CCK-IS-2 sample shows no evidence of the typical trimodal signature in under- and overlying Assemblage 2 strata (Figure 4.16.). Instead, age populations in this sample are scattered between 2.35 and 1.79 Ga, with peaks at 2.30, 2.08 and 1.92, along with some >2.5 Ga Archean ages. This age distribution is unusual because 2.4-2.0 Ga detrital zircon ages are rare in Neoproterozoic passive margin sediments of the southern Canadian Cordillera (Gehrels and Ross, 1998; Hadlari et al., 2021; Matthews et al., 2017; Ross and Bowring, 1990). These age probabilities correspond well with the Chinchaga (2.19-2.09 Ga), Buffalo Head (2.32-1.99 Ga), and Wabamun (2.32 Ga) terranes that form the basement of northern Alberta, northern Saskatchewan, and N.W.T. However, the fact that this signature is present in only one sample and not duplicated in sandstone-filled channel units that immediately underlie and overlie ICC4B, suggests that this change in sediment source was not only profound

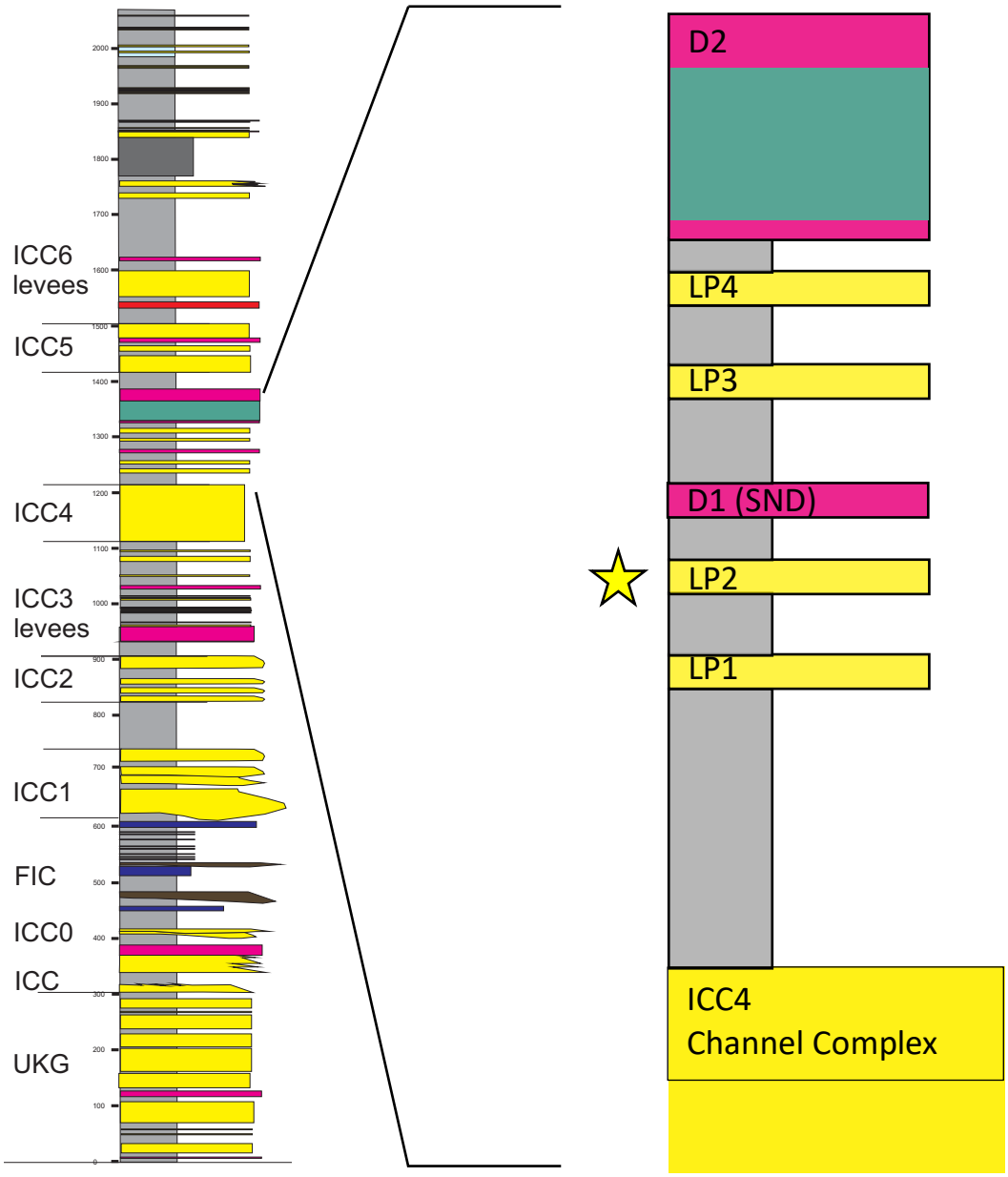

Figure 4.15. Location of ICC4B within the Isaac Formation at the Castle Creek study area. Yellow star marks the stratigraphic location of the anomalous samples

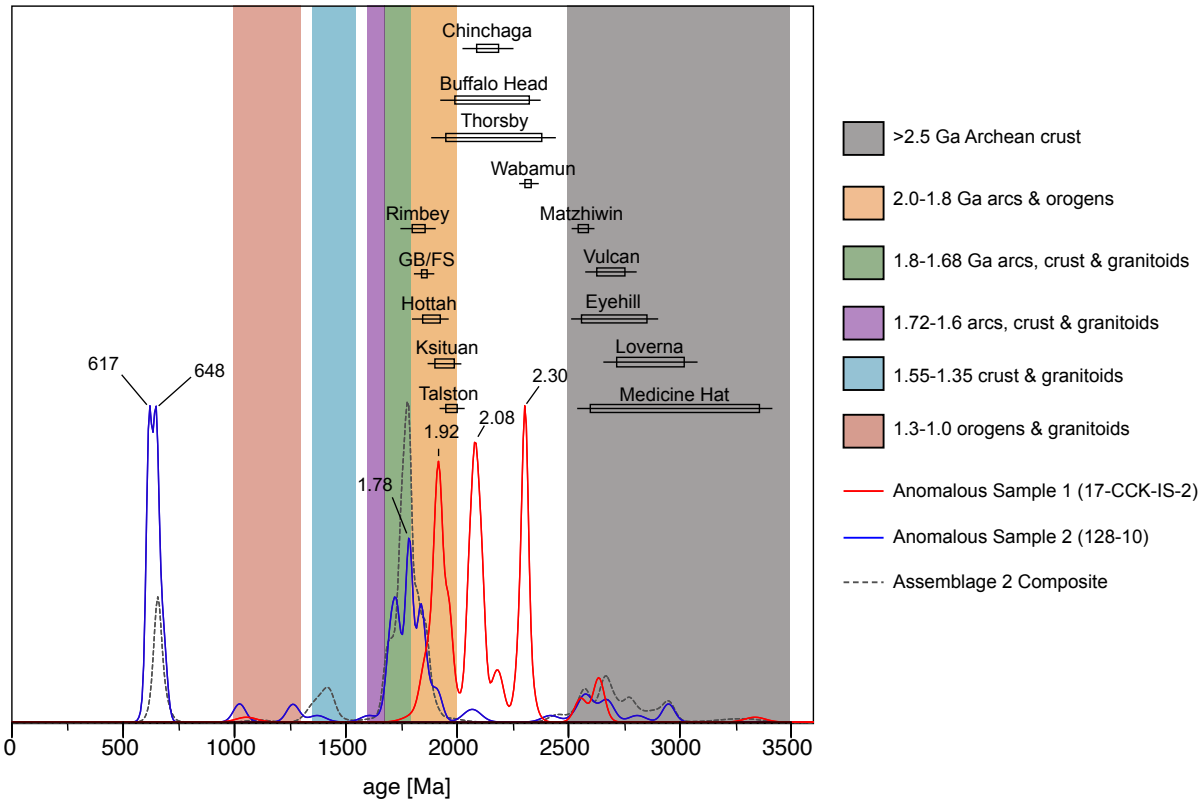

Figure 4.16. Composite kernel density estimation for all U-Pb zircon data for the anomalous samples of ICC4B, with <1% probability of concordance were filtered from the data set. N is the number of samples; n is the number of measurements. Coloured regions correspond to major crystalline provenances of the Laurentian craton. Significant proximal sources are noted on the diagram with age ranges.

but also very short-lived and quickly returned to the characteristic trimodal signature of Assemblage 2.

The second anomalous sample (128-10) is ~ 1 m stratigraphically above 17-CCK-IS-2 and shows the typical trimodal signature of Assemblage 2, with peaks at 648 Ma and 1.78 Ga (ranges from 1.94 to 1.65 Ga), and a scattering of > 2.5 Ga Archean ages (Figure 4.16.), but uniquely a sharp age probability at 617 Ma, with 15 grains ranging in age from 625 to 595 Ga. Generally, it is thought that the period between 650-580 Ma was a time of relative tectonic quiescence with no known ca. 620 Ma magmatic rocks in the southern Canadian Cordillera.

However, several recent studies from the northwestern U.S. have reported mafic magmatism between 620-600 Ma (Brennan et al., 2020; Provow et al., 2021). The late Ediacaran Browns Hole Formation (Brigham Group) of northern Utah comprises <140 m of volcaniclastic rocks with interbedded mafic-volcanic flows. Apatite U-Pb geochronology suggests a crystallization age of 613 ± 12 Ma (2σ) for the intercalated volcanic member (Provow et al., 2021). Additional evidence for coeval mafic magmatism is in central Idaho, where the lower Clayton Mine quartzite (ca. 667 Ma) is intruded by a 601 ± 27 Ma gabbroic sill, suggesting that mafic magmatism, possibly associated with rifting, was active at this time (Brennan et al., 2020). These dates fall within the error for our 617 ± 16 Ma age peak and may be coincident with late-stage rift-related mafic magmatism prior to the transition to a passive margin. Although possible, it is important to note the absence of igneous rocks with crystallization ages between 620-600 Ma north of central Idaho.

4.4 Sediment routing patterns in the Neoproterozoic Windermere Supergroup, southern Canadian Cordillera

The integration of a suite of geochemical provenance techniques reveals a series of significant shifts in the geochronology and geochemistry of deep-water clastic rocks from the upper Kaza Group to the base of the Cunningham Formation. These results are summarized in Figure 4.17, showing changing trends in major elements, trace elements, isotopic ratios, and U-Pb dates, for the three identified assemblages. Together, these provenance proxies indicate a transition from a mixture of cratonic and intermediate-mafic Laurentian basement sources (Assemblage 1), to mixed cratonic and local Neoproterozoic felsic igneous source (Assemblage 2), and finally to an exclusively Laurentian cratonic source (Assemblage 3). A map with all western Laurentia basement rocks is shown in Figure 4.18, and hypothetical catchment and drainage pathways for each assemblage are illustrated in Figure 4.19.

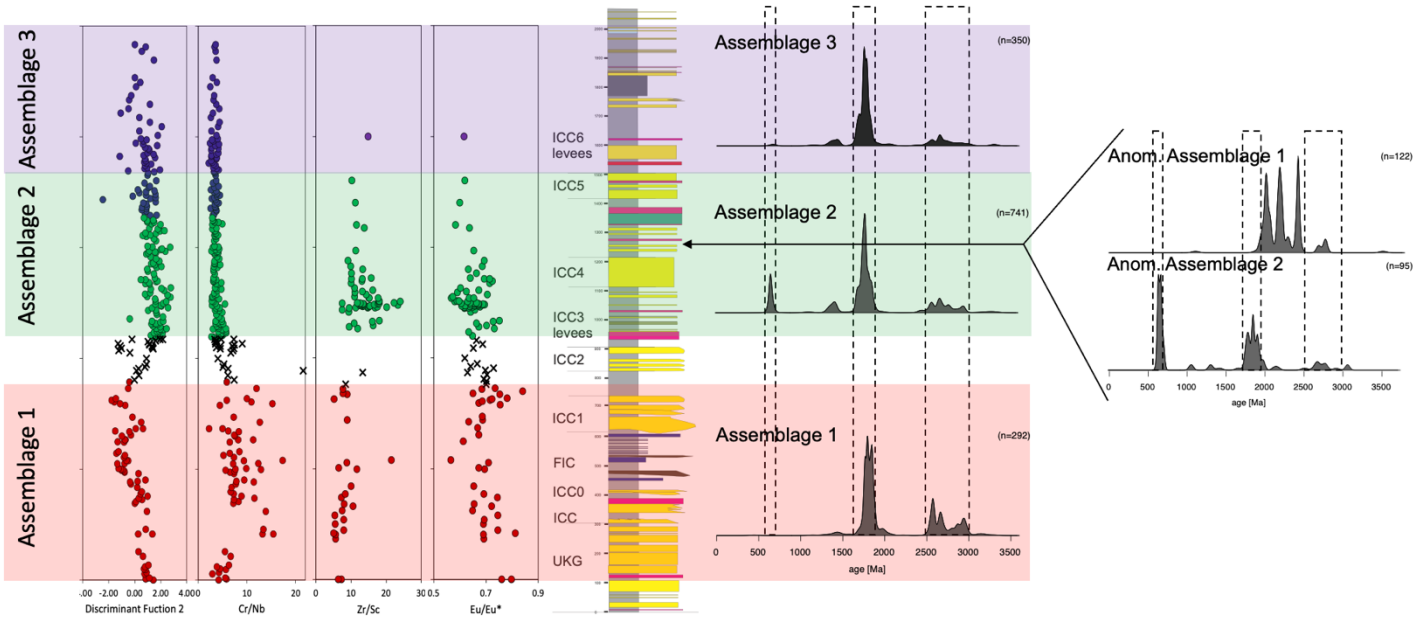

Figure 4.17. Summary of provenance proxies for assemblages 1, 2 and 3, showing major and trace element ratios: a) discriminant function; b) Cr/Nb, c) Zr/Sc, d) Eu/Eu*. Also shown are compiled detrital zircon U-Pb data for each assemblage, showing most common age populations.

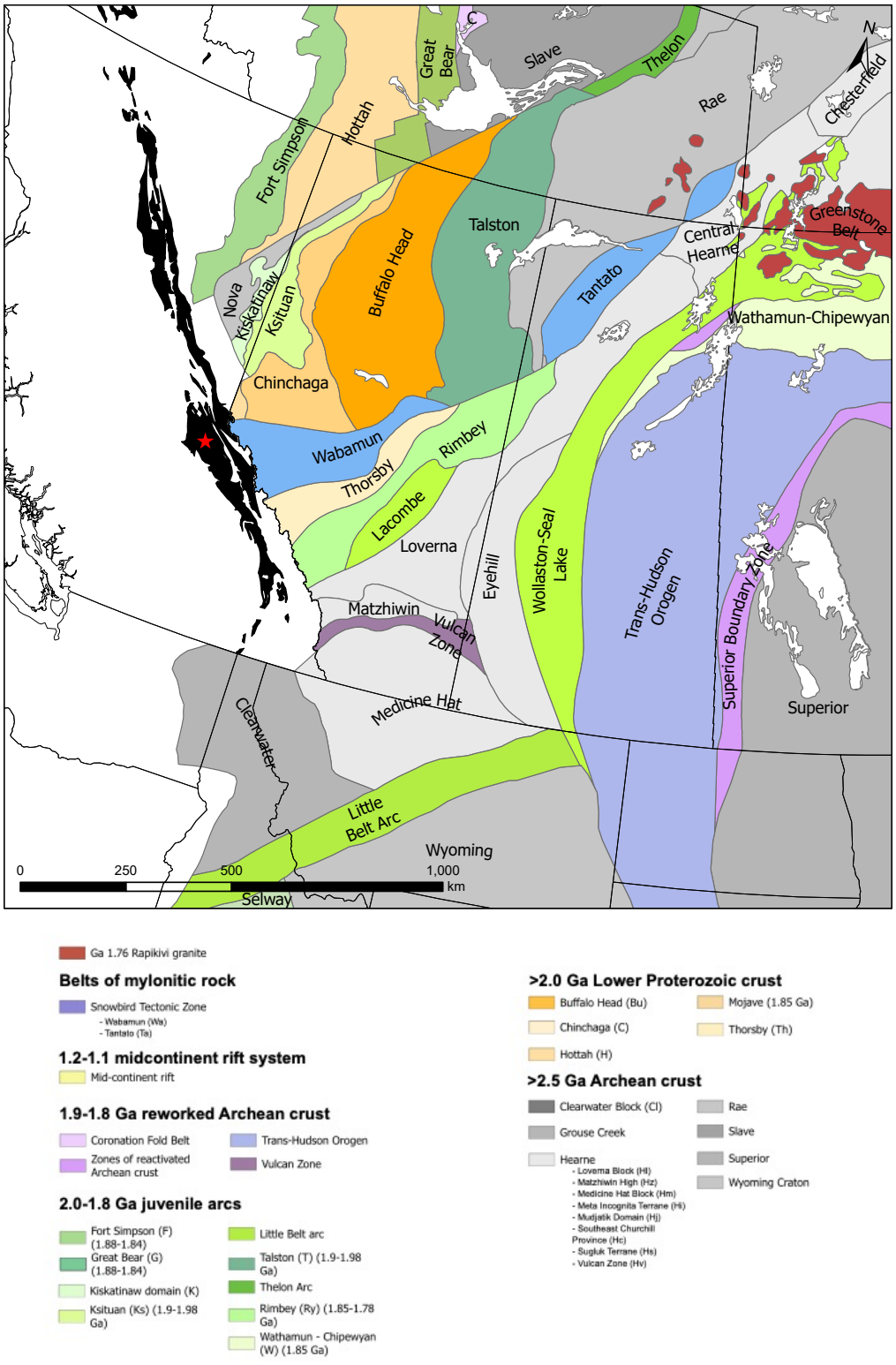

Figure 4.18. Map of basement terranes (exposed and subsurface) in western Laurentia. Black shaded area represents Windermere Supergroup deposits; red star is the location of the Castle Creek study area. Geological data from Open Government Canada, BC Geological Survey Digital Geology, Government of Alberta Open Data, USGS Open Data Bedrock Geology maps.

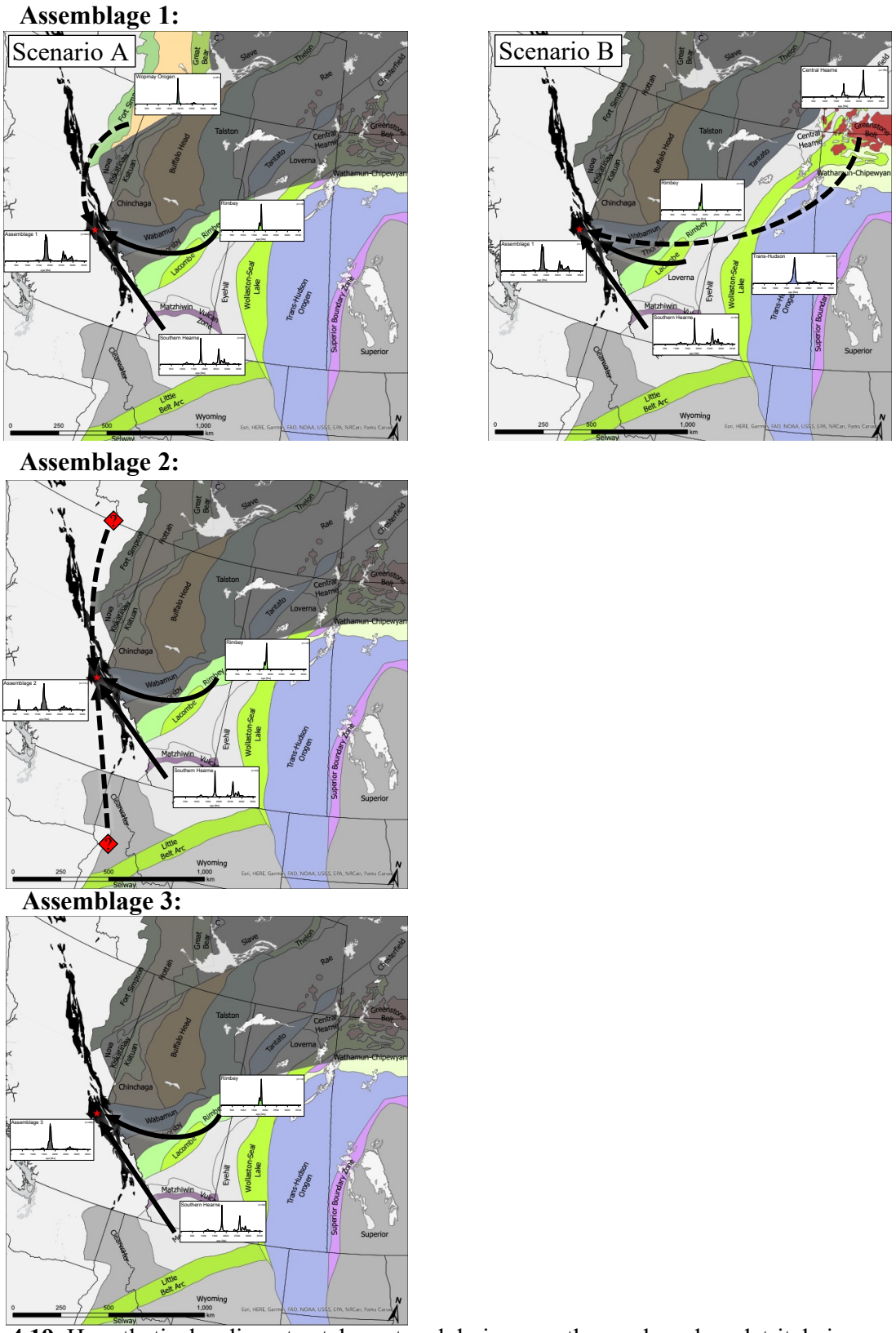

Figure 4.19. Hypothetical sediment catchment and drainage pathways based on detrital zircon signatures superimposed on sub-Paleozoic subcrop map. Darker tinted areas represent non-sourced areas; lighter areas represent the potential regional drainage basin. Black solid and dotted arrows represent most likely and less likely sediment source pathways, respectively.

Assemblage 1 is characterized predominantly by an old (>1.7 Ga) cratonic source with significant additional input from an intermediate-mafic source. The cratonic source has numerous potential sources in the Precambrian basement domains of Laurentia but is likely derived primarily from the Rimbey domain and southern Hearne province due to their proximity to the Windermere basin. Two potential sources for the additional intermediate-mafic source (see also Chapter 5.2), include: a) the northern Wopmay Orogen, and b) Archean greenstone belts from in the central Hearne and Slave cratons. Scenario A could provide an intermediate-mafic geochemical signature from the terranes that make up the Wopmay Orogen, specifically the Fort Simpson, Hottah, Great Bear terranes, which also would be consistent with detrital zircon and Nd isotopic data. However, this scenario requires sediment to traverse several 2.4-2.0 Ga terranes that lie between the CC study area and the Wopmay Orogen magmatic belts, including the Kiskatinaw, Ksituan, Chinchaga, and Buffalo Head terranes. However, the absence of 2.4-2.0 Ga detrital zircons makes this scenario problematic. Furthermore, there is no evidence of a north-south paleoflow direction. Alternatively, sediment of intermediate-mafic composition may have been derived from Archean mafic and ultramafic suites in the central Hearne province supracrustal belt of northern Saskatchewan, Manitoba and Nunavut – one of the most laterally extensive Neoarchean “greenstone” terranes in the Canadian shield. This model (Scenario B) is more consistent with the generally accepted opinion that sediment dispersal systems in the Neoproterozoic traversed northern Laurentia in a roughly east to west direction (Hadlari et al., 2021; Matthews et al., 2017; Saylor and Sundell, 2021).

Assemblage 2 is characterized by the appearance of ca. 655 Ma detrital zircon population, and the disappearance of the intermediate-mafic source rock signature of Assemblage 1. The resulting detrital signature reflects mixing of two distinct sources. Like

Assemblage 1, the Mesoproterozoic and Archean detrital zircon signatures are attributed to the southern Hearne and associated Rimbey domain. The more distal central Hearne and Trans-Hudson domains are less significant compared to Assemblage 1, as noted by fewer ca. 1.85 Ga ages. This may be attributed to a greater flux of sediment from local sources or a reduced sediment supply from distal sources. The source of the ca. 655 Ma age peak, however, is more uncertain. This age peak appears abruptly at the base of ICC3 and remains significant throughout ICC4, although the relative abundance of the peak varies between samples. The strength of the peak gradually decreases from ICC5 to ICC6 and then is absent in strata above ICC6. This may suggest that the peak represents unroofing and erosion, followed by gradual depletion. The only Neoproterozoic igneous rocks known to have crystallized between ~ 660-640 Ma are a suite of 665-651 Ma alkalic felsic plutons in central Idaho (Lund et al., 2009), and the 650-640 Ma Pool Creek syenite in the Yukon Territory (Pigage and Mortensen, 2004). If the detrital zircon signature came from the Pool Creek syenite to the north, the absence of 2.4-2.0 Ga zircons, like in Scenario A of Assemblage 1, becomes problematic. When considering a southern source for the 655 Ma peak, for example alkalic plutonic suites in central Idaho, no previous studies have suggested a significant sediment routing system from the south in the southern Canadian Cordillera. However, there is extensive evidence for active tectonism between 650 and 635 Ma in the southern United States, particularly in the Death Valley region where angular unconformities formed by block rotation, buried normal faults, and associated olistostrome and fanglomerate deposits have been reported (Nelson et al., 2020). This may suggest that the same episode of tectonism that formed magmatic units in the southern United States was also active in the southern Canadian Cordillera, possibly suggesting that tectonic quiescence occurred later

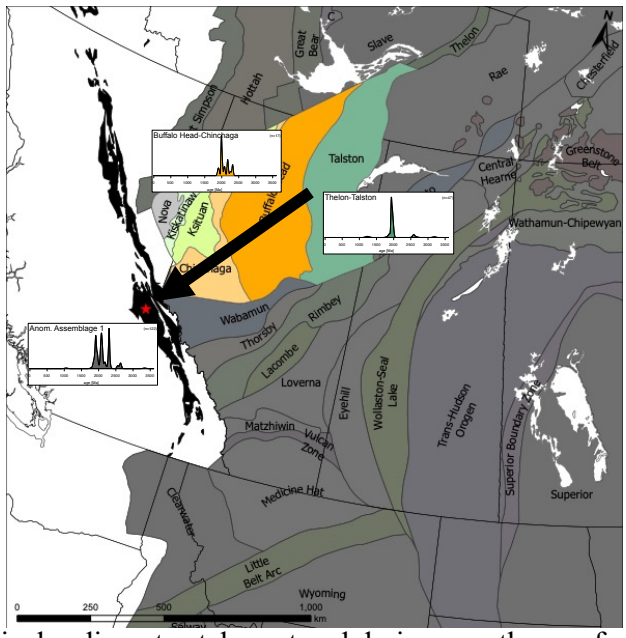

Figure 4.20. Hypothetical sediment catchment and drainage pathways for anomalous ICC4B sample based on detrital zircon signatures superimposed on sub-Paleozoic subcrop map. Highlighted area indicates the probable sediment catchment and the solid black arrow the most likely drainage pathway.

than prevously hypothesized. A third possibility is that 655 Ma zircons may be derived from rare, isolated intrusive units related to late-stage rifting in the SCC. Interestingly, the 617 Ma peak in Anomalous Sample 1 of ICC4B may also reflect anorogenic magmatism, and based on its large relative abundance but isolated occurrence (one sample), a source located in close proximity to the study area would seem most probable.

The most likely source for anomalous Sample 2 in ICC4B (17-CCK-IS-2), is the 2.4-2.0 Ga Chinchaga and Buffalo Head domains, and the Talston arc to the northeast of the deep-water Windermere turbidite basin (Figure 4.20). Being restricted to a single sample, and then reverting to the regional Assemblage 2 signature, indicates that one or at most a small number of successive transport events were affected by this dramatic change in sediment provenance – a change that otherwise had no obvious effect on sedimentological, lithological or stratigraphic characteristics. This would suggest a catastrophic, possibly single transport event that

overwhelmed the general sediment transport pattern. Although highly speculative, one possible scenario could be an energetic, high-volume glacial outburst event or major slope failure that spawned an anomalous transport event – an event that might have equivalence in the carbonate-rich Contessa bed in the otherwise siliciclastic deep-water strata of the Miocene Marnoso Arenacea Formation in northern Italy (Amy and Talling, 2006).

Assemblage 3 has a signature similar to Assemblage 2 but lacks the ca. 655 Ma peak. Given the major ca. 1.75 Ma peak, and absence of the ca. 1.85 peak of Assemblage 1, the principal sediment sourced was mostly likely the southern Hearne and Rimbey domains.

Chapter 5: Summary and Future Work

The Windermere Supergroup is a 7–9 km-thick continental rift-to-drift succession associated with the breakup of Rodinia and subsequent development of a passive continental margin and deposition of mostly siliciclastic deep-marine strata. Using a variety of geochemical datasets this study focuses on a 2.5 km-thick succession of basin-floor to slope deposits exposed in the Castle Creek study area of east-central British Columbia. Eleven sandstone samples were collected for detrital zircon U-Pb geochronology and a suite of mudrocks with ~ 10 m vertical sample spacing for whole-rock isotopic and elemental analysis.

Initially, the objective of this thesis was to document the geochemical changes in proximity to a geochronologically anomalous sample in ICC4B and therein elucidate changes on the pattern of regional sediment supply. However, with newly collected data it became clear that the unusual nature of sample was isolated to a single observation and led to a secondary objective to study the broad-scale provenance trends through the entire transect of basin floor to continental slope succession exposed at Castle Creek. This thesis has made several original contributions toward the understanding of temporal changes in sediment provenance and sediment supply during development of the continent-margin Neoproterozoic Windermere turbidite system in the southern Canadian Cordillera. These contributions and recommendations for future work are highlighted next.

5.1 Contributions

Methods:

1. ***Collection of high temporal resolution dataset:*** This thesis involved the collection of a suite of closely spaced (~1-10 m) mudrock samples supplemented with variably spaced detrital zircon samples from strata of the upper Kaza Group and Isaac Formation. The

purpose was to identify temporal changes in sediment source. This high level of stratigraphic resolution, especially in terms of the detrital zircon data, is uncommon in sediment provenance studies, but here allowed for the identification of provenance subgroups with greater confidence. Nonetheless, it is recognized that for most provenance studies a more moderate sample spacing (~10-20 m) is most likely sufficient, although smaller scale trends may not be identified.

2. ***Integration of detrital zircon and isotope studies:*** In this study detrital zircon and whole-rock isotope data were collected and analyzed. Both data sets were able to independently discriminate discrete provenance assemblages and therein temporal changes in sediment supply. More specifically, isotopic ratios for Nd and Sr were found to supplement geochronology data by providing information on the comparative contribution of juvenile versus old, cratonic material. A weakness of whole-rock isotope data is that it cannot identify a specific source region, especially when multiple sediment sources are involved and the amount of mixing is unknown. Single grain LA-ICP-MS analysis, which targets individual grains, would eliminate this issue and may be a useful addition in future work.
3. ***Usefulness of major and trace element contents as indicators of source rock type:*** Major and trace elements from whole-rock digestions showed some variation at small scales but generally followed large-scale trends between assemblages. Major elements, through discriminant function analysis, were shown to be highly effective in identifying unique provenance assemblages. Trace element analyses helped distinguish mafic from felsic sources using abundances of ferromagnesian elements, and elemental ratios such as Th/Sc, La/Yb, and REE trends. Collectively, these data provide a useful supplement to detrital zircon and isotope data for provenance interpretations.

Insights on the Windermere Supergroup in the SCC:

4. ***Three geochemically distinct assemblages in the upper Kaza Group (basin floor) to Isaac Formation (continental slope) transect:*** The geochemistry and geochronology of the studied mudrock samples reveal three distinct clusters. Assemblage 1 consists of mudstones from the UKG to ICC1. The detrital zircon ages from Assemblage 1 sandstones have a characteristic northwestern Laurentia bimodal distribution with major populations between 3.0 to 2.5 Ga and 1.9-1.75 Ga, and a notable absence of grains between 2.5 and 2.0 Ga. This zircon age distribution, in addition to low $\varepsilon_{Nd}(0)$ values, are consistent with derivation from nearby Precambrian basement domains in the subsurface of western Canada. Major elements from Assemblage 1 mudstones plotted on a provenance discrimination diagram also indicate an intermediate igneous to mafic igneous provenance, which is supported by trace element data showing low Th/Sc and Zr/Sc, high Co/Th, high Cr abundance, and a more poorly developed Eu/Eu_N*. This additional input was likely derived from Archean mafic and ultramafic suites from the Central Hearne province supracrustal belt, one of the most laterally extensive Neoarchean "greenstone" terranes in the Canadian shield. Assemblage 2 consists of mudstones in the interval from ICC3 to ICC5. Like Assemblage 1, zircon age distributions are consistent with derivation from nearby Precambrian basement domains in the subsurface of western Canada but uniquely exhibit a 655 Ma detrital zircon age population and higher $\varepsilon_{Nd}(0)$ values. On a provenance discrimination diagram most samples plot in fields for felsic igneous and quartzose sedimentary provenance. High Th/Sc and Zr/Sc, low Co/Th, and low concentrations of Cr and Ni suggest a mostly continental source. These indicators suggest a significant Neoproterozoic felsic igneous rift-related source component for

Assemblage 2. In the interval between ICC1 and ICC3 geochemical data show a progressive upward transition related to the progressive increase in the contribution of the Assemblage 2 provenance. Assemblage 3 comprises mudstones from ICC6 to the base of the Cunningham Formation, and like Assemblage 1 exhibits a bimodal detrital zircon signature characteristic of a western Laurentia source. However, in the provenance discrimination diagram samples in the lower part of Assemblage 3 plot in the felsic igneous provenance field, with some in the quartzose sedimentary provenance field, but stratigraphically upwards trend towards an increasingly more intermediate and mafic igneous composition. Additionally, Assemblage 3 lacks the input of juvenile ca. 655 Ma sources of Assemblage 2, and therefore marks the return to the characteristic bimodal Laurentian signature.

5. ***A mostly western Laurentian craton source for strata at Castle Creek:*** Major and trace element analysis, and Sr-Nd isotopic composition of strata of the Neoproterozoic Windermere Supergroup at the Castle Creek study area indicate derivation primarily from upper continental crust. This is indicated by the enrichment of LILE and LREE, $^{87}Sr/^{86}Sr(t)) > 0.71$, $\varepsilon Nd\ (t) < -10$, and negative $f^{Sm/Nd}$ values. Most of the samples contain detrital zircon age populations with a characteristic northwestern Laurentia bimodal distribution with major age populations between 3.0 to 2.5 Ga and 1.9-1.75 Ga, and notably an absence of ages between 2.5 and 2.0 Ga. This zircon age distribution, in addition to low $\varepsilon_{Nd}(0)$ values, are consistent with derivation from nearby Precambrian basement domains in the subsurface of western Canada. The 3.0 to 2.5 Ga age population matches that of multiple Archean terranes that comprise western Laurentia. This age population has peaks at 2.94 Ga, 2.66 Ga, and 2.57 Ga, which correspond well with the

Medicine Hat Block (ca. 3.28-2.50 Ga), as well as subdivisions of the southern Hearne province, specifically the Matzhiwin domain (ca. 2.59 Ga), Vulcan domain (ca. 2.75-2.63 Ga), Eyehill domain (ca. 2.84-2.56 Ga) and Loverna domain (ca. 3.04-2.71 Ga). The 1.9-1.75 Ga age population, with peaks at 1.85 Ga and 1.79 Ga, is like that of the Rimbey (1.85-1.79 Ga).

6. ***Evidence of late-stage magmatism, possibly related disassembly of Rodinia:*** Assemblage 2 is characterized by a major 655 Ma peak, which contrasts the general assumption of broad subsidence and tectonic quiescence along the passive margin of Laurentia from 650 to 580 Ma (Link et al., 1987). The youngest known rifting event in the Canadian Cordillera is the Gataga Volcanic assemblage of northeastern B.C. (689 ± 4.6 Ma) (Fanning and Link, 2004; Lund et al., 2003). Records of Cryogenian magmatic activity also include volcanic and intrusive alkalic suites in Idaho and Utah (665-650 Ma) (Fanning and Link, 2004), and the Pool Creek syenite and associated dykes in southeast Yukon Territory (650-640 Ma) (Pigage and Mortensen, 2004). Additionally, there is extensive evidence for active tectonism between 650 and 635 Ma in the southern United States, particularly in the Death Valley region, and includes angular unconformities formed by block rotation, buried normal faults, and associated olistostrome and fanglomerate deposits (Nelson et al., 2020). It is unlikely that the 655 Ma population was derived from the north due to an absence of 2.4-2.0 Ga detrital zircons in the samples (derived from intervening basement terranes), and the fact that no paleocurrent data to date in the SCC has indicated a northern source to the WSG. The most likely source is the southern source, or potentially local 660-650 Ma magmatism in the general northwestern Laurentian catchment that has no counterparts in previously dated Precambrian basement

in the North American Cordillera. This may suggest that the same episode of tectonism that generated the magmatic units in the southern United States was also active in the southern Canadian Cordillera, and therefore the timing of tectonic quiescence occurred later than previously hypothesized.

5.2 Future Work

1. ***Analysis of detrital zircon samples by LA-ICP-MS methods, including analysis of Hf isotopic ratios:*** The original scope of this thesis included the Lu-Hf isotope system to help in the identification of provenance sources. However, Lu-Hf analyses were not able to be completed due to the long-term closure of the isotope laboratory. Hf isotope data from single zircon grains are particularly useful for studying crustal–mantle evolution over geologic history because zircon is a ubiquitous accessory mineral in granitoids and high-grade metamorphic rocks, and records Hf isotope composition at the time of crystallization. By targeting detrital zircons previously dated using U-Pb methods, it is possible to better constrain their origin, such as which grains came from magmatic versus volcanic or felsic versus mafic sources.
2. ***Further sampling in other localities and at other stratigraphic levels in the WSG in the SCC:*** Additional sampling would help determine if the assemblages recognized in this study are observed regionally, and therein test the reliability of these provenance assemblages as a regional correlation tool. Also, sampling of strata in the middle and lower Kaza groups, in addition to the stratigraphically higher Cunningham and Yankee Belle formations, would provide a more complete assessment of sediment provenance for the entire Windermere turbidite system. Areas where this could be done include North Jumbo Creek in southeast B.C. where a continuously exposed succession extending from

rift-related strata of the Toby Formation to continental rocks of the Cambrian Hamill Group that unconformably overlie the WSG crop out. Additionally, archived and previously unanalyzed mudrock and sandstone samples from the work of Dr. Margot McMechan (GSC Calgary) would extend the geochemical characterization of Windermere strata northward into the central Rocky Mountains.

References

Aalto, K.R., 1971. Glacial Marine Sedimentation and Stratigraphy of the Toby Conglomerate (Upper Proterozoic), Southeastern British Columbia, Northwestern Idaho and Northeastern Washington. Canadian Journal of Earth Sciences, 8(7): 753-787.

Absar, N., Raza, M., Roy, M., Naqvi, S., Roy, A., 2009. Composition and weathering conditions of Paleoproterozoic upper crust of Bundelkhand craton, Central India: Records from geochemistry of clastic sediments of 1.9Ga Gwalior Group. Precambrian Research, 168(3-4): 313-329.

Aitken, J.D., 1969. Documentation of the sub-Cambrian unconformity, Rocky Mountain Main Ranges, Alberta. Canadian Journal of Earth Sciences, 6(2): 193-200.

Ali, S. et al., 2014. The provenance of Cretaceous to Quaternary sediments in the Tarfaya basin, SW Morocco: Evidence from trace element geochemistry and radiogenic Nd–Sr isotopes. Journal of African Earth Sciences, 90: 64-76.

Amedjoe, C.G., Gawu, S.K.Y., Ali, B., Aseidu, D.K., Nude, P.M., 2018. Geochemical compositions of Neoproterozoic to Lower Palaeozoic (?) shales and siltstones in the Volta Basin (Ghana): Constraints on provenance and tectonic setting. Sedimentary Geology, 368: 114-131.

Amy, L.A., Talling, P.J., 2006. Anatomy of turbidites and linked debrites based on long distance (120 x 30 km) bed correlation, Marnoso Arenacea Formation, Northern Apennines, Italy. Sedimentology, 53(1): 161-212.

Armstrong-Altrin, J.S. et al., 2015. Provenance and depositional history of continental slope sediments in the Southwestern Gulf of Mexico unraveled by geochemical analysis. Continental Shelf Research, 95: 15-26.

Armstrong-Altrin, J.S. et al., 2013. Geochemistry of the Jurassic and Upper Cretaceous shales from the Molango Region, Hidalgo, eastern Mexico: Implications for source-area weathering, provenance, and tectonic setting. Comptes Rendus Geoscience, 345(4): 185-202.

Armstrong-Altrin, J.S., Ramos-Vázquez, M.A., Zavala-León, A.C., Montiel-García, P.C., Tyrrell, S., 2018. Provenance discrimination between Atasta and Alvarado beach sands, western Gulf of Mexico, Mexico: Constraints from detrital zircon chemistry and U-Pb geochronology. Geological Journal, 53(6): 2824-2848.

Arnott, R.W.C., 2007. Stratal architecture and origin of lateral accretion deposits (LADs) and conterminuous inner-bank levee deposits in a base-of-slope sinuous channel, lower Isaac Formation (Neoproterozoic), East-Central British Columbia, Canada. Marine and Petroleum Geology, 24(6-9): 515-528.

Basu, A., 2017. Evolution of Siliciclastic Provenance Inquiries, Sediment Provenance, pp. 5-23.

Bergen, A.L., Cunningham, C.M., Terlaky, V., Arnott, R.W.C., 2022. Influence of channelized-flow density structure on the stratal architecture of deep-marine levee deposits. Journal of Sedimentary Research, 92(4): 381-403.

Bhatia, M.R., 1983. Plate tectonics and geochemical composition of sandstones. The Journal of Geology, 91(6): 611-627.

Bhatia, M.R., Crook, K.A.W., 1986. Trace element characteristics of greywackes and tectonic setting discrimination of sedimentary basins. Contributions to Mineralogy and Petrology, 92: 181-193.

Bizimis, M., Scher, H.D., 2016. Neodymium Isotopes, Encyclopedia of Engineering Geology. Encyclopedia of Earth Sciences Series, pp. 1-6.

Boghossian, N.D., Patchett, P.J., Ross, G.M., Gehrels, G.E., 1996. Nd Isotopes and the Source of Sediments in the Miogeocline of the Canadian Cordillera. The Journal of Geology, 104: 259-277.

Bond, G.C., Kominz, M.A., 1984. Construction of tectonic subsidence curves for the early Paleozoic miogeocline, southern Canadian Rocky Mountains: Implications for subsidence mechanisms, age of breakup, and crustal thinning. Geological Society of America Bulletin, 95: 155-173.

Bowring, S.A., Podosek, F.A., 1989. Nd isotopic evidence from Wopmay Orogen for 2.0-2.4 Ga crust in western North America. Earth and Planetary Science Letters, 94: 217-230.

Box, S.E., Pritchard, C.J., Stephens, T.S., O'Sullivan, P.B., 2020. Between the supercontinents: Mesoproterozoic Deer Trail Group, an intermediate age unit between the Mesoproterozoic Belt–Purcell Supergroup and the Neoproterozoic Windermere Supergroup in northeastern Washington, USA. Canadian Journal of Earth Sciences, 57(12): 1411-1427.

Brennan, D.T., Pearson, D.M., Link, P.K., Chamberlain, K.R., 2020. Neoproterozoic Windermere Supergroup Near Bayhorse, Idaho: Late-Stage Rodinian Rifting Was Deflected West Around the Belt Basin. Tectonics, 39(8).

Burwash, R.A., Cavell, P.A., Burwash, E.J., 1988. Source terranes for Proterozoic sedimentary rocks in southern British Columbia: Nd isotopic and petrographic evidence. Canadian Journal of Earth Sciences, 25: 824-832.

Burwash, R.A., Culbert, R.R., 1976. Multivariate geochemical and mineral patterns in the Precambrian basement of western Canada. Canadian Journal of Earth Sciences, 13(1): 1-18.

Cameron, E.M., Hattori, K., 1997. Strontium and neodymium isotope ratios in the Fraser River, British Columbia: a riverine transect across the Cordilleran orogen. Chemical Geology, 137: 243-253.

Campbell, R.B., Mountjoy, E.W., Young, F.G., 1973. Geology of the McBride Map-Area, British Columbia.

Carter, S.C., Griffith, E.M., Clift, P.D., Scher, H.D., Dellapenna, T.M., 2020. Clay-fraction strontium and neodymium isotopes in the Indus Fan: implications for sediment transport and provenance. Geological Magazine, 157(6): 879-894.

Chaudhuri, A., Chatterjee, A., Banerjee, S., Ray, J.S., 2020. Tracing multiple sources of sediments using trace element and Nd isotope geochemistry: provenance of the Mesozoic succession in the Kutch Basin, western India. Geological Magazine, 158(2): 359-374.

Chen, L. et al., 2019. Provenance and palaeoenvironment of Upper Devonian Shetianqiao Formation mudstones in Shaoyang Sag, Xiangzhong Depression, Central China. Geological Journal, 55(1): 934-948.

Colpron, M., Logan, J.M., Mortensen, J.K., 2002. U-Pb zircon age constraint for late Neoproterozoic rifting and initiation of hte lower Paleozoic passive margin of western Laurentia. Canadian Journal of Earth Sciences, 39: 133-143.

Condie, K.C., Wronkiewicz, D.J., 1990. The Cr/Th ratio in Precambrian pelites from the Kaapvaal Craton as an index of craton evolution. Earth and Planetary Science Letters, 97: 256-267.

Cousens, B., Facey, K., Falck, H., 2002. Geochemistry of the late Archean Banting Group, Yellowknife greenstone belt, Slave Province, Canada: simultaneous melting of the upper mantle and juvenile mafic crust. Canadian Journal of Earth Sciences, 39(11): 1635-1656.

Cox, R., Lowe, D.R., Cullers, R.L., 1995. The influence of sediment recycling and basement composition on evolution of mudrock chemistry in the southwestern United States. Geochimica et Cosmochimica Acta, 59: 2919-2940.

Crichton, J.G., Condie, K.C., 1993. Trace Elements as Source Indicators in Cratonic Sediments: A Case Study from the Early Proterozoic Libby Creek Group, Southeastern Wyoming. The Journal of Geology, 101: 319-331.

Crowley, J.L., 1999. U-Pb geochronologic constraints on Paleoproterozoic tectonism in the Monashee complex, Canadian Cordillera: Elucidating an overprinted geologic history. Geological Society of America Bulletin, 111(4): 560-577.

Cullers, R., 1988. Mineralogical and chemical changes of soil and stream sediment formed by intense weathering of the Danburg granite, Georgia, U.S.A. Lithos, 21.

Cullers, R.L., 2000. The geochemistry of shales, siltstones and sandstones of Pennsylvanian–Permian age, Colorado, USA: implications for provenance and metamorphic studies. Lithos, 51: 181-203.

Cullers, R.L., 2002. Implications of elemental concentrations for provenance, redox conditions, and metamorphic studies of shales and limestones near Pueblo, CO, USA. Chemical Geology, 191: 305-327.

Devlin, W.J., Bond, G.C., 1988. The initiation of the early Paleozoic Cordilleran miogeocline: evidence from the uppermost Proterozoic - Lower Cambrian Harnill Group of southeastern British Columbia. Canadian Journal of Earth Sciences, 25: 1-19.

Devlin, W.J., Bond, G.C., Brueckner, H.K., 1985. An assessment of the age and tectonic setting of volcanics near the base of the Windermere Supergroup in northeastern Washington: implications for latest Proterozoic - earliest Cambrian continental separation. Canadian Journal of Earth Sciences, 22: 829-837.

Devlin, W.J., Brueckner, H.K., Bond, G.C., 1988. New isotopic data and a preliminary age for volcanics near the base of the Windermere Supergroup, northeastern Washington, U.S.A. Canadian Journal of Earth Sciences, 25: 1906-1911.

Dickinson, W.R., 2004. Evolution of the North American Cordillera. Annual Review of Earth and Planetary Sciences, 32(1): 13-45.

Dillard, K.A., Pope, M.C., Coniglio, M., Hasiotis, S.T., Lieberman, B.S., 2007. Stable isotope geochemistry of the lower Cambrian Sekwi Formation, Northwest Territories, Canada: implications for ocean chemistry and secular curve generation. Paleogeography, Paleoclimatology, Paleoecology, 256(174-194).

Eisbacher, G.H., 1985. Late proterozoic rifting, glacial sedimentation, and sedimentary cycles in the light of Windermere deposition, western Canada. Paleogeography, Paleoclimatology, Paleoecology, 51: 231-254.

Eriksson, K.A., Campbell, I.H., Palin, J.M., Allen, C.M., Bock, B., 2004. Evidence for Multiple Recycling in Neoproterozoic through Pennsylvanian Sedimentary Rocks of the Central Appalachian Basin. The Journal of Geology, 112: 261-276.

Evans, J.A., Zalasiewicz, J.A., Chopey-Jones, A., 2009. Facies effects on the behaviour of Nd and Sr isotope systems in turbidite mudrocks during diagenesis. Sedimentology, 56(4): 863-872.

Eyster, A., Ferri, F., Schmitz, M.D., Macdonald, F.A., 2018. One diamictite and two rifts: Stratigraphy and geochronology of the Gataga Mountain of northern British Columbia. American Journal of Science, 318(2): 167-207.

Fanning, C.M., Link, P.K., 2004. U-Pb SHRIMP ages of Neoproterozoic (Sturtian) glaciogenic Pocatello Formation, southeastern Idaho. Geology, 32(10).

Fedo, C.M., Eriksson, K.A., Krogstad, E.J., 1996. Geochemistry of shales from the Archaean (~3.0) Bhuwa Greenstone belt, Zimbabwe: implications for provenance and source-area weathering. Geochimica et Cosmochimica Acta, 60(10): 1751-1763.

Floyd, P.A., Leveridge, B.E., 1987. Tectonic Environment of the Devonian Gramscatho Basin South Cornwall: Framework Mode and Geochemical Evidence from Turbiditic Sandstones. Journal of the Geological Society, London, 144: 531-542.

Fraino, P.E., Arnott, R.W.C., Navarro, L., 2022. The influence of sediment supply on the stratigraphic evolution of an ancient passive margin deep-marine slope channel system, Windermere Supergroup, British Columbia, Canada. Journal of Sedimentary Research, 92(3): 232-256.

Frost, C.D., Burwash, R.A., 1986. Nd evidence for extensive Archean basement in ,the western Churchill Province, Canada. Canadian Journal of Earth Sciences, 23(9): 1433-1437.

Gammon, P.R., Arnott, R.W.C., Ross, G.M., 2007. Architectural Relationships Between Channels, Levees, and Debris Flows: Isaac Channel 6, Castle Creek South, Lower Isaac Formation, Windermere Supergroup, British Columbia, Canada. Atlas of deep-water outcrops: AAPG Studies in Geology.

Garver, J.I., Royce, P.R., Smick, T.A., 1996. Chromium and nickel in shale of the Taconic Foreland: a case study for the provenance of fine-grained sediments with an ultramafic source. Journal of Sedimentary Research, 66(1): 100-106.

Garzione, C.N., Patchett, P.J., Ross, G.M., Nelson, J., 1997. Provenance of Paleozoic sedimentary rocks in the Canadian Cordilleran miogeocline: a Nd isotopic study. Canadian Journal of Earth Sciences, 34: 1603-1618.

Gehrels, G.E., Ross, G.M., 1998. Detrital zircon geochronology of Neoproterozoic to Permian miogeoclinal strata in British Columbia and Alberta. Canadian Journal of Earth Sciences, 35: 1380-1401.

Gifford, J.N., Malone, S.J., Mueller, P.A., 2020. The Medicine Hat Block and the Early Paleoproterozoic Assembly of Western Laurentia. Geosciences, 10(7).

Hadlari, T. et al., 2021. Provenance of the Incipient Passive Margin of NW Laurentia (Neoproterozoic): Detrital Zircon from Continental Slope and Basin Floor Deposits of the Windermere Supergroup, Southern Canadian Cordillera. Lithosphere, 2021(1).

Harlan, S.S., Heaman, L.M., LeCheminant, A.N., Premo, W.R., 2003. Gunbarrel mafic magmatic event: A key 780 Ma time marker for Rodinia plate reconstructions. Geology, 31(12): 1053-1056.

Harnois, L., 1988. The CIW index: a new chemical index of weathering. Sedimentary Geology, 55: 319-322.

Hauck, T.E., Pană, D., DuFrane, S.A., 2017. Northern Laurentian provenance for Famennian clastics of the Jasper Basin (Alberta, Canada): A Sm-Nd and U-Pb detrital zircon study. Geosphere.

Hawkesworth, C.J., Kemp, A.I., 2006. Evolution of the continental crust. Nature, 443(7113): 811-7.

Hiscott, R.N., 1984. Ophiolitic source rocks for Taconic-Age flysch: trace-element evidence. Geological Society of America Bulletin, 95: 1261-1267.

Hoffman, P.F., 1988. United plates of America, the birth of a craton: Early Proterozoic assembly and growth of Laurentia. Ann. Rev. Earth Planet. Sci, 16: 543-603.

Hoffman, P.F. et al., 2017. Snowball Earth climate dynamics and Cryogenian geology-geobiology. Science Advances, 3(11): 43.

Jefferson, C.W., Parrish, R.R., 1988. Late Proterozoic stratigraphy, U-Pb zircon ages, and rift tectonics, Mackenzie Mountains, northwestern Canada. Canadian Journal of Earth Sciences, 26: 1784-1801.

Jenkyns, H.C., Jones, C.E., Grocke, D.R., Hesselbo, S.P., Parkinson, D.N., 2002. Chemostratigraphy of the Jurassic System: applications, limitations and implications for palaeoceanography. Journal of the Geological Society, London, 159: 351-378.

Johnson, C.M., Winter, B.L., 1999. Provenance analysis of lower Paleozoic cratonic quartz arenites of the North American midcontinent region: U-Pb and Sm-Nd isotope geochemistry. Geological Society of America Bulletin, 111(11): 1723-1738.

Kendall, B.S., Creaser, R.A., Ross, G.M., Selby, D., 2004. Constraints on the timing of Marinoan "Snowball Earth" glaciation by 187Re–187Os dating of a Neoproterozoic, post-glacial black shale in Western Canada. Earth and Planetary Science Letters, 222(3-4): 729-740.

Kuiper, Y.D., Shields, C.D., Tubrett, M.N., Bennett, V., Buchwaldt, R., 2014. Age and provenance of a Paleoproterozoic to Devonian Canadian Cordilleran sequence of metasedimentary rocks, Thor-Odin dome, southeastern British Columbia. Geological Society of America Bulletin, 126(9-10): 1259-1274.

Lan, Q. et al., 2014. Tectonics, topography, and river system transition in East Tibet: Insights from the sedimentary record in Taiwan. Geochemistry, Geophysics, Geosystems, 15(9): 3658-3674.

Li, Z.-X., Evans, D.A.D., Halverson, G.P., 2013. Neoproterozoic glaciations in a revised global palaeogeography from the breakup of Rodinia to the assembly of Gondwanaland. Sedimentary Geology, 294: 219-232.

Li, Z.X. et al., 2008. Assembly, configuration, and break-up history of Rodinia: A synthesis. Precambrian Research, 160(1-2): 179-210.

Link, P.K., Christie-Blick, N., Devlin, W.J., Elston, D.P., Horodyski, R.J., Levy, M., Miller, J.M.G., Pearson, R.C., Prave, A., Stewart, J.H., Winston, D., Wright, L.A., and Wrucke, C.T., 1993. Middle and late Proterozoic stratified rocks in the western U.S. Cordillera, Colorado Plateau, and Basin and Range Province. In: J.C. Reed, J.M.E.B., R.S. Houston,

P.K. Link, D.W. Rankin, P.K. Sims, and W.R. Van Schmus (Ed.), Precambrian: Conterminous U.S., The Geology of North America: Geological Society of America Decade of North American Geology Series, pp. 474-690.

Long, L.E., 1999. Rubidium-Strontium method. In: Marshall, C.P., Fairbridge, R.W. (Eds.), Encyclopedia of Geochemistry. Kluwer Academic Publishers, Dordrecht, The Netherlands.

Lund, K. et al., 2009. SHRIMP U-Pb dating of recurrent Cryogenian and Late Cambrian-Early Ordovician alkalic magmatism in central Idaho: Implications for Rodinian rift tectonics. Geological Society of America Bulletin, 122(3-4): 430-453.

Lund, K., Aleinikoff, J.N., Evans, K.V., Fanning, C.M., 2003. SHRIMP U-Pb geochronology of Neoproterozoic Windermere Supergroup, central Idaho: Implications for rifting of western Laurentia and synchroneity of Sturtian glacial deposits. Geological Society of America Bulletin, 115(3): 349-372.

Mackinder, A., Cousens, B.L., Ernst, R.E., Chamberlain, K.R., 2019. Geochemical, isotopic, and U–Pb zircon study of the central and southern portions of the 780 Ma Gunbarrel Large Igneous Province in western Laurentia. Canadian Journal of Earth Sciences, 56(7): 738-755.

Matthews, W., Guest, B., Madronich, L., 2017. Latest Neoproterozoic to Cambrian detrital zircon facies of western Laurentia. Geosphere, 14(1): 243-264.

McCulloch, M.T., Wasserburg, G.J., 1978. Sm-Nd and Rb-Sr Chronology of Continental Crust Formation. Science, 200: 1003-1011.

McDonough, M.R., Parrish, R.R., 1991. Proterozoic gneisses of the Malton Complex, near Valemount, British Columbia: U-Pb ages and Ndisotopic signatures. Canadian Journal of Earth Sciences, 28: 1202-1216.

McLennan, S.M., 2001. Relationships between the trace element composition of sedimentary rocks and upper continental crust. Geochemistry, Geophysics, Geosystems, 2(4): n/a-n/a.

McLennan, S.M., Taylor, S.R., McCulloch, M.T., Maynard, J.B., 1990. Geochemical and Nd-Sr isotopic composition of deep-sea turbidites: Crustal evolution and plate tectonic associations. Geochimica et Cosmochimica Acta, 54: 2015-2050.

McMechan, M.E., 2000. Vreeland Diamictites – Neoproterozoic glaciogenic slope deposits, Rocky Mountains, northeast British Columbia. . Bulletin of Canadian Petroleum Geology, 48(3): 246-261.

McMechan, M.E., 2015. The Neoproterozoic succession of the central Rocky Mountains, Canada. Bulletin of Canadian Petroleum Geology, 63(3): 243-273.

Meija, J. et al., 2016. Isotopic compositions of the elements 2013 (IUPAC Technical Report). Pure and Applied Chemistry, 88(3): 293-306.

Middelburg, J.J., Van der Weijden, C.H., Woittiez, J.R.W., 1988. Chemical processes affecting the mobility of major, minor and trace elements during weathering of granitic rocks. Chemical Geology, 68: 253-273.

Moorbath, S., 1964. The rubidium-strontium method. Geological Society, London, Special Publications, 1(1): 87-99.

Moynihan, D.P., Strauss, J.V., Nelson, L.L., Padget, C.D., 2019. Upper Windermere Supergroup and the transition from rifting to continent-margin sedimentation, Nadaleen River area, northern Canadian Cordillera. GSA Bulletin, 131(9-10): 1673-1701.

Murphy, D.C., 1987. Suprastructure/infrastructure transition, east-central Cariboo Mountains, British Columbia: geometry, kinematics and tectonic implications. Journal of Structural Geology, 9(1): 13-29.

Murphy, D.C., Walker, R.T., Parrish, R.R., 1991. Age and geological setting of Gold Creek gneiss, crystalline basement of the Windermere Supergroup, Cariboo Mountains, British Columbia. Canadian Journal of Earth Sciences, 28: 1217-1231.

Murphy, J.B., 2000. Tectonic influence on sedimentation along the southern flank of the Late Paleozoic Magdalen Basin in the Canadian Appalachians: Geochemical and isotopic constraints on the Horton Group in the St. Marys basin, Nova Scotia. GSA Bulletin, 112(7): 997-1011.

Narbonne, G.M., Aitken, J.D., 1995. Neoproterozoic of the Mackenzie Mountains, northwestern Canada. Precambrian Research, 73: 101-121.

Nelson, L.L. et al., 2020. Geochronological Constraints on Neoproterozoic Rifting and Onset of the Marinoan Glaciation from the Kingston Peak Formation in Death Valley, California (USA). Geology, 48(11): 1083-1087.

Nesbitt, B.E., Muehlenbachs, K., 1997. Paleo-hydrogeology of late Proterozoic units of southeastern Canadian Cordillera. American Journal of Science, 297: 359-392.

Nesbitt, B.E., Young, G.M., 1984. Prediction of some weathering trends of plutonic and volcanic rocks based on thermody- namic and kinetic considerations. Geochimica et Cosmochimica Acta, 48: 1523-1534.

Nesbitt, H.W., 1979. Mobility and fractionation of rare earth elements during weathering of a granodiorite. Nature, 279.

Nesbitt, H.W., Young, G.M., 1982. Early Proterozoic climates and plate motions inferred from major element chemistry of lutites. Nature, 299: 715-717.

Nie, J. et al., 2012. Integrated provenance analysis of a convergent retroarc foreland system: U–Pb ages, heavy minerals, Nd isotopes, and sandstone compositions of the Middle Magdalena Valley basin, northern Andes, Colombia. Earth-Science Reviews, 110(1-4): 111-126.

Ootes, L. et al., 2017. A Paleoproterozoic Andean-type iron oxide copper-gold environment, the Great Bear magmatic zone, Northwest Canada. Ore Geology Reviews, 81: 123-139.

Paravidini, G. et al., 2021. Combined use of Sm–Nd isotopes and lithogeochemistry in the sedimentary provenance of the southern Ediacaran-Cambrian Bambuí foreland basin system, Brazil. Journal of South American Earth Sciences, 111.

Phan, T.T., Gardiner, J.B., Capo, R.C., Stewart, B.W., 2018. Geochemical and multi-isotopic (87Sr/86Sr, 143Nd/144Nd, 238U/235U) perspectives of sediment sources, depositional conditions, and diagenesis of the Marcellus Shale, Appalachian Basin, USA. Geochimica et Cosmochimica Acta, 222: 187-211.

Pigage, L.C., Mortensen, J.K., 2004. Superimposed Neoproterozoic and Early Tertiary alkaline magmatism in the La Biche River area, southeast Yukon Territory. Bulletin of Canadian Petroleum Geology, 52(4): 325-342.

Post, R.T., Long, D.G.F., 2008. The Middle Cambrian Mount Roosevelt Formation (new) of northeastern British Columbia: Evidence for rifting and development of the Kechika Graben System. Canadian Journal of Earth Sciences, 45: 483-498.

Potter, P.E., Maynard, J.B., Depetris, P.J., 2005. Provenance of Mudstones, Mud and Mudstones. Springer, pp. 157-174.

Potter, P.E., Maynard, J.B., Pryor, W.A., 1980. Sedimentology of shale : a study guide and reference source. Springer-Verlag, New York.

Price, R.A., 1981. The Cordilleran foreland thrust and fold belt in the southern Canadian Rocky Mountains. Geological Society special publication, 9(1): 427-448.

Provow, A.W. et al., 2021. Revised Maximum Depositional Age for the Ediacaran Browns Hole Formation: Implications for Western Laurentia Neoproterozoic Stratigraphy. Lithosphere, 2021(1).

Rainbird, R.H. et al., 1997. Pan-continental River System Draining Grenville Orogen Recorded by U-Pb and Sm-Nd Geochronology of Neoproterozoic Quartzarenites
and Mudrocks, Northwestern Canada. The Journal of Geology, 105: 1-17.

Reid, L.F., Simony, P.S., Ross, G.M., 2002. Dextral strike-slip faulting in the Cariboo Mountains, British Columbia: a natural example of wrench tectonics in relation to Cordilleran tectonics. Canadian Journal of Earth Sciences, 39(6): 953-970.

Richard, P., Shimizu, N., Allègre, C.J., 1976. 143Nd/146Nd, a natural tracer: an application to oceanic basalts. Earth and Planetary Science Letters, 31: 269-278.

Rollinson, H., Pease, V., 2021. Using Trace Element Data, Using Geochemical Data To Understand Geological Processes. Cambridge University Press, pp. 96-156.

Rooney, A.D. et al., 2014. Re-Os geochronology and coupled Os-Sr isotope constraints on the Sturtian snowball Earth. Proceedings of the National Academy of Sciences, 111(1): 51-56.

Roser, B.P., Korsch, R.J., 1986. Determination of tectonic setting of sandstone-mudstone suites using SiO2 content and K2O/Na2O ratio. The Journal of Geology, 94(5): 635-650.

Ross, G.M., 1991. Tectonic setting of the Windermere Supergorup revisited. Geology, 19: 1125-1128.

Ross, G.M., Arnott, R.W.C., 2007. Regional Geology of the Windermere Supergroup, Southern Canadian Cordillera and Stratigraphic Setting of the Castle Creek Study Area, Canada. Atlas of deep-water outcrops: AAPG Studies in Geology, 56.

Ross, G.M., Bloch, J.D., Krouse, H.R., 1995. Neoproterozoic strata of the southern Canadian Cordillera and the isotopic evolution of seawater sulfate. Precambrian Research, 73: 71-99.

Ross, G.M., Bowring, S.A., 1990. Detrital zircon geochronology of the Windermere supergroup and the tectonic assembly of the southern Canadian cordillera. Journal of Geology, 98: 879-893.

Ross, G.M., Murphy, D.C., 1988. Transgressive stratigraphy, anoxia, and regional correlations within the late Precambrian Windermere grit of the southern Canadian Cordillera. Geology, 16: 139-143.

Ross, G.M., Parrish, R.R., 1991. Detrital zircon geochronology of metasedimentary rocks in the southern Omineca Belt, Canadian Cordillera. Canadian Journal of Earth Sciences, 28: 1254-1270.

Ross, G.M., Parrish, R.R., Winston, D., 1992. Provenance and U-Pb geochronology of the Mesoproterozoic Belt Supergroup (northwestern United States): implications for age of deposition and pre-Panthalassa plate reconstructions. Earth and Planetary Science Letters, 113: 57-76.

Rudnick, R.L., 1995. Making continental crust. Nature, 378(6557): 571-578.

Rudnick, R.L., Gao, S., 2014. Composition of the Continental Crust. Elsevier, pp. 1-51.

Saylor, J.E., Sundell, K.E., 2021. Tracking Proterozoic–Triassic sediment routing to western Laurentia via bivariate non-negative matrix factorization of detrital provenance data. Journal of the Geological Society, 178(3).

Singh, S.K., Rai, S.K., Krishnaswami, S., 2008. Sr and Nd isotopes in river sediments from the Ganga Basin: Sediment provenance and spatial variability in physical erosion. Journal of Geophysical Research, 113(F3).

Smith, M.D., Arnott, R.W.C., Ross, G.M., 2014. The Old Fort Point Formation: Redefinition and formal subdivision of a distinctive stratigraphic marker in the Neoproterozoic Windermere Supergroup, southern Canadian Cordillera. Bulletin of Canadian Petroleum Geology, 62(1): 1-13.

Stevenson, R.K., Whittaker, S., Mountjoy, E.W., 2000. Geochemical and Nd isotopic evidence for sedimentary-source changes in the Devonian miogeocline of the southern Canadian Cordillera. Geological Society of America Bulletin, 112(4): 531-539.

Stewart, J., 2005. Eolian deposits in the Neoproterozoic Big Bear Group, San Bernardino Mountains, California, USA. Earth-Science Reviews, 73(1-4): 47-62.

Stewart, J.H., 1972. Initial Deposits in the Cordilleran Geosyncline: Evidence of a Late Precambrian (<850 m.y.) Continental Separation. Geological Society of America Bulletin, 83: 1345-1360.

Stewart, J.H. et al., 1999. Neoproterozoic (?) to Pennsylvanian Inner-Shelf, Miogeoclinal Strata in Sierra Agua Verde, Sonora, Mexico. Revista Mexicana de Ciencias Geológicas, 16(1): 35-62.

Tao, S. et al., 2017. Geochemistry of the Shitoumei oil shale in the Santanghu Basin, Northwest China: Implications for paleoclimate conditions, weathering, provenance and tectonic setting. International Journal of Coal Geology, 184: 42-56.

Taylor, S.R., McLennan, S.M., 1985. The continental crust: Its composition and evolution. Blackwell Scientific Pub.,Palo Alto, CA, United States, Medium: X; Size: Pages: 328 2008-02-08 Blackwell Scientific Publications, Inc., 667 Lytton Avenue, Palo Alto, CA 94301. pp.

Taylor, S.R., McLennan, S.M., 1995. The geochemical evolution of the continental crust. Reviews of Geophysics, 33(2): 241.

Terlaky, V., Arnott, R.W.C., Talling, P., 2014. Matrix-rich and associated matrix-poor sandstones: Avulsion splays in slope and basin-floor strata. Sedimentology: n/a-n/a.

Terlaky, V., Rocheleau, J., Arnott, R.W.C., Talling, P., 2015. Stratal composition and stratigraphic organization of stratal elements in an ancient deep-marine basin-floor succession, Neoproterozoic Windermere Supergroup, British Columbia, Canada. Sedimentology, 63(1): 136-175.

Thériault, R.J., Ross, G.M., 1991. Nd isotopic evidence for crustal recycling in the ca. 2.0 Ga subsurface of western Canada. Canadian Journal of Earth Sciences, 28: 1140-1147.

Villenueve, M.E. et al., 1993. Tectonic subdivision, and U-Pb Geochronology of the Crystalline Basement of the Alberta Basin, Western Canada. Geological Survey of Canada Bulletin, 447: 1-86.

Villenueve, M.E., Thériault, R.J., 1991. U-Pb ages and Sm-Nd signature of two subsurface granites from the Fort Simpson magnetic high, northwest Canada. Canadian Journal of Earth Sciences, 28: 1003-1008.

Walker, J.F., 1926. Geology and mineral deposits of Windermere map-area, British Columbia. Geological Survey of Canada, Memoir 148.

White, W.M., 2013. Trace elements in igneous processes, Geochemistry. Wiley-Blackwell, pp. 268-321.

Whitmeyer, S.J., Karlstrom, K.E., 2007. Tectonic model for the Proterozoic growth of North America. Geosphere, 3(4): 220-259.

Wronkiewicz, D.J., Condie, K.C., 1989. Geochemistry and mineralogy of sediments from the Ventersdorp and Transvaal Supergroups, South Africa: Cratonic evolution during the early Proterozoic. Geochimica et Cosmochimica Acta, 54: 343-354.

Yonkee, W.A. et al., 2014. Tectono-stratigraphic framework of Neoproterozoic to Cambrian strata, west-central U.S.: Protracted rifting, glaciation, and evolution of the North American Cordilleran margin. Earth-Science Reviews, 136: 59-95.

Young, F.G., Campbell, R.B., Poulton, T.P., 1973. The Windermere Supergroup of the Southeastern Canadian Cordillera, Belt Symposium, Moscow, Idaho, USA.

Young, G.M., 1984. Proterozoic plate tectonics in Canada with emphasis on evidence for a late Proterozoic rifting event. Precambrian Research, 25: 233-256.